Department of Precision and Microsystems Engineering

Wettability-controlled permeability of porous PDMS membranes for drug delivery in the brain

K.S.L. Tio

TUDelft
Delft
University of
Technology

Challenge the future

Wettability-controlled permeability of porous PDMS membranes

for drug delivery in the brain

by

K.S.L. Tio

to obtain the degree of Master of Science
at the Delft University of Technology,
to be defended publicly on Tuesday September 25, 2018 at 03:00 PM.

Student number:	4633210
Project duration:	September 12, 2017 – September 25, 2018
Thesis committee:	Dr. Ir. M. Tichem, TU Delft, chair
	Dr. L. Sasso, TU Delft, supervisor
	Dr. P. Fanzio, TU Delft, supervisor
	Dr. U. Olcese, UvA
	Dr. Ir. M. Langelaar, TU Delft

An electronic version of this thesis is available at `http://repository.tudelft.nl/`.

TUDelft

Preface

The idea of a drug delivery implant in the brain to aid the recovery of a stroke was triggered by the fact that current drug delivery methods are lacking, because of either systemic side effects by intravenous injection or multiple invasive procedures for local injection. An implant can provide local drug delivery, while reducing the amount of surgeries to two. This initiated a collaboration between the University of Amsterdam and Delft University of Technology.

This research is about exploring the basic concept for a controlled local drug delivery device and thereby, providing the initial step towards such a device. Many possible design options concerning materials and activating stimuli were evaluated and summarized. The foundations were laid for the fabrication procedure of porous PDMS membranes and its surface modifications. The findings from the literature survey were used to devise a project outline. The relevant methods and results of the project were documented and discussed in the format of a typical journal. Porous PDMS membranes were characterized. A phantom brain material, agarose gel, was used to test the permeability of the membrane. These results were then compared to the same experiment on mouse brains.

I would like to thank my supervisors Luigi Sasso and Paola Fanzio for their guidance, enthusiasm, and kindness. I'm also grateful for the opportunity to collaborate with Umberto Olcese who showed me the basics in brain research and tested the membrane on mouse brains with me. Furthermore, I want to thank professors, postdocs, PhDers, and students from the MNE department for making time for me to provide training on certain equipment and for fruitful discussions. Finally, I want to thank lab support for their hard work in maintaining the work flow in and around the labs.

K.S.L. Tio
Delft, September 2018

Contents

1

Introduction

A stroke is the reduction of the blood supply in the brain. Brain cells, called neurons, have no energy reserves causing a chain reaction of events upon energy deprivation leading to cell damage or death in the worst case. With time as the most important determining factor, a stroke will commonly result in disability or even death. The current treatment focuses on the removal of the blockage or repair of the blood vessel. However, there are still other strategies that can be utilized. Drugs can help in the prevention of additional damage after the stroke and in the recovery of brain functionality. A great part of the drug effectiveness depends on the drug delivery. Especially in the brain, systemic side effects and invasiveness of the procedure nullify the positive effect of drug administration. Therefore, a device is envisioned to enable localized drug delivery functional for a period of time.

In order to design a drug delivery implant for the brain, the clinical background and state-of-the-art are provided to put the desired device into perspective. From this information, the requirements of this device are deduced.

1.1. Clinical background

Basic knowledge is provided for understanding the clinical background of strokes and the motivation for designing a solution for the improvement of stroke recovery. First, a brief overview is given of the structure of the brain and its protective layers. Then, an introduction to the medical background of strokes is made for greater understanding of the biological events during and after a stroke. Finally, the current treatment for strokes is discussed.

1.1.1. Structure of the brain

The brain functions as the processing and signaling organ in the body and is part of the central nervous system. The brain receives information from the environment through the sensory system, processes this information, and initiates a reaction resulting in a signal to another organ. This essential, but fragile organ has many forms of protection: shielding out of bone by the skull, lymphatic functioning and damping by cerebrospinal fluid (CSF), and selective barrier from substances in the blood stream called the blood-brain barrier (BBB). The main cell type that processes information in the brain are neurons.

The brain and spinal cord are surrounded by a set of membranes called meninges. In mammals, the meninges consists of three membranes: dura mater, arachnoid mater, and pia mater as displayed in Figure 1.1. The dura mater is the thickest and stiffest layer of the three closest to the skull. The membrane in the middle is the arachnoid mater named after its spider web-like appearance. It is covered by a layers of epithelium with tight junctions that form an impermeable membrane for CSF. Between the arachnoid mater and pia mater is the subarachnoid space which contains the CSF. The thin membrane called pia mater is adhered to the surface of the brain referred to as cerebral cortex.

1.1.2. Pathophysiology of stroke

A stroke is defined as the loss of blood flow which can quickly lead to cell death in the brain. It can be caused by a blockage in a blood vessel restricting the blood flow which is called an ischemic stroke. Another type of stroke is a hemorrhagic stroke which is the result of a blood leakage from the vessel. Both types of strokes

1
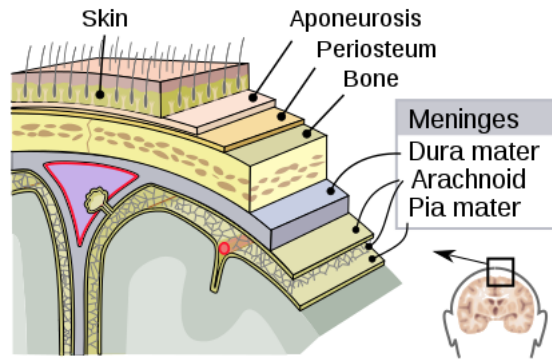
Figure 1.1: Graphical representation of the layers surrounding the brain [14]

lead to the reduction of blood flow which in turn will result in a depletion of key substances such as oxygen and glucose. In the brain deprivation of energy begins within minutes, due to high metabolism of neurons, triggering a pathophysiological sequence of events as displayed in Figure 1.2.
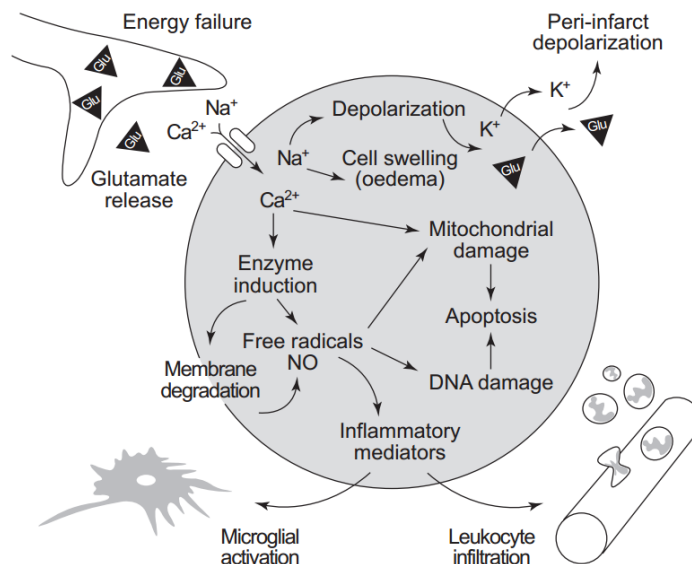
Figure 1.2: Simplified overview of stroke pathophysiology [27]

First of all, the lack of oxygen causes the cells to produce energy by means of anaerobic glycolysis which produces lactate. The increase of lactate will increase the acidity of the cell and its surroundings causing the activation of particular enzymes that produce free radicals and degrade structural proteins of the cell membrane [89]. Free radicals can initiate an inflammatory response and react irreversibly with important cellular components like mitochondria and DNA [51].

Another consequence from the lack of energy is the depolarization of neurons and glia, disabling the signaling function of these cells. During this process a neurotransmitter, glutamate, is released in the extracellular environment causing influx of Ca^{2+}, Na^+, and Cl^- and efflux of K^+. This causes the affected cells to swell (oedema), increasing the pressure in the brain and other detrimental intracellular effects by the excess of Ca^{2+} [27]. The increased concentration of K^+ and glutamate cause depolarization in surrounding tissue around the site of the stroke. The damage in this region is potentially or at least partially reversible [130]. Repolarization requires a high amount of energy which also add to the deprivation of energy [29].

As mentioned earlier, inflammatory response is a result of a stroke. The damage is not immediate, but develops in a time span of days in contrast with depolarization, swelling, cell membrane degradation, and apoptosis which happen in a matter of seconds to hours. This longer time frame allows for a treatment that aims to prevent damage due to inflammation, instead of repairing it. These damaging mechanisms are prominent

during a specific period of time as displayed in Figure 1.3.
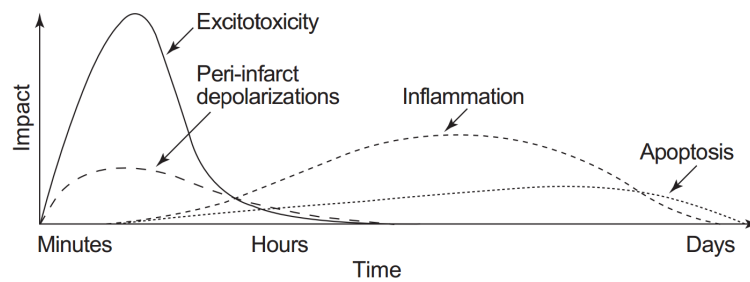
Figure 1.3: The impact of damaging mechanisms after stroke over time [27]

The regions affected by the stroke are referred to as the core and penumbra as visualized in Figure 1.4. The core is defined as the region where the stroke occurs and is characterized by irreversible damage. The area surrounding the core is called penumbra in which neurons can potentially be restored to their functional state.
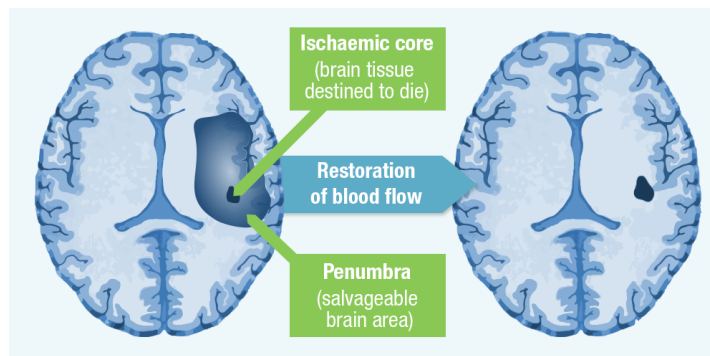
Figure 1.4: Definition of the resulting regions after stroke [52]

1.1.3. Treatment of strokes

General stroke treatment consists of monitoring and stabilizing essential variables, such as body temperature, blood pressure, and oxygen saturation. Even though lots of research is done on the treatment of strokes with the help of drugs, the only recommended treatment by the European Stroke Organisation is a drug called recombinant tissue plasminogen activator (rtPA) that helps with the breakdown of blood cloths [1]. Intra-venous rtPA has been proven to be effective in the recovery, but only when administered within three hours after the occurrence of the stroke [81].

The drug treatments for strokes can be divided into three approaches: recanalization, neuroprotection, and neural repair. With recanalization the goal is to restore the blood flow by means of removing the clot. Whereas, neuroprotective drugs strive to diminish further damage to the penumbra by interfering with steps of the stroke cascade. Drugs for neural repair aim to enhance brain plasticity in order to regain the lost neural functionality. Many drugs are being researched, but only rtPA has been approved for clinical use. Effective drugs for protecting and repairing neurons are difficult to introduce, since extensive testing is required which can take years and in most cases the systemic side effects offset the improvement too much to be worth it.

To prevent negative systemic effects, drugs must be locally administered. With the current available technology it is required to inject directly into the cortex, but this is not possible without causing damage by the penetration of the needle. Drug delivery through a vein will require high concentrations which cause undesired effects in healthy tissue. A manner to locally release drugs without penetration of the cortex might be a solution to improving long-term stroke treatment using neural protective and repairing drugs. This lead to the idea of a drug delivery implant which is further explored in the next section.

Table 1.1: Overview of the various drug delivery methods rated based on their performance. Rating: ++ excellent, + good, +− average, − mediocre, −− poor

Delivery route	Method	Minimally invasive	Drug delivery efficiency	No systemic side effects	Status
Local	Local injection	−−	++	++	Clinic
	Epi-cortical application	−	+	+	Clinic
	Epi-cortical implant	−	+	++	To be designed
	Intranasal delivery	+	+−	+	Research
Systemic	Intravenous injection	++	−−	−−	Clinic
	Ultrasound & microbubbles	++	−	++	Research

1.2. State-of-the-art tools for brain

To explore de possibilities for a drug delivery implant for the brain, the state-of-the-art is to be defined. Since there is no similar device to directly compare this implant to, the state-of-the-art is divided in three approaches. First, a comparison is made between different drug delivery routes to the brain. Next, brain implants used for recording and stimulation of brain activity are described and parallel characteristics are found for a drug delivery implant. Moreover, a short overview of implantable drug delivery devices for other applications. The combined information will clearly define the lacking features of the available tools to improve stroke treatment. Finally, the defining features of the ultimate device can be deduced aimed to improve the current stroke treatment.

1.2.1. Drug delivery routes

Drug delivery devices can be divided into two delivery routes: local and systemic. The local route is generally more invasive than systemic which means that more tissue damage is caused during the procedure and more healing time will be required. Local routes do have the advantage of a higher drug delivery efficiency resulting in a reduction of systemic side effects. The systemic route has an additional disadvantage that requires the drug to pass through the blood-brain barrier. Table 1.1 summaries the various methods and its features that are explained below in more detail.

Local routes   The first method to insert therapeutics is through local injection. Using stereotaxic equipment and a micro-injector the therapeutics are directly inserted into the core or penumbra of the stroke [104]. The damage associated with the injection is dependent on the size of the needle which can be minimized. No major damage will be induced, however there is a risk of inflammation [37]. Therefore, other less invasive treatments have been developed.

Epi-cortical application is less invasive than local injection, although the procedure in itself is still considered moderately invasive compared to systemic routes, since it is still required to open up the skull. In this procedure a hydrogel filled with therapeutics is applied on the surface of the cortex [23]. The transport of the drugs is in this case dependent on the diffusion through the healthy brain region to reach the penumbra and core. Large drug particles will be less effective or not effective at all, since these cannot diffuse or only very slowly through the dense brain tissue [74].

Intranasal delivery is also considered a local route, though the traveled distance of the drug compared to epi-cortical application has increased. In this procedure the therapeutics are inserted through the nose and travel via the olfactory region to the brain. This procedure is considerably less invasive compared to local injection and epi-cortical applications. Drug delivery efficiency can be increased with the use of nanocarriers, but it is still relatively low [61]. Systemic side effects in short-term researches were not detected, but more study on this subject is required.

Systemic routes   Intravenous injection uses the systemic route and is generally the most accepted clinically, because it is the least invasive procedure. The drug is injected with a needle into the blood stream. Due to the large travel distance and the blood-brain barrier, drug delivery efficiency is the lowest compared to other techniques. To acquire the required amount of drugs at the target site, a large amount of drugs must be administered causing systemic side effects [137]. Delivery carriers, such as biodegradable nanoparticles, can be used to increase the delivery efficiency [104].

A relatively new researched method uses ultrasound and microbubbles to deliver the drugs to the brain. Ultrasound is used to burst microbubbles causing the blood-brain barrier to open temporarily. It has been found that drug delivery efficiency is increased. The method has been tested in animals and it is found that the BBB could be repeatedly disrupted without evident damage making this a promising non-invasive technique for targeted drug delivery to the brain [85].

Ultimately, there is no perfect drug delivery method. In clinical settings it is still preferred to inject drugs in blood vessels. The most balanced trade-off between invasiveness and local drug delivery is achieved with the epi-cortical implant. It still makes a compromise on invasiveness compared to intravenous injection, but it avoids additional damage to the brain by not penetrating the cortex as is the case with local injection. The device to be designed is supposed to be the improved version of the epi-cortical method using a hydrogel. The new device will aim to provide better spatial and temporal control over the drug released and to allow for integration of other features such as electrodes for diagnostics.

1.2.2. Brain recording and stimulating implants

Various implants for the brain have been developed already. Their purpose is not drug delivery, but monitoring and stimulating brain activity. There are different types of devices available as visualized in Figure 1.5. Implantable brain recording devices are either penetrating into the brain or non-penetrating placed on top of the cortex.
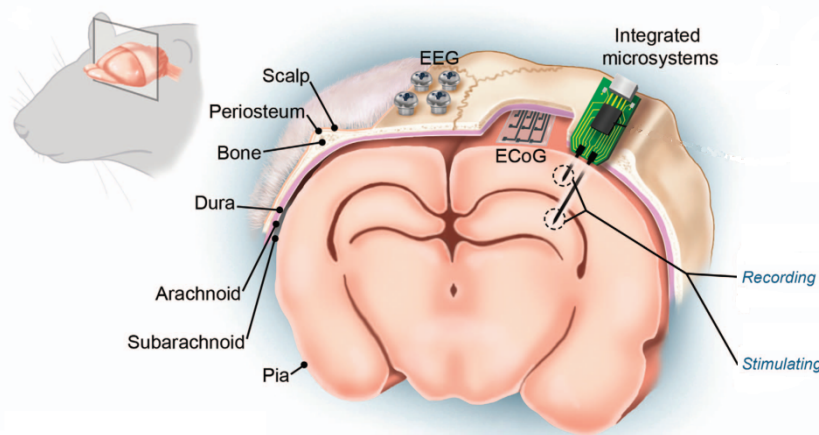
Figure 1.5: Graphical representation of the different brain recording devices and their respective placement. Adapted from [107].

Stiff electrode arrays that penetrate the cortex with needle-like structures are called Michigan and Utah array [107]. Stiff materials are used to be able to penetrate the cortex, but the large mechanical difference between the array and the brain tissue will cause additional stress that can damage brain tissue. Electrocorticograms (ECoG) is a flexible alternative that sits above the cortex, either subdural or epidural [124]. ECoG arrays are therefore less invasive than the Michigan and Utah array and causes less mechanical stress at the surface of the cortex. A flexible implant also provides a larger contact surface, because it can adjust its shape to the curved structure of the cortex. Therefore, ECoG will be used as a starting point for the drug releasing brain implant. An example of an ECoG made out of a thin polyimide substrate platinum electrodes is given in Figure 1.6. The research on long-term tissue response with these electrode arrays has been extensively studied [111]. The knowledge obtained from these studies can be used in the design of the implantable drug delivery device. Important topics include the insertion trauma, the body's immune response, and strain-induced damage from mechanical mismatch.

1.2.3. Implantable drug delivery devices

The idea of a drug releasing implant was already devised in 1989 by During et al. [28]. They made a polymeric matrix with dopamine which was slowly released over time after implantation. The drug release rate increased as the implant degrades. Thereafter, others have made degradation-based drug delivery brain implants. An example is the earlier explained epi-cortical application with a hydrogel that increases the ease of use due to its injectable form [23].

Another interesting use of the degradation-based drug release is electrical stimulation generated by neu-
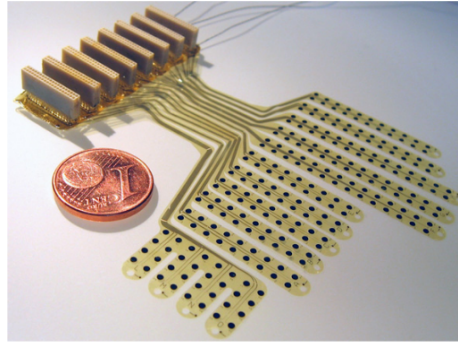
Figure 1.6: Assembled ECoG interface [105]

ral electrodes [126]. A drug is incorporated into a conductive polymer, polypyrrole, that is added as a coating over the neural electrode. Upon cyclic voltammetric stimulation, the drug can be locally released at any chosen time. The drawback is that multiple drugs cannot be independently released, unless different drug coatings on different electrodes are applied which decreases the spatial resolution for drug release. Furthermore, the required total dosage must be integrated into the coating, since a refill requires removal and re-insertion of the device.

Using a mechanical approach, a microfluidic device has been designed to locally release drugs in the brain [95]. The design is basically a probe, which is used to monitor brain activity, with a microchannel and an opening at the end of the probe. The drug can reach its target without the need of diffusion through the brain, however the probe needs to penetrate the cortex.

As concluded from the previous Section 1.1 there is a need for local drug release. Research on the state-of-the-art has shown that there is potential for an local drug delivery method without penetration of the cortex. The envisioned device can be seen as an improved version of the epi-cortical hydrogel with better spatial and temporal control. Additionally, single-use drug-coated devices can be evolved into a microfluidic system to allow for multiple drug administrations and replenishing of different drugs after implantation. With these ideas in mind, the requirements of the device are formulated.

1.3. Requirements device
The goal is to design a device that can locally administer drugs in the brain at any chosen time. Before such a device can be used in a clinical setting, it must apply to certain requirements and undergo in vitro and in vivo experiments in rats or mice to ensure its safety and effectiveness for clinical use. The important requirements for this device are listed and explained below.

- Functionality
    - Local drug administration in plane of surface cortex
    - External controlled drug release, preferably wireless
    - Store drugs or preferably option to connect to external source
    - Integration of electrodes

- Properties
    - Biocompatible
    - Low stiffness
    - Functional for period of time of implantation
    - Dimensions (mouse/rat vs human)

- Handling
    - Packaging
    - Sterilization

- Implantation surgery

- Fixation

1.3.1. Functionality
It is required to release the drug only at the targeted sites, since the drugs can have negative effects on healthy cells. Furthermore, the pinpointing of the location for the drug is in plane of the surface of the cortex like with ECoG. Internal localization would also be possible in the direction perpendicular to the cortex surface by a penetrating drug delivery device. This would improve the control of targeted drug release, but this is much more invasive with a high possibility of damaging cells during implantation. Moreover, it is required that the activation of the drug releasing mechanism is external, so that the skull can be closed up after implantation. Ultimately, the best activation is wirelessly controlled such that it allows free movement.

It is both possible to store drug in the device, but preferably the drug is supplied by an external source. If the measuring electrodes are implemented in the device, there will nevertheless be cables going out of the skull, therefore an external source for the drug only adds minimal stress to the patient. This also allows for independent multiple drug administration which will greatly improve the effectiveness of the device. There are different drugs that need to be released during certain phases of recovery. In the early phase neuroprotective drugs are administered to prevent damaging mechanisms after stroke as explained in Section 1.1.2. After the initial phase and the neural regions have been stabilized, drugs focusing on repair can be administered.

Integration of electrodes will provide additional functionality to the drug delivery device. Electrodes are required for the final product to be able to measure neuron activity which helps in the diagnosis and the decision of the required drug administration. For example, an increase of neural activity in the surrounding region of the stroke can be measured, indicating the spreading depolarizations of neurons. There are also commercial brain electrode devices available that can be used to built this device around. In an ideal device, a fully automated system could be made by using the measurements for in a controlled feedback loop.

1.3.2. Properties
Since the device is implanted, the biocompatibility of the complete device is very important to prevent harm to the body. Biocompatibility is a broad term that includes both short-term and long-term body response. A fast responses can be expected in the case of toxicity, whereas slow responses are associated with the body's immune system. An immune response will be triggered as a reaction of the body to foreign material. If no prevention measures are taken, as a result proteins will adhere to the surface, eventually encapsulating the device. Moreover, degradation can occur after being implanted for some time resulting in possibly toxic degradation products. Biocompatibility is also tissue specific, for skin tissue is less delicate than brain tissue. Neurons are very sensitive to changes in the environment, thus the stimuli-responsive mechanism must not alter the chemical environment, such as concentration of ions and pH, because these can disturb the electrical potential of neurons which can cause depolarization. Some heating is allowed, but the temperature can only be changed within a very limited range near body temperature. This is related to the functional temperature range of essential proteins. Overheating will cause irreversible damage in proteins called denaturation.

The material must be flexible to be able to reshape to the curves of the cortex' surface. Furthermore, damage the outer cells is prevented, because the stress at the interface will be reduced [111]. Note that this property is related to the thickness, as well as, the stiffness of the material.

The treatment takes a few weeks, therefore the device must be functional for at least one month. The materials used must avoid degradation, especially the materials used for the releasing mechanism, for this time period to assure a working device. Note that degradation products might have a negative influence on the biocompatibility, even though they might be harmless before degradation. Moreover, fouling of membranes is a common problem mainly described for filtering systems [88]. This results in the blocking of pores and thus prevent drug release.

For the dimensions it is important to note that there are different requirements for the device used for in vivo experiments and the device used for humans. The main difference is that the physical sizing limits at the scale of a mouse's or rat's brain versus a human's brain. Not only is the brain of a mouse and a rat much smaller than in a human, the surface structures are very different. The brain of these small rodents are relatively smooth compared to the grooves present in the human brain. Furthermore, the procedure of the implantation in humans is that the skull gets closed up or the device can even be inserted through a slit, while with small rodents it is too difficult to surgically close the brain. A protective coating is used in this case. Therefore, the thickness of the device for a rodent is less important than with the human device, since in a

mouse the thickness is not limited by the space between the dura mater and the brain. It should be aimed to design for the smallest of surface area, because the strain will be lower and there is less material for the immune system to react to [111].

1.3.3. Handling

These requirements will become important at a later stage in the design of the complete device, but to provide some perspective, these requirements will be shortly explained. First, proper packaging is essential to have electronics in the device without harming biological tissue or losing signal. Furthermore, any implant must be sterilized before implantation. Sterilization is essential for the prevention of infections. It must be taken into account that the device can be effectively sterilized without destroying its functionality. Moreover, the surgery to insert the implant should be minimally invasive. To expand, a stiff implant or an implant with a temporary holder can be inserted through a slit, while a compliant implant without a holder will require a larger insertion hole. Lastly, the device must not move after placement to prevent inaccurate drug administration.

1.3.4. Priority of requirements

As described in Section 1.2.2 electrodes have already been integrated on flexible substrates. The findings from studies on ECoG can be adapted and integrated after the drug releasing mechanism has been realized. Naturally, the control and microfluidic system are also dependent on the design of the drug releasing mechanism. The largest and most logical contribution towards the final device as described in this section is the design of the mechanism to locally release drugs. Therefore, this will be the focus of the next sections.

Some of the other mentioned requirements are involved in the design choices in Chapter 2. Choosing the drug releasing mechanism will mostly involve biocompatibility and potential for external control. For the material choice, biocompatibility and low stiffness are prioritized, but options for sterilization are also noted.

2

Design considerations

There are various ways to deliver the drug to the targeted regions in the brain. In the first place, the basis of the device - the substrate material is chosen from a selection of materials used in flexible implantable electrodes. Next, stimuli-responsive mechanisms are briefly compared from which the best suitable stimulus is deducted. Finally, the specific system is appointed from a more extensive analysis of the available mechanisms of the chosen stimulus.

2.1. Substrate materials

The substrate material is the basis of the implantable device. Most important property to consider for any implant is biocompatibility. Specifically for implants for the brain, stiff materials can create micromotion produced by everyday body movements like breathing [38]. This induces a shear stress at the interface between the implant and the cells leading to damage and even cell death under excessive stress [24].

ECoG are flexible electrodes for implantation in the brain as explained in Section 1.2.2. Since the substrate material of the drug delivery implant has the same criticial requirements as for ECoG, the materials to be compared are already used in ECoG applications in Table 2.1 on page 10. The selection of materials consists out of polydimethylsiloxane (PDMS), polyimide, parylene C, and liquid crystal polymer (LCP).

Properties   Brain tissue has an elastic modulus of about $1\,\mathrm{kPa}$. PDMS comes closest to this mechanical property, thus the least stress is caused at the brain interface compared to the other materials. Water absorption is an important property, especially for in vivo applications combined with the integration of electrodes in this context specifically. The difference in the amount of water absorbed by the substrate material and the electrode layer will cause a mismatch in the expansion of these materials at the interface. This can result in delamination of the two layers, if this mismatch is too large. Once again, PDMS has the lowest water absorption of its peers.

Out of the selected materials, PDMS is the only hydrophobic material. Wettability is a critical factor in fluid dynamics at the scale at which capillarity plays an important role. Furthermore, hydrophobic materials adsorb free-floating biological substances [103]. However, wettability can be altered by coatings or surface modifications.

Most researched materials for ECoG have USP class VI which means that the material is suitable for implantable applications. These materials also apply to ISO 10993 a set of standards evaluating the biocompatibility. The exception is polyimide which has not been officially certified yet, but preliminary in vivo biocompatibility tests have shown promising results [92].

Fabrication   In terms of fabrication, PDMS is the most accessible. The fabrication process for PDMS is well-known using either replica molding or spin-coating and no expensive equipment is required. However, PDMS is not the best option to scale-up manufacturing. Multiple molds or larger wafers can be used to reduce production time, but a batch process will be less efficient than roll-to-roll processes. Parylene C is used as a coating, so it needs to be combined with another supporting material [96]. LCP are usually bought in commercially available sheets. The fabrication is relatively complicated to the other materials. Bonding and surface modification techniques are available for all materials.

Integration   There are features that might be useful depending on the drug releasing mechanism. Looking at the optical transparencies, all materials but LCP are optical transparent for microscopic analysis. PDMS and parylene C are even transparent in the UV-region. All materials can be sterilized for implantation. Only the adhesion of metals to PDMS is poor, thus it will require an extra production step, when electrodes are added [96].

*All in all, **PDMS** is the best material to use for prototyping a drug releasing device considering the available materials and equipment in the department. Furthermore, PDMS has its Young's modulus closest to the brain's value. Water absorption is the lowest in PDMS amongst the other materials, thus it will expand the least in wet environments such as inside the body lowering the chance of delamination between different material layers. The integration of electrodes in a later stage is more difficult than with the other materials, because the adhesion between PDMS and metals is very poor.*

Table 2.1: Comparison of substrate materials used in flexible implantable electrodes

Property	Material			
	PDMS	Polyimide	Parylene C	LCP
Young's modulus	1-10 MPa	0.1-50 GPa	3 GPa	10-18 GPa
Water absorption	0.03%	0.5%	0.1%	<0.04%
Wettability: water contact angle	Hydrophobic: 110°	Hydrophilic: 82°	Hydrophilic: 78°	Hydrophilic: 80°
USP class	VI	-	VI	VI
Biocompatibility	ISO 10993	In vivo	ISO 10993	ISO 10993
Fabrication & patterning	Molding, spin-coating	Molding, spin-coating	Vapor deposition polymerization	Commercial sheet
	Curing: 25-200°C	Curing: 350°C in nitrogen		Microfabrication
Bonding/surface modification	(Oxygen) Plasma	(Oxygen) Plasma	Oxygen plasma	Oxygen plasma
Optical transmission	240 - 1100 nm	64-91.6% visible	<1% @wavelength 281 nm	-
Sterilization	Ethanol, UV	Gamma, EtO, e-beam	Gamma, EtO, e-beam	Gamma, steam
Electrode integration	Very poor	Vapor deposition, sputtering	Encapsulation	Surface modification
Ref.	[6, 54, 91, 96]	[84, 92]	[40, 83]	[21, 42]

2.2. Stimuli

A membrane is a barrier that selectively lets substances through. To change the selectivity of a membrane, its pores can be opened or closed by certain triggers. Such a sophisticated membrane can be found, for example around cells. The cell membrane contains pores and receptors that can activate opening and closing of the pore in the presence of a particular substance. Many researchers have been inspired by this to design new stimuli-responsive membranes that can aid in other applications such as self-adjusting systems, valves in microfluidic devices, and filtering. Some of these techniques might be applicable for local drug release by an external trigger.

There are various kinds of stimuli and mechanisms to choose from. To obtain an insight of the available options, the different stimuli are explored. One important aspect is the ability of external triggering, however the first few stimuli mentioned do not allow external triggering by itself. Nevertheless, they might be useful when combined with another stimulus that is externally ellicitable. Furthermore, the viability of the particular stimulus in the intracranial environment is discussed.

2.2.1. Environmental stimuli

Temperature   Temperature-responsive polymers are one of the most commonly used stimuli-responsive material. These polymers exhibit a low critical solution temperature (LCST) which can be carefully fine-tuned by changing the chemistry of the polymer. Below LCST the chains are swollen and hydrophilic. Rising the temperature above LCST makes the polymer undergo a phase transition making the chains hydrophobic and thus compact. This mechanism has been used for drug delivery with copolymer of N-isopropylacrylamide (NIPAAm) and acrylamide (AAm) the LCST can be tuned to be above body temperature ($\approx 37°C$), but below hyperthermia ($\approx 42°C$) [90, 133].

pH and ion   Another stimulus to change polymer conformation is pH [131]. However, especially in the brain, the pH can affect ion channels in neurons potentially disrupting their electrical activity. The polymer can be made responsive to the presence of a specific ion or the ion strength can also be used as a trigger [136]. However, for the same reason as for the pH, ions play an important role in the electrical activity of neurons. Therefore, these stimuli cannot be used as main trigger, but they still might be useful as a complementary condition that satisfies the liquid composition in the brain.

Molecule   Like in cell membranes, particular molecules can be used to activate the release of drug. The possibilities can range from proteins to glucose [19]. This mechanism can be used as a reactive system, for specific molecules that characterize for example an immune response.

2.2.2. Remote controllable stimuli

While the previous mentioned stimuli are dependent on the environment, the following stimuli are activated independently of the environment allowing the integration of a remotely controlled mechanism. Stimuli to be discussed in this category are light, magnetic, ultrasound and electric triggers.

Light   Light is an attractive option, when chemical potential changes are undesired and on demand drug release is required. Systems using light can be divided into two groups: UV/visible light and near-infrared radiation (NIR). UV/visible light is considered as a group, because photochromic units such as azobenzene and spiropyran undergo reversible trans-cis isomerization by the absorption of UV-light and visible light. This mechanism can be used by switching between these two types of light to open and close a pore [73, 75] or trap and release particles [8, 98]. In contrast, NIR-triggered mechanisms are based on the generated heat by NIR-responsive materials such as gold nanomaterials [120, 133]. These materials absorb the light in near-infrared region to produce heat that can be combined with temperature-responsive material to create a drug releasing mechanism. Recently, mechanisms using upconversion nanoparticles are studied. These particles can convert longer wavelength in NIR to shorter wavelengths in UV range [70].

UV and visible light have a low penetration depth through the skin and underlying tissue, thus can only be used in near contact. Furthermore, there is a risk to damage tissue depending on the intensity and the exposure time [141]. Waveguides may be used to guide the light to precise locations within the device to counter these problems. With NIR, deeper tissue penetration is possible and the risk of damaging cells is much lower than with UV and visible light under the same circumstances [53].

Magnetic   Compared to other stimuli, the magnetic field's interaction with biological molecules is very low making it another attractive option. Magnetic fields and materials can be used in different ways. Magnetic particles can be implemented in an elastic membrane that deforms as a magnetic field is applied [101]. A magnetic field can also be used to guide magnetic nanoparticles to the target location. Additionally, these particles can be used for non-invasive imaging [123]. When applying a high frequent alternating magnetic field and combining magnetic particles with thermo-responsive materials, an opening and closing pore can be designed [36]. The magnetic particles can be trapped in a membrane with temperature-responsive nanogels that upon heating shrinks making the membrane permeable [47].

Table 2.2: Overview of remote controllable stimuli and their feasibility for brain implantable drug delivery. Rating: ++ excellent, + good, +− average, − mediocre, −− poor

Stimulus	Spatial control	Dose precision	Biocomp- atibility	Interference	Integration
Light	++	+	+−	No	Waveguide
Magnetic	−	+−	+	Yes	Magnetizable implant
Ultrasound	+	+	+	No	High intensity focused ultrasound
Electric	+−	++	−	Yes	Wiring

The problem with using magnetic mechanisms is that accurate magnetic targeting is difficult to obtain in vivo. External magnetic fields have difficulties reaching deeper tissues and the resolution is poor. Implanted magnets are therefore preferred [50, 102]. Magnetic fields will also interfere with the measurement of electrical activity in neural electrodes. For that reason it is required that the magnetic drug delivery system can be turned off, when measuring the neuronal activity.

Ultrasound   Ultrasound is also a viable external stimulus, because of its relatively deep penetration depth in tissue no invasive triggering system is required [77]. Ultrasound is a pressure wave which can heat structures as the contained energy is absorbed. This process can temporarily affect the blood-brain barrier [86] and can break structures such as microbubbles filled with therapeutics at the target location [46]. However, there is also the possibility of harming the tissue, since temperature can rise quickly with high-intensity focused ultrasound (HIFU) [117]. Using HIFU is required to obtain high spatial control [65]. If penetration through the skull is achieved with decent resolution [22], ultrasound will be an attractive alternative for an easy, external application for remote drug release with breakable nanoparticles. Applying ultrasound on polymeric materials such as PDMS makes the material locally more permeable. Ultrasound causes so-called cavitations which is the formation and collapsing of microbubbles within the polymeric network. These cavitations are believed to enhance particle release by adding a convective term to a normally diffusion limited system [63]. The increase in permeability triggered by ultrasound can be enhanced by adding mesoporous silica to the PDMS matrix [60].

Electric   Electrical mechanisms are mostly associated with microfluidic systems in which they are used as valves. A piezoelectric micropump can be used to displace a certain volume out of the channel [56]. Furthermore, an electrochemical pump is made by electrolysis which generated bubbles to enlarge a bellow pushing fluid outwards [66]. Although, precise dosing can be achieved, these systems are relatively bulky that will result in a large footprint, stiff brain implants with relatively low spatial control for drug release. Moreover, the induced electric fields can influence neural activity [5, 34].

The advantages and disadvantages of the various remote controllable stimuli for drug delivery devices are summarized in Table 2.2. Stimuli are compared based on the possible spatial control, dose precision, biocompatibility of the stimulus, its effect on neural activity measurements and how the stimulus can be applied or integrated.

*For the application of an in vivo drug delivery device, **light** as the activating stimulus seems to be the most promising, because of its high spatial resolution providing local dosage, relatively fast actuation allowing control over the dose, good biocompatibility when used with limited power intensity and exposure time, and no interference with neural activity measurements.*

2.3. Type of light
As mentioned before, light can be applied as UV/visible light or NIR. These two groups have vastly different mechanisms, even though the difference in stimulation is only a matter of wavelength. A comparison is made in Table 2.3 on page 14 in terms of general fabrication steps, possible side effects of the mechanism for in vivo settings, performance, power consumption in possible mechanisms, achievable spatial resolution

and the different types of integration. These points of attention to be explained in more detail in the following paragraphs.

Fabrication   The fabrication of NIR-responsive mechanisms involve materials that induce the photothermal effect upon NIR irradiation. Gold nano particles (NPs) can convert NIR-light into heat that can induce the collapse of thermoresponsive polymers [133]. A photothermal agent must be selected based on mainly their biocompatibility. However, due to their small size, adverse systemic effects might be introduced [97]. Coatings have been developed to increase their biocompatibility, but their long-term in vivo effects are still unknown [113]. A NIR-responsive membrane can be made by incorporating the photothermal NPs into a hydrogel matrix [120]. To ensure the biocompatibility of the membrane, covalent bonding of the gold NPs to the hydrogel is preferred, but this would require an additional fabrication step and the introduction of another intermediate chemical. Furthermore, a hydrogel that changes between 37-42°C must be formulated which requires the careful tweaking in chemical composition. Lastly, the hydrogel must be attached to the substrate material for assembled drug delivery device. The adhesion of the interface between relatively soft and hard material is proven to be difficult [16].

UV/visible light mechanisms generally require a photochromic unit which is connected to a spacer molecule on the surface of the substrate material or integrated in the bulk material. While NIR-responsive mechanisms require four critical fabrication steps that have to be investigated, UV/visible light has only two. Within the provided time frame for this project a mechanism using UV/visible light is more feasible in terms of ease of fabrication, because every fabrication step optimization. Additionally, the risk increases with the number of procedures.

Side effects   For both mechanisms there are side effects that are produced during activation of the mechanism. In the case with photothermal, the thermoresponsive polymer will be heated causing its surroundings to be heated as well. The heating of cells is possible up to the upper limit of 42°C, when proteins start to denature [90]. Furthermore, there is a risk of potentially toxic photothermal nanoparticles to be released from the hydrogel, when particles are not well bonded to the matrix or the bonding is affected by other factors. Additionally, photochemical damage can be induced by high irradiation intensities and long exposure times [53].

Although, the goal of UV/visible light mechanisms is not to heat the material, local heating of a few degrees is still possible depending on the setup. The risk of photochemical damage is also much larger with UV than with NIR, therefore much lower irradiation intensities and shorter exposure times can be utilized [141].

Performance   Performance is a difficult quality to compare, due to inconsistency between the reported mechanisms in the characterization of performance. Generally, the photothermal mechanisms are relatively quick in their response. The reverse response is dependent on heat dissipation, which is a slower response than heating. However, UV/visible light mechanisms are slower to respond overall varying from 10 minutes in optimized systems to several hours. The performance is not solely dependent on the chosen mechanism and materials, but optimization within a certain setup will probably have more impact on the overall performance, since most reported mechanisms showcase proof of concepts without any optimization.

Power consumption   In NIR-responsive mechanisms, NIR-light promotes the permeability in a membrane. This permeable state is sustained by continuous irradiation, because heat constantly dissipates from the system. UV/visible light irradiation is mainly required for switching between the open and closed state. While photodimerizing photochromic units only open and close under the influence of two different wavelengths, photoisomerization can be opened with a particular wavelength light and closed by another wavelength light, heat dissipation or darkness.

Spatial resolution   Theoretically, the highest optical resolution can be obtained with UV-light due to its shortest wavelength as derived from the diffraction limit: $R = \lambda/(2\text{NA})$. Thus, the resolution is theoretically about 3 times better with UV-light than with NIR-light. Nevertheless, the possible resolution with NIR-light is good enough, when compared to the dimensions of electrodes in ECoG.

__UV/visible light__-responsive mechanisms will be further investigated, because they have generally less fabrication steps, less side effects and provides a more flexible choice in integration of the mechanism compared to NIR-responsive mechanisms.

Table 2.3: Comparison of NIR and UV/visible light

	NIR + thermoresponsive polymer	UV/Vis + photochromic unit
Fabrication	• Synthesis of photothermal NPs • Adhesion of NPs to hydrogel • Synthesis of hydrogel (LCST ±40°C) • Adhesion of hydrogel to substrate	• Modifying photochromic units • Bonding to substrate
Side effects	• Heating hydrogel • Released nanoparticles • Photochemical damage	• Local heating • Photochemical damage
Performance	Response (<7 min)	Response (10 min - several hours)
Power consumption	Heating: opening	Isomerization: opening/switching Dimerization: switching
Spatial resolution $\propto \lambda$	NIR: 700-2500 nm	UV: 200-350 nm; Vis: 400-700 nm
Integration	• Responsive bulk material • Responsive pore size • Composite with nanogel	• Responsive bulk material • Responsive pore size • Composite with nanogel • Impellers in pore • Pore cap

2.4. Integration of photochromic unit

UV/visible light responsive mechanisms are produced by integrating specific photochromic units. There are many different photochromic units which are compared in Table 2.4 on page 15. These responsive molecules are categorized according to their type of response to light. Coumarin and thymine are examples of photodimerizing molecules [68, 132, 132]. Photodimerization is a process in which two monomers can form one dimer which closes the pore. Secondly, photoresponsiveness can occur in the form of photoisomerization. In the case of azobenzene, the molecule undergoes a trans-cis isomerization under the influence of certain wavelengths of light. Spiropyran has multiple forms depending on the light and also pH. A relatively new phenomenon is photo-responsive pH-jump systems. Malachite green carbinol base (MGCB) is such a system that can emit hydroxide ions increasing the local pH by dissociation to malachite green cations due to light irradiation. Recombination with the hydroxide ions reverses MGCB to its original state, thereby reducing the pH [44].

The movement of drug particles is instigated by two transport mechanisms. The first mechanism is diffusion in which particles move from a high to a low concentration. In this case the solvent is static. In contrast with diffusion, convection is the bulk flow of the solvent including the particles. In diffusion the speed at which the particles move is determined by Brownian motion, whereas in convection the velocity of the flow determines the movement of the particles, thereby being better controllable and faster.

Diffusion and convection in a pore can be controlled by two main strategies: blocking and wettability. Blocking stops the diffusion of particles through the pore and can be opened to let the particle to move freely again. Wettability is a material property to control the flow. A hydrophobic surface halts the flow, whereas a hydrophilic surface promotes it.

2.4.1. Blocking

Blocking mechanisms that are controlled by UV-light can be achieved by responsive pores or bulk material. Responsive pores in a membrane can either decrease in size with azobenzene [75] or can be capped with coumarin/thymine [68, 132, 132], azobenzene molecular complexes [18, 115], or spiropyran [138] to restrain the diffusion of particles through the pore. Azobenzene can be grafted to the surface. By irradiation of UV-light, the molecule switches from trans to cis form, decreasing its effective length and thus increasing the size of the pore. This process is called trans-cis photoisomerization. When azobenzene is grafted inside a pore, the effective size of the pore can be controlled by light as depicted in Figure 2.1.

Capping mechanisms that use photodimerization such as coumarin rely on the location of the two monomers that can form a dimer together as depicted in Figure 2.2a. The most optimal blocking of the pore is achieved, when two monomers at opposite sides of the pore dimerize, whereas the photoisomerization of azobenzene

Table 2.4: Comparison of photochromatic units and their applications

| Mechanism	Photochromic unit	Type	Description	Fabrication	Ref.
Photodime-rization	Coumarin	Cap	Coumarin gate on mesoporous bioactive glass (MBG)	Grafting of modified coumarin	[68]
		Cap	Cap of copolymer methyl methacrylate (MMA) and coumarin moieties grafted on hollow mesoporous silica nanoparticles (MSNs)	Grafting of modified coumarin	[132]
	Thymine	Cap	Cap of thymine dimers on MSNs	Grafting of thymine on modified MSN	[43]
Trans-cis photoiso-merization	Azobenzene	Stalk	Azobenzene ligands lining on mesoporous silica	Self-assembly of azobenzene-containing organosilane	[75]
		Cap	Azobenzene stalk with alpha-cyclodextrin cap on MSN	Grafting of modified azobenzene stalk with alpha-cyclodextrin	[115]
		Cap	Supramolecular assembly between azobenzene and cyclodextrin on PDMS	LBL assembly of PDDA/PAA-Azo and PDDA/PAA-CD	[18]
		Hydrogel	Photo-triggered DNA hybridization in azobenzene-containing hydrogel	Grafting of DNA and azobenzene to hydrogel network	[100]
		Hydrogel	Azobenzene on cyclodextrin sliding crosslinker in hydrogel	Grafting of azobenzene to cyclodextrin. Gelation with dimethyl-sulfoxide (DMSO)	[106]
Photoisom-erization	Spiropyran	Cap	Nitrospiropyran-functionalized caps on MSN pores.	Grafting of nitrospiropyran on modified MSN	[138]
		Hydrogel	Self-protonating spiropyran- and acrylic acid-containing NIPAM hydrogel	White light polymerization with photo-initiator (PBPO)	[140]
Photo-responsive pH-jump system	Malachite green carbino base (MGCB)	Cap	MGCB-containing MSN capped with i-motif DNA	Self-assembly of MGCB	[44]
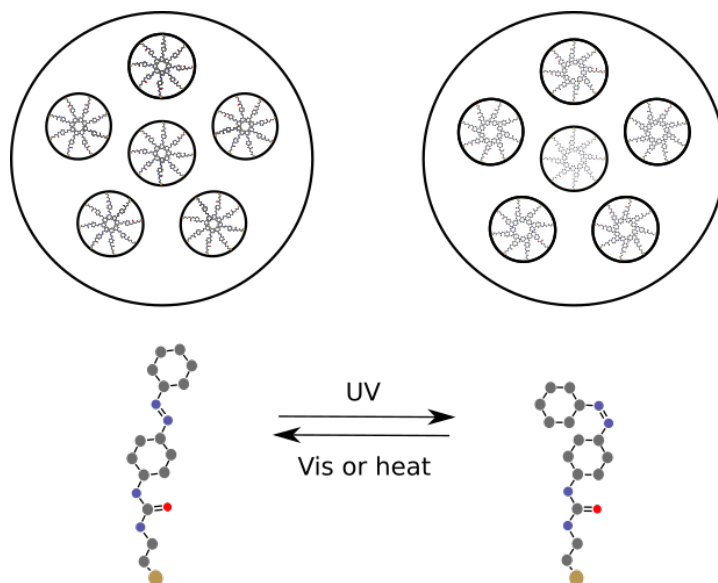
Figure 2.1: Schematic of grafted azobenzene for switchable pore size. Adapted from [72]

is independent of other azobenzene molecules. In these capping systems two monomers have to be close to each other by chance to dimerize.

Coumarin and azobenzene can be integrated into one system with increased performance [139]. Zhu et al. found that coumarin had a lower release rate than azobenzene. This suggests that coumarin is still partially blocking in the open-state. One important requirement for both mechanisms is that pores must be at nanoscale to be effective. The effectiveness of the mechanism is also highly dependent on the optimal grafting density. Low grafting density results in insufficient blocking, while too dense grafting can obstruct movement of neighboring molecules.

Capping mechanisms that use azobenzene can be combined with another molecule to form a complex. When trans azobenzene is combined with cyclodextrin, a host-guest complex is formed as illustrated in Figure 2.2b. Cyclodextrin is shaped like a hollow, truncated cone. Trans azobenzene slides inside the hollow cavity of cyclodextrin in aqueous environments. This complex decreases the free volume compared to azobenzene by itself, thereby increasing the blocking performance inside a pore. To maintain the functionality after cyclodextrin separates from cis-azobenzene, the stalk and a molecule larger than the cavity of cyclodextrin can be attachted to azobenzene [115]. Furthermore, nitrospiropyran has been used as a capping mechanism. When the pore is closed, the nitrospiropyran strands cluster together, because of hydrophobic interactions. Upon UV irradiation, spiropyran changes to its protonated form. Electrostatic repulsion causes the grafted strands to seperate, thereby opening the pore [138]. Similarly to azobenzene, spiropyran complexes can be utilized as a cap, however these mechanisms are irreversible [9].

Stimuli-responsiveness can also be integrated in a bulk material such as a hydrogel in which the permeability through the polymer network can be controlled by its local density or valving mechanisms are made using the ability of a hydrogel to change its volume. Most reported photo-responsive hydrogels switch between their solution and gel state which can be used for one time drug delivery [114]. Hydrogels that can be used for reversible drug delivery mechanisms are hydrogels that can change their volume through swelling and deswelling. These type of photo-responsive hydrogels are made using azobenzene [100, 106] and spiropyran [140]. Hydrogels can be implemented as an opening and closing pore gate by deformation as seen in Figure 2.3 or a bulk material in which molecules can diffuse through, when the hydrogel is swollen. Hydrogels also influence bulk flow, as for swelling there is a flow going inwards and for deswelling the flow is outwards. The difficulty in the fabrication is that direct adhesion of a hydrogel to a substrate, due to the difference in mechanical properties. Delamination of the different layers can occur over time. A medial layer can be used to reduce the stresses at the interface [16].

2.4.2. Wettability
The wettability of the substrate plays an important role in a phenomenon the capillary effect which allows a liquid to flow in a microchannel without the need for an external force such as pressure. A measure for
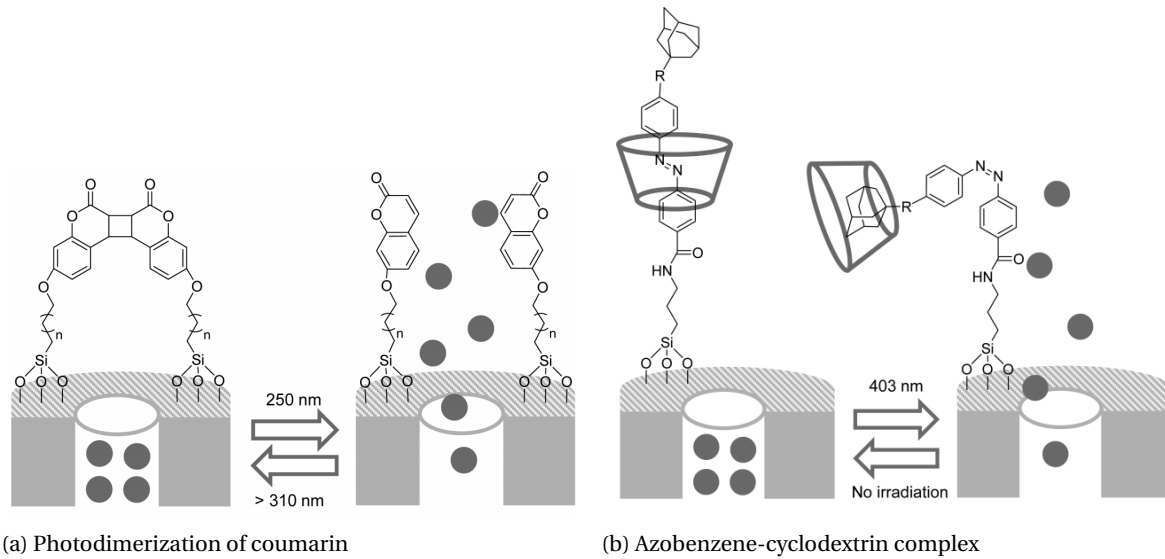
(a) Photodimerization of coumarin   (b) Azobenzene-cyclodextrin complex

Figure 2.2: Examples of capping mechanisms. Reproduced from [10].

(a) Adaptive pore size by expansion/contraction of the hy-
drogel inside a pore

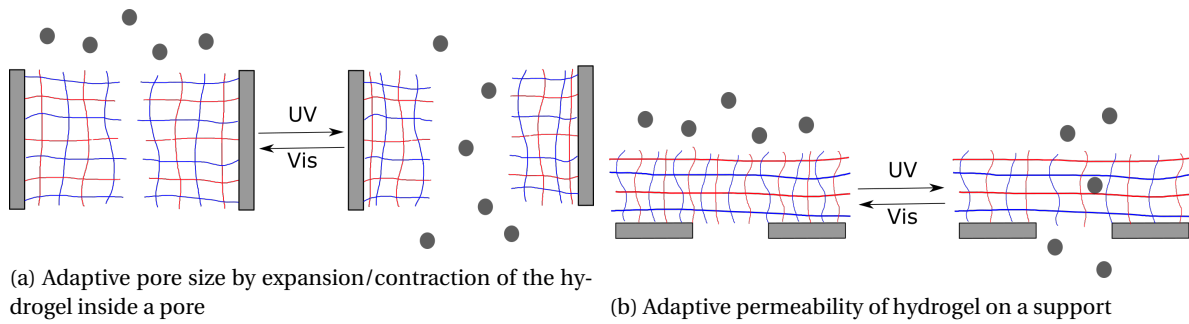(b) Adaptive permeability of hydrogel on a support

Figure 2.3: Examples of hydrogels used to control permeability in a pore/membrane

wettability is the contact angle which is the angle between the solid-liquid and liquid-gas interface contact lines. A water contact angle below 90° is called hydrophilic and above 90° is hydrophobic.

Capillary rise is the phenomenon that causes the meniscus to rise in a narrow, vertical tube to a height above the liquid height far away from the tube. The capillary rise h is governed by Equation 2.1.

$$h = \frac{2\gamma\cos\theta}{\rho g r} \tag{2.1}$$

where $\gamma = 0.073\,\mathrm{J\,m^{-2}}$ is the surface tension of the water-air interface at 20 °C [2], θ is the contact angle, ρ is the density of the liquid in $\mathrm{kg\,m^{-3}}$, $g = 9.81\,\mathrm{m\,s^{-2}}$ is the gravitational acceleration and r is the radius in m.

In the case of a hydrophilic material, the capillary rise is positive and the liquid will rise against gravity. The meniscus shape is concave. However, hydrophobic materials have a negative capillary rise and the meniscus height is lower than the bulk liquid. In this case the meniscus is convex. This distinction is illustrated in Figure 2.4. Thus, the wettability of the pores in a membrane controls the liquid movement. When combined with a wettability switching surface, a valve can be produced. However, the problem is that after wetting of the surface, the reverse process has a high activation barrier which may only be theoretically achieved with pores smaller than 5 nm [125]. Consequently, larger valves relying on the wettability are considered one-time use until dried.

Wettability switching   Since wettability controls the direction of capillary rise, a surface that is able to switch between hydrophobic and hydrophilic states can be used to control the liquid flow in a microchannel. The most well-known example for a reversible wettability surface makes use of a thermo-responsive polymer, poly(N-isopropyl acrylamide) (PNIPAm) [76].
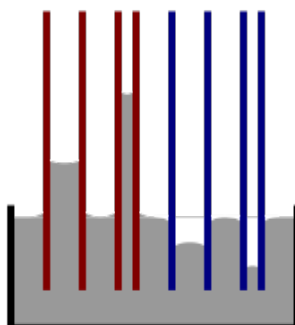
Figure 2.4: The effect of hydrophilic and hydrophobic material on the capillary rise

For reversible light-induced systems, azobenzene is the most researched. Another molecule belonging to this group is spiropyran. Inorganic materials such as ZnO and TiO$_2$ can be used as a photo-responsive coating. These systems are summarized in Table 2.5.

Azobenzene is generally found to be more hydrophilic as cis isomer and less hydrophilic as trans isomer due to a change in the dipole moment [26]. Pei et al. found that the type of end group combined with azobenzene and its orientation on the substrate has a larger influence on the wettability than the dipole moment [99]. This was shown by using an hydrophilic end group and a hydrophobic side chain connected to azobenzene. In its trans isomer the surface was hydrophilic and when irradiated by UV-light the cis isomer made it less hydrophilic.

Surface roughness is also an important factor and combined with azobenzene or spiropyran superhydrophilic and superhydrophobic surface can be obtained. Lim et al. found that increasing the surface roughness could increase the difference in water contact angle from 5° up to 148° for grafted azobenzene on silicon wafers [67]. Similarly, spiropyran has been grafted onto etched silicon to change the contact angle from 140° to 43° [127].

Azobenzene is the most versatile photochromic unit that can be grafted on the inside of a pore for blocking purposes, can change wettability of the surface, or can be integrated in a hydrogel. For blocking or wettability controlled mechanisms, the pores must be small, because the effective length change of azobenzene by itself is only a few angstroms and the activation barrier in larger pores is too high. The change in wettability is only around 8°, but can be heavily influenced by the end group and the surface roughness. Hydrogels have the potential to have better performance without the limitation in pore size, but this depends on the integration and optimization of hydrogel's properties. Generally, the fabrication of hydrogels require more steps and it thus takes longer to optimize the process and the resulting performance. When it comes to adhesion, grafted molecules are more robust than hydrogels, since molecules are attached individually, while a hydrogel has to be adhered as a bulk material leading to internal forces that might cause delamination. *Therefore, grafting* **azobenzene** *is chosen, because of its ease of fabrication and potentially a better durability.*

Table 2.5: Comparison of photoresponsive materials that switch their wettability

Photoresponsive material	Description	Water contact angle	Fabrication	Ref.
Azobenzene	Hydrophilically substituted azobenzenes on silicon surface	Vis: 57° UV: 65°	Grafting of carboxylic acid-functionalized azobenzene by reaction on aminosilane-functionalized silicon	[99]
	Azobenzene-modified SAMs on Si(111)	Vis: 73.9° UV: 68.2°	Grafting of hydroxyl-modified azobenzene by reaction on carboxylic acid-functionalized silicon	[26]
	Azobenzene on increased surface roughness by multilayer film	Vis: 152° UV: <5°	Layer-by-layer deposition of (SiO$_2$/PAH) polyelectrolyte multilayer on silicon. Grafting of carboxylic acid-functionalized azobenzene by reaction on aminosilane-functionalized multilayer	[67]
Spiropyran	Spiropyran-containing polymer brushes grafted on roughened silicon	Vis: 139° UV: 43°	Spiropyran monomer polymerization by atom transfer radical polymerization (ATRP) on roughened silicon by laser etching	[127]
Spiropyran (azobenzene, salicylide-neaniline)	Chromophore-functionalized coating based on Polysilsesquioxanes	Vis: 75° UV: 46°	Spin- or dip-coating poly(methylsilsesqioxane)-poly(pentafluoro-phenyl acrylate) (PMSSQ-PPFPA) hybrid polymer onto the desired surface. Grafting of amino-functionalized chromophore	[57]
ZnO	Hierarchical structured ZnO mesh film	Vis: 152° UV: 0°	Dip coating of mesh in ZnO solution and annealing at 420 °C to form crystal seeds. Crystallization in solution of zinc nitrate hydrate and methenamine	[118], [119]
TiO$_2$	TiO$_2$-coated aerogel	Vis: 140° UV: 0°	Coating of aerogels with TiO$_2$ by chemical vapor deposition	[58]
	Nitrogen-doped TiO$_2$ nanorod film	Vis: 135° UV: 0°	N-doped TiO$_2$ nanoparticles formed by hydrothermal method. Suspended in water and dried to form film.	[128]

3

Fabrication process

The various approaches for the fabrication process of a porous PDMS membrane and the modification of PDMS with azobenzene for a switchable wettability surface are examined and compared in this chapter. A fabrication method is concluded based on the feasibility of the execution in this thesis.

3.1. Porous PDMS membrane

There are two approaches to make a porous PDMS membrane. The first method by Huh et al. [49] uses spin coating to achieve a membrane thickness of $10\,\mu$m. The other approach is replica molding which produces generally thicker membranes. Both methods are to be explained in more detail and compared.

3.1.1. Thin porous PDMS membrane

The protocol to make a porous PDMS membrane of $10\,\mu$m thick is defined by Huh et al. [49]. The general fabrication steps are visualized in Figure 3.1. First, uncured PDMS is spin coated on silanized PDMS which is used as a support. Next, the uncured PDMS layer is placed on a silicon master with pillars made by photolithography and pressed together using a weight. This arrangement is cured, after which the silicon master can carefully be removed. The membrane can be removed by irreversible bonding to another part of the final PDMS structure which in this reported case was the part containing the microchannel.
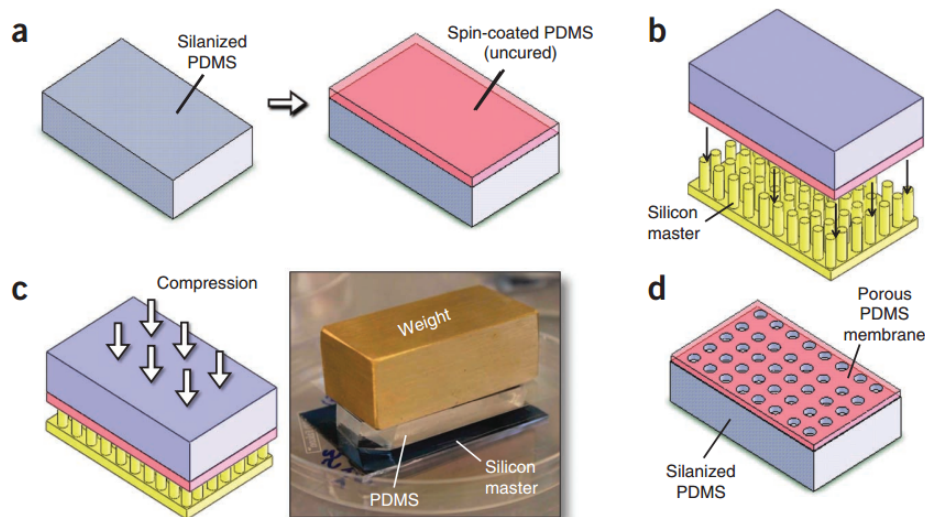

Figure 3.1: Fabrication process of thin porous PDMS membranes as described by Huh et al. [49]

Table 3.1: Comparison between fabrication methods for porous PDMS membranes

Thin membrane	Thick membrane
Smaller pores possible	Faster and easier fabrication
More prone to breakage	Easier handling

3.1.2. Thick porous PDMS membrane

Another way to make a porous PDMS membrane is with replica molding. The main steps of the fabrication process is visualized in Figure 3.2. A high resolution 3D-printer is available for prototyping of the mold. The simplest design is an array of pillars surrounded by walls. The thickness of the membrane is determined by the wall height. If a membrane is too thin, it will break upon removal from the mold. To decrease the membrane thickness beyond this point, supports are needed to help lifting the membrane out of the mold.
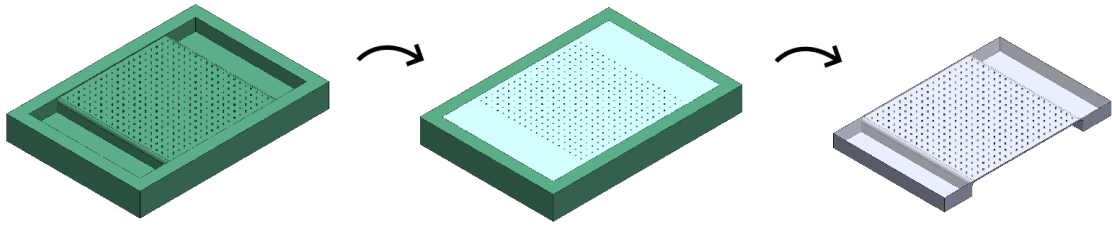

Figure 3.2: Replica molding for thick PDMS membranes

A comparison between the two methods is summarized in Table 3.1. Thin membranes allow for smaller pores than in thicker membranes, because the height of the pillars in the mold can be lowered for thin membranes. Shorter pillars are less likely to break, thus making it possible to decrease the diameter of the pillars resulting in narrower pores. However, thin membranes are very prone to breakage and are therefore require careful handling. In contrast, thick membranes are more robust and much easier to handle. The most striking advantage of membranes made using replica molding is easier and faster fabrication.

3.2. PDMS functionalization

The next step is to modify the PDMS surface with azobenzene to ultimately make a smart membrane. This section focuses on the formulation of a protocol to graft azobenzene on PDMS. Specific and general grafting methods for azobenzene and PDMS are explored, while considering the feasibility of the fabrication with the available equipment and the stability of the type of bonding for potential use as an implant.

3.2.1. Layer-by-layer assembly

The starting point is to find a reported method that describes grafting of azobenzene on PDMS. Cheng et al. [18] was the only research group that modified PDMS with azobenzene. They used layer-by-layer (LbL) self-assembly to form a multilayer structure of adsorbed polyanion and polycations layered alternately to the substrate to form a multilayer structure. Grafting of azobenzene to PDMS is done in three steps: synthesis of acrylamide-azobenzene, synthesis of poly(acrylic acid)-azobenzene (PAA-Azo), and LbL assembly on PDMS. The multilayer structure consists of PAA-Azo alternated with poly(diallyldimethylammonium chloride) (PDDA).

The LbL technique can be applied to any substrate and layer thickness can be controlled at nanoscale. However, the stability and structure of the LbL assembly is dependent on many factors such as concentration and ionic strength of the polyelectrolytes used, solvent, temperature, and pH [87]. To increase the stability chemical, polymers can be crosslinked to produce a multilayer assembly [79]. Covalent bonding azobenzene requires of crosslinking PAA and PDDA, however it has not been reported before. Without crosslinking the stability of (PDDA/PAA) is at least 48 hours [3]. Furthermore, the procedure itself is tedious, because the substrate has to be cycled through the two solutions and washed with DI water every time. Advanced chemical equipment for refluxing is also required to synthesize PAA-Azo, thus making it difficult to reproduce this

procedure in our department.

3.2.2. Conjugation strategies

There is no optimal solution for grafting azobenzene on PDMS, thus general conjugation strategies are investigated. Surface modifications of PDMS are usually initiated by oxidizing the surface. Next, The formed hydroxyl groups are able to covalently bond with alkoxysilanes with a functional end group of choice in a process called silanization. Well-defined reactions are available for particular combinations of end groups to covalently bond azobenzene.

Surface oxidation PDMS is commonly oxidized by plasma, UV, or oxidative solution treatment. After oxidation, hydroxyl groups are formed on the surface which has become hydrophilic. The effectiveness of the different treatments vary with plasma being the most effective out of the three.

Plasma is a gas-like substance consisting of charged particles. Gases such as air, oxygen and nitrogen, can be used to create plasma. Other tunable variables are pressure and power used during the treatment. Due to its fast and effective procedure, it has become the most popular choice for PDMS grafting. Another well-known usage is for bonding of PDMS to glass and PDMS to PDMS for the fabrication of microfluidic devices.

UV treatment is much slower than with plasma, but promises deeper oxidation of the PDMS without cracking of the surface [12]. A 30 minute UV/ozone treatment has been used in combination with silanization to bond PEG spacers to PDMS [94].

A HCl/H_2O_2 solution can be used to activate the PDMS surface. The main advantage is that no expensive equipment is required. Sui et al. used this method in assembled microfluidic devices to functionalize inside the channels. The HCl/H_2O_2 solution was passed through the channel for the duration of 5 minutes [112]. PDMS is also oxidized by submergence for 10 minutes in piranha solution which is usually a mixture of H_2O_2 and H_2SO_4 at a volume ratio of 1:3 [25]. Furthermore, another wet method of oxidizing PDMS is by reacting in 1M NaOH for 24h [110]. However, the water contact angle of oxidized PDMS was measured to be close to the value of PDMS before oxidation [48].

Silanization Published articles have mostly described azobenzene being functionalized on mesoporous silica. Azobenzene ligands are organized in the pore by self-assembled monolayer (SAM) and covalently bonded by silanization which is the formation of covalent Si-O-Si bonds between an alkoysilane and OH-groups at the substrate's surface. An alternative to the LbL method can be created by modifying azobenzene as suggested in previous reports and choosing an appropriate surface treatment for PDMS.

Silanization is a common method to functionalize PDMS by covalent Si-O-Si bonds between a silanes and OH-groups at the substrate's surface. Silanes are often used as coupling agents, since they can introduce new functional end groups to the surface. The general structure consists of the functional or reactive group on one end and up to three hydrolyzable groups at the other end separated by an alkyl spacer and silicon atom as displayed in Figure 3.3.
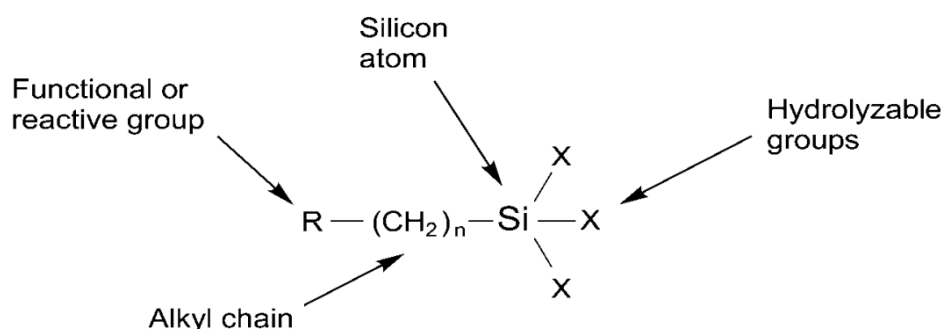

Figure 3.3: The general structure of a silane with a functional group on one end connected by an alkyl spacer and silicon atom to three hydrolyzable groups. Reproduced from [45].

Silanol derivatives will form hydrogen bonds and thus clump together in solution. The alkoxy groups prevent polymerization of silanol groups. For that reason alkoxysilanes are the most commonly used for surface modification. However, at room temperature alkoxy groups are unreactive with hydroxyl groups as

is without hydrolysis to form the highly reactive silanol. 3-aminopropyltriethoxysilane (APTES) is the most commonly used aminosilane that belongs to the alkoxysilanes. Besides an amino end group, APTES has three ethoxygroups available for bonding to the hydroxyl rich surfaces. Silanes with other reactive groups may be used. However, APTES is preferred, because of its frequent usage in research and established protocol on PDMS.

Amine reactions The PDMS surface can be modified by silanization with functional end groups such as amino, carboxylate, hydroxyl, and thiol. From this point, there are many different strategies to react these end groups with a complementary group which is either attached to azobenzene or an intermediary molecule. Amine reactions can be used to covalently bond an amino silane to carboxylates, isothiocyanates, sulfonyl chlorides, and aldehydes. The chemical reactions are summarized in Figure 3.4.

NHS (n-hydroxysuccinimide) esters are the most popular crosslinker for amine-reactions. NHS is relatively water-insoluble, thus it must first be dissolved in an organic solvent before addition to a water-based solution. For these situations a water-soluble variant, sulfo-NHS (N-hydroxysulfosuccinimide), is used. Sulfo-NHS contains a hydrophilic group, while keeping the same reactive properties of NHS. Combined with EDC (1-ethyl-3-(3-dimethylaminopropyl)carbodiimide hydrochloride) it can be used to react with a carboxylate group to form an active ester which can react with an amine to form a stable amide bond. This reaction, however, competes with hydrolysis in water. Hydrolyzed molecules cannot be used to react with amines. The reaction is fast and highly efficient.

Isothiocyanates only form a stable product with primary amines. Reactions are encouraged in alkaline environments. Isotiocynates are, however, unstable in aqueous solutions and it is therefore recommended to be stored dessicated in the fridge or freezer.

Sulfonyl chlorides reacts with an amine to form a sulfoamide bond at the cost of a chlorine atom. Reactions are performed in alkaline conditions and may also be executed in organic solvents. The reactions with amine groups compete with hydrolysis, but the rate of hydrolysis is much slower than the formation of sulfoamide bonds. In any case, care must be taken in storage, as moisture will degrade molecule.

Aldehydes react with amine groups to form an unstable Schiff base which can be reduced by sodium borohydride or sodium cyanoborohydride to form a secondary amine bond. This reaction, called reductive amination, is more dominant at high pH. Sodium cyanoborohydride is preferred over sodium borohydride, because the latter also reduces aldehyde to hydroxyls, hence a lower efficiency.

Crosslinkers Azobenzene with a functional group can be directly coupled to complementary silane or a crosslinker between azobenzene and silane. Crosslinkers can be used to increase the distance between the two target molecules known as the spacer arm length. They can be purchased with various reactive ends. For PDMS popular crosslinkers are glutaraldehyde and dextran.

Glutaraldehyde is one of the most used crosslinkers in bioconjugation. Chuah et al. have it used to graft collagen to PDMS [20]. The PDMS surface is first oxidized and silanized with APTES. The amine-functionalized PDMS is submerged in a solution of glutaraldehyde and sequentially, in a solution of collagen.

Similarly, **dextran** is used as a crosslinker to graft proteins on PDMS. Dextran is a long polysaccharide with molecular weight larger than 1,000 Dalton. It is highly water-soluble, due to its many hydroxyl groups. For each repeating unit of dextran, two sodium periodate molecules are consumed to form two aldehydes which can then be used to react with amines from APTES to form Schiff bases [82]. A covalent bond is formed by reductive amination using sodium borohydride or sodium cyanoborohydride [45]. Long polymer chains can be attached to the surface with only a few bonds with amines. When dextran is partially oxidized and bonded to the surface, it can be then be fully oxidized to provide sites for other amine-containing molecules. This is especially useful, when the grafting density of APTES on PDMS is low. Using dextran could potentially increase the grafting density of the target molecule.
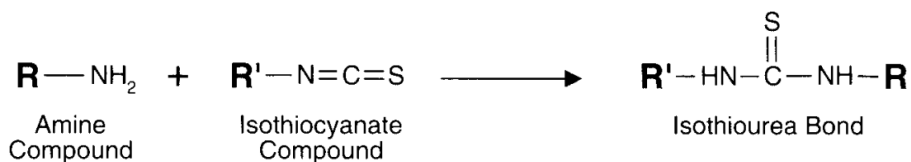
3.2.3. Azobenzene modification

All reported methods use silanization to attach azobenzene to mesoporous silica interiors. There is no comparison made between the chemical properties of the different combinations. The type of azobenzene molecule is rather chosen in terms of availability of components and ease of fabrication.
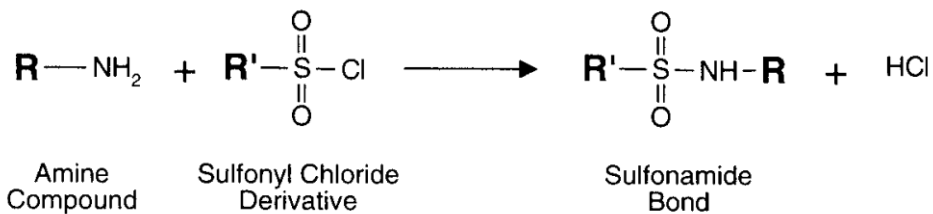
There are two main strategies that can be defined. In the first strategy the silane is coupled to the azobenzene before reacting to the substrate. This will require the modification of an azobenzene-containing molecule
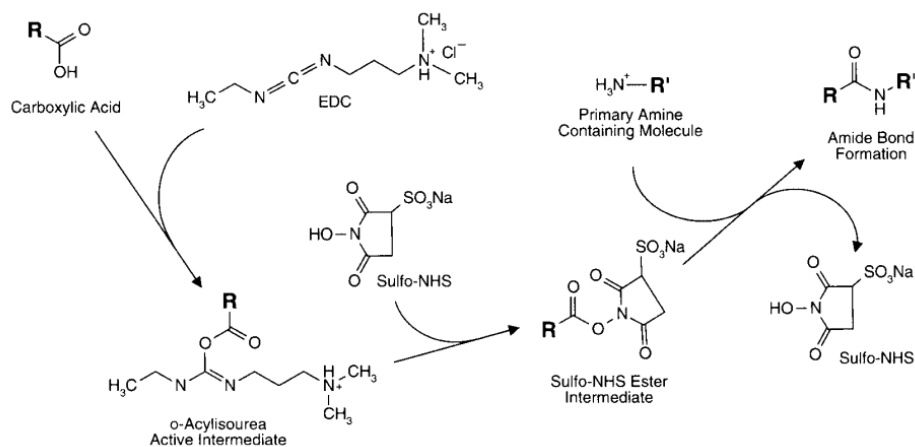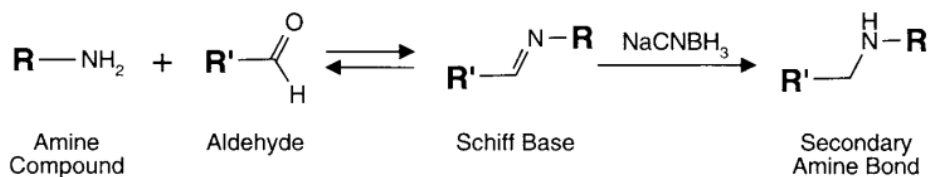
(a) EDC and sulfo-NHS

(b) Isothiocyanate

(c) Sulfonyl chloride

(d) Aldehyde

Figure 3.4: Chemical reactions schemes with amine. Reproduced from [45]

which requires refluxing equipment which are not available in our department. The modification of the azobenzene molecule also requires multiple steps which can take days in total. The second strategy is a two-step method in which first the substrate is silanized using a silane and then it is reacted to azobenzene combining the reactive end groups.

An important factor to consider is the available azobenzene variants by the chemical supplier, Sigma-Aldrich. Azobenzene-containing molecules with various functional end groups are listed in Table 3.2 on page 27. Some chemicals in this list are very dangerous, while others are relatively harmless. For this reason azobenzene and 4-aminoazobenzene are not taken into consideration. Thus, for this project modified-azobenzene can be purchased with an amine, carboxylic acid, NHS ester, sulfonyl chloride, and isotiocyanate compound.
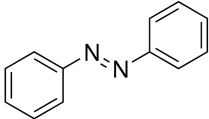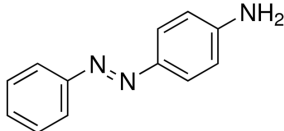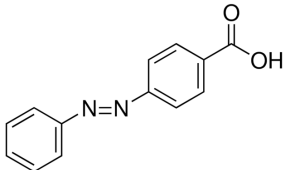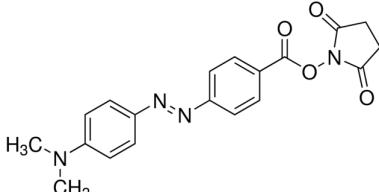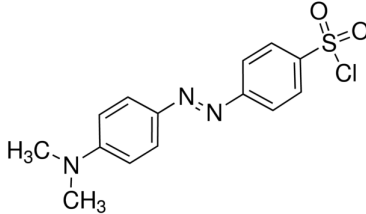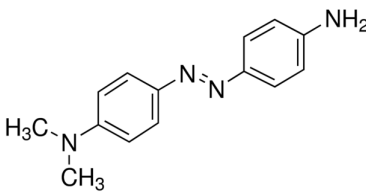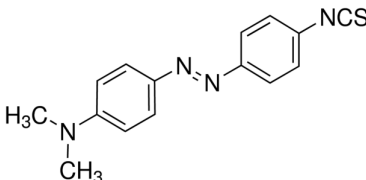
3.2.4. Process overview

LbL assembly is the only method that describes a method to adhere azobenzene to a PDMS surface. The long-term stability of the multilayer structure, that is not covalently bonded, is unknown. Since the implant needs to be functional for at least one month, LbL assembly is not the ideal option. In this project, a fabrication method is chosen that involves covalent bonding. The option that uses dextran seems the most promising, because the method has been used on PDMS in several studies before. Moreover, an azobenzene can be purchased that contains an amine compound. Furthermore, the grafting density is less dependent of the aminosilane layer.

The process for grafting of azobenzene on a PDMS surface is displayed in Figure 3.5 on page 28. First, the PDMS surface is activated using a plasma treatment to form hydroxyl groups. The activated PDMS is treated with APTES to obtain an amine-functionalized surface. Meanwhile, dextran is partially oxidized with sodium periodate. The PDMS with amine groups is treated with oxidized dextran to form Schiff bases. These bonds are then reduced with sodium borohydride to obtain covalent, secondary amine bonds. The dextran-functionalized PDMS is then further oxidized with sodium periodate. Next, amine-containing azobenzene is introduced to the oxidized dextran to form Schiff bases which are then reduced again with sodium borohydride. The protocol that explains the process step-by-step is found in Appendix A.2.

In conclusion, the functionalization of the PDMS membrane will be produced by grafting APTES, oxidized dextran, and amino-containing azobenzene with covalent bonds. LbL assembly is still a good option, in case there are problems with silanization. Other methods need to be explored, if the stability of LbL is proven to be insufficient.

Table 3.2: List of available azobenzene molecules at Sigma-Aldrich. The degree of hazardousness is indicated with a category where 1 indicates a greater hazard category than 2, and A is a greater hazard than B.

| Name	SKU	Chemical structure	Safety
Azobenzene	424633		Acute toxicity, oral+inhalation (cat. 4), germ cell mutagenicity (cat. 2), carcinogenicity (cat. 1B), specific target organ toxicity - repeated exposure (cat. 2), acute aquatic toxicity (cat. 1), chronic aquatic toxicity (cat. 1).
4-aminoazobenzene	46130		Carcinogenicity (cat. 1B), acute aquatic toxicity (cat. 1), chronic aquatic toxicity (cat. 1)
4-(Phenylazo)benzoic acid	479624		Skin irritation (cat. 2), eye irritation (cat. 2), specific target organ toxicity - single exposure (cat. 3)
4-[4-(Dimethylamino) phenyl-azo]benzoic acid N-succinimidyl ester	9278		-
4-(Dimethylamino) azobenzene-4'-sulfonyl chloride	39068		Skin corrosion (cat. 1B)
N,N-Dimethyl-4,4'-azodianiline	379298		Skin irritation (cat. 2), eye irritation (cat. 2), specific target organ toxicity - single exposure (cat. 3)
4-(4-Isothiocyanato-phenylazo)-N,N-dimethylaniline	317802		Respiratory sensitization (cat. 1), skin sensitization (cat. 1)
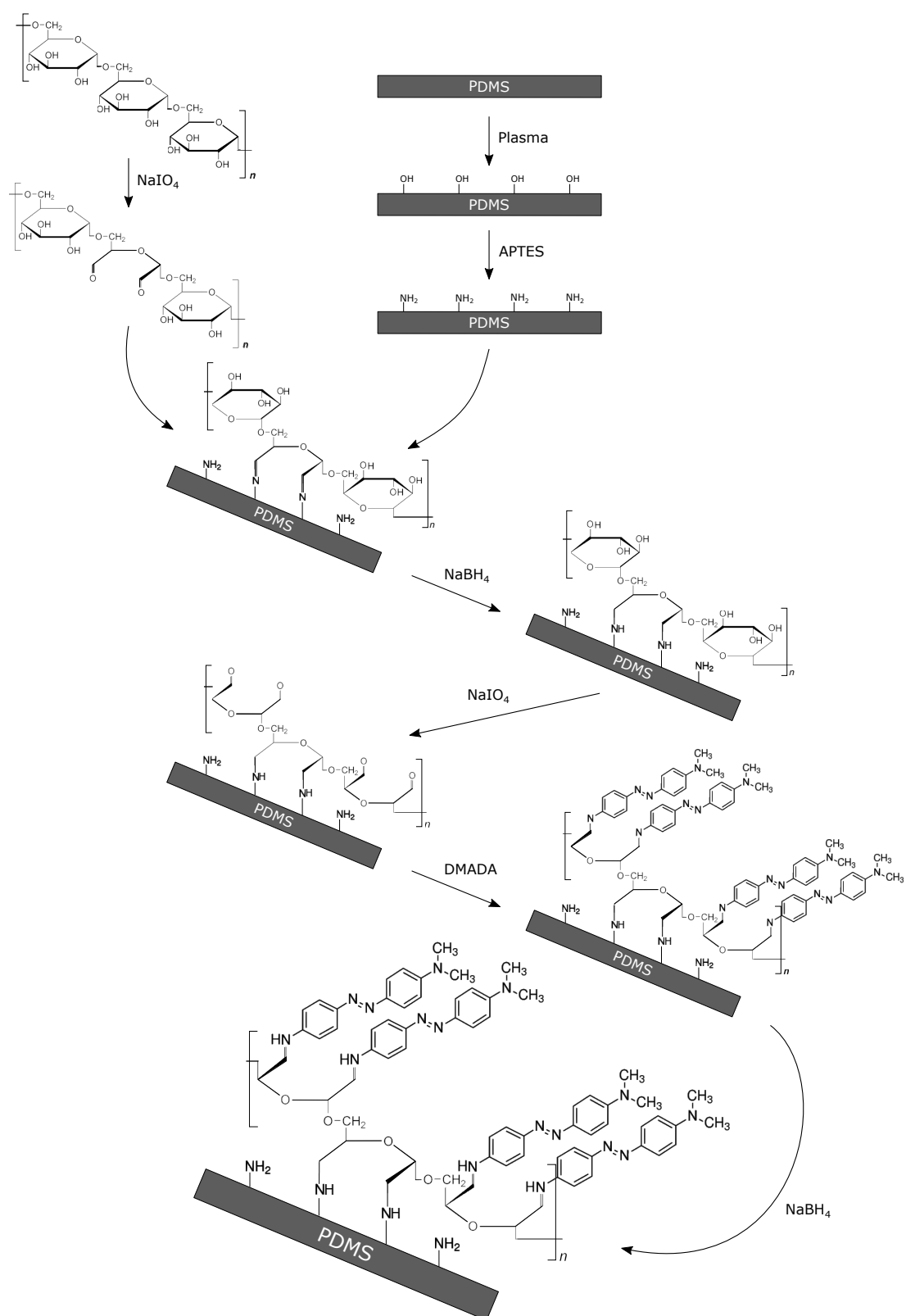
Figure 3.5: Schematic of the grafting procedure of amine-containing azobenzene PDMS with dextran.

4
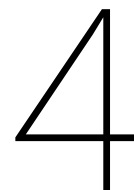
Project outline

In this chapter the outline of the master's thesis project is described by defining the project goals, planning containing the steps to reach the goals, and possible risks that might be encountered. The actual execution of this planning is documented in Appendix B-E, whereas the next chapter will present the relevant results in the form of a paper.

4.1. Project goals

Within a time span of about 45 ECTS, the goal of this project is set to fabricate a membrane that can change its permeability locally by activation of light and to test its feasibility for drug delivery for the brain. To achieve this goal there are three objectives: successful fabrication of a porous PDMS membrane, grafting of azobenzene on the PDMS surface, and demonstration of controlling the permeability.

For the integration of the membrane in the final device, there are a few specific benchmarks to be set. It is desired to achieve a pore spacing of about $30\,\mu$m as this is the electrode spacing in one of the more recent researched ECoG [59], but spacings of up to 1 mm are still usable [124]. Furthermore, if a working mechanism with azobenzene is achieved, the response time should be constant to be able to predict the dose and it is nice to have the closing response time as short as possible to lower the minimum dose. Long-term stability is a critical property to make the use of an implant worthwhile, thus the mechanism must be intact for at least one month.

4.2. Planning

The project consists of the fabrication and characterization of which each is subdivided as listed below. Some are labeled to indicate that this step has some risk (R) or high risk (HR) which is further explained in the next section. Some characterization methods are not available (NA) in the PME department.

Fabrication

- Porous membrane (R)

- Azobenzene-grafted membrane (HR)

- Integration membrane in microfluidic device (R)

Characterization

- Porous membrane with and without surface modifications

    - Morphology: microscopy, SEM

    - Chemistry: FTIR (NA), Raman spectroscopy

    - Functionality: water contact angle, UV-Vis spectroscopy (NA), AFM (HR), Raman spectroscopy (R)

- Application

    - Permeability: agar, mouse brain

Proof of concept demonstration

- Pore resolution

- Response time

- Stability

The milestones include fabrication and characterization of a porous membrane, azobenzene-grafted membrane, and microfluidic system which are displayed in a schematic in Figure 4.1 to roughly indicate how long each part should take.
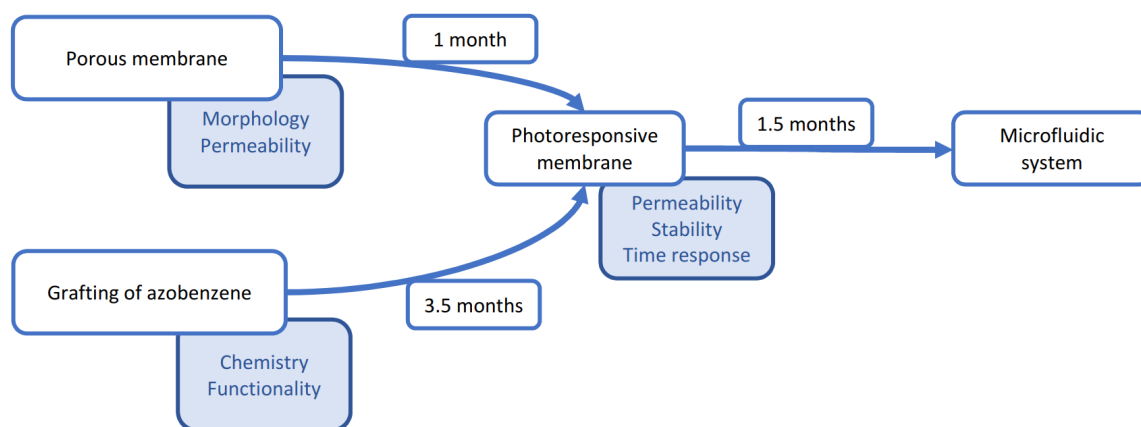

Figure 4.1: The process of the project including the estimated time.

Each milestone is to be fabricated, analyzed and characterized. First a porous PDMS membrane is fabricated and the morphology is characterized by visualization methods such as optical microscopy and scanning electron microscopy (SEM). In SEM the surface of a sample is irradiated with an electron beam in vacuum. Information about the topography is obtained from secondary or backscattered electrons. PDMS is not conductive, thus to prevent charging, samples must be coated with a thin layer of a noble metal. Imaging using SEM is, therefore, more time consuming than with optical microscopy.

Then azobenzene is covalently bonded on PDMS. Since this has not been reported before, a lot of time would be needed to alter and optimize the protocol. The modified membrane is compared to the pristine membrane in terms of chemistry and functionality. Surface changes are initially verified by water contact measurements, because PDMS modified with APTES and dextran should become more hydrophilic [32]. The presence of the grafted molecules and the formation of chemical bonds are confirmed by Raman spectroscopy and Fourier transform infrared spectroscopy (FTIR). Raman spectroscopy is prioritized, because it is readily accessible in the department, whereas FTIR measurements can only be arranged at a different department. Both are a type of vibrational spectroscopy used to identify molecular vibrations that are characteristic for the chemical composition. In Raman spectroscopy, incident photons can interact with the sample which causes a difference in energy between incident and scattered photons known as the Raman effect. The resulting shift in frequency can be measured to identify certain chemical bonds. The Raman effect relies on the polarizability which means that symmetric moieties with distributed electron clouds result in strong Raman bands [62]. In IR spectroscopy, if the vibration caused by incident light is able to change the dipole moment, energy will be absorbed. This resonance occurs at the natural frequency of the specific bond. Instead of using a monochromatic light as used in Raman spectroscopy, FTIR uses light containing many frequencies to measure the amount of absorbed, transmitted or reflected light. The light beam is slightly modified between each data point by making use of a Michelson interferometer. The resulting signal is a interferogram which is translated with Fourier transform to a spectrum. FTIR is able to detect asymmetric bonds such as O-H, making it a complementary to Raman spectroscopy for identifying chemical compositions.

Next, the switching functionality of grafted azobenzene has to be verified. The most popular method for this is UV-Vis spectroscopy [4, 71, 72, 93, 121, 122], which measures the absorption at different wavelengths in the UV-Vis spectrum. The trans and cis isomers will show distinctive absorption peaks at about 350 and 450 nm, respectively. There is no UV-Vis spectrophotometer in the department, so other methods are preferred. AFM can be used to measure the difference in height between the two isomers given that azobenzene is grafted on a flat surface of PDMS and that azobenzene layer is grafted uniformly and aligned perpendicular to the surface [31]. However, El Garah et al. performed this measurement on a wafer, whereas in this project the measurement is performed on a sticky surface of PDMS making AFM a high risk option. Raman spectroscopy has also been proven to identify different characteristic graphs of the two isomers on a flat substrate [55]. However, there is no UV laser available at a wavelength of around 350 nm in our department. A difference in the water contact angle should be measurable [26, 67, 99]. Nevertheless, visible light is required to image the contact angle making the measurement less accurate.

The permeability of a membrane is to be demonstrated in an application relevant setup. Ideally, membranes are tested on actual brains, however this would be inhumane. Therefore, a phantom material is to be used. 0.6% agarose gel is commonly used in brain infusion studies [17]. The gel is cheap and easy to fabricate. A benefit over an actual brain is that agarose gel is transparent. Diffusion of colored liquids can be followed real-time, whereas a brain must be sliced to determine the amount of diffusion. Only a few tests should be performed on the brain to determine whether agar is a reasonable substitute. Pristine PDMS membranes are to be compared to azobenzene-modified membranes.

For the proof of concept of localized drug delivery, there are a few parameters to be quantified. Long-term stability is determined by performing the characterization after 2 weeks and also a month later. Next, time response for switching between trans- and cis-isomers is measured. This value can be used to determine a dose and it can be evaluated how easy it is to achieve the desired dose consistently. Lastly, the membrane is tested on its temperature dependency. The membrane has to be functional at 37°C. After characterization of the photoresponsive membrane, the integration into a microfluidic system initiated.

4.3. Risks

The highest risk of this project is expected to be the grafting of azobenzene on PDMS. Other risks to be considered are the characterization of the functionality of the grafted membrane and its integration into a microfluidic device. Expectations of the potential problems and possible solutions will be described.

4.3.1. Grafting of azobenzene

The grafting of azobenzene on PDMS has a relatively high risk. First of all, there is no established protocol. This will required tweaking of many variables of such as treatment time, temperature, and chemical composition. The surface of PDMS can be activated with plasma or an oxidative solution. Even if silanization does not work out, there is still the option to graft azobenzene using LbL assembly.

Hydrogen bonds   Grafting density can be insufficient, when other hydrogen bonds are formed instead of the intended covalent bond. Examples of possible interactions between an alkoxysilane with an amino-group and a silicon oxide surface are illustrated in Figure 4.2. In example c,d, and e the grafting would seem successful, however the long-term stability of the graft will be significantly reduced due to the the weak hydrogen bonds. Hydrogen bonded silanes are easily washed away with water [7].
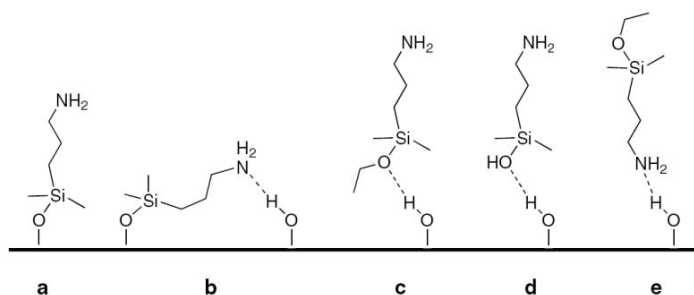

Figure 4.2: Examples of bonds and unintentional interactions between aminopropylethoxysilane and an oxidized silicon oxide substrate [7]

Steric hindrance   Grafting density can be too low for proper functionality. This can be caused by steric hindrance which mostly applies to grafting methods using larger molecules. Grafted molecule chains will obstruct incoming molecules from moving towards the substrate's surface. In grafting from this is less of a problem, since the molecules for grafting are relatively small [80].

Surface roughness   The surface roughness of native PDMS or PDMS that was in contact with the mold can influence the performance of the grafted azobenzene. On an uneven surface the grafted molecule chains will be aligned more chaotically instead of perpendicular to the surface. This will prevent incoming molecules from bonding to the surface. Additionally, the molecular motion of grafted azobenzene are more likely to be obstructed by neighbouring molecules. In the case that surface roughness should be decreased, a layer can be added between the substrate and the spacer to compensate for the roughness of PDMS [18]. On the other hand, it was found that an increased surface roughness can increase the difference in water contact angle between the two states of azobenzene [67].

4.3.2. Other risks

Porous membrane   A detailed protocol is available to fabricate a thin, porous PDMS membrane [49]. The pore dimensions might be a problem, because using this protocol the pore diameter will be in the micron range, and thus is still relatively large compared to the length change of 3.4 Å [72] between trans-cis isomerizations of azobenzene. The method can be adapted to produce smaller pores by an intermediate spacing layer or longer spacer molecule to attach the azobenzene. The easiest method to execute is to layer several membranes in which the pores are only slightly overlapping [129]. The effective pore size becomes smaller, but the membrane becomes thicker. Another approach is to increase the change in effective end-to-end distance between the trans-cis isomers [11]. This is not a simple adjustment, for it is required that the molecular extension is stiff and does not bunch up like a loose rope. There is also the possibility that the photochemistry is changed of the azobenzene molecules.

Characterization of the functionality   There is a risk in the characterization of the switching behavior. UV-Vis spectroscopy is not be available in the department. Other techniques can be used, but there is less material to compare the measurements with. In AFM measurements are made on a flat surface instead of in a pore [31]. Since the height difference caused by the isomerization between trans and cis is small (3.4 Å [72]) a high-resolution AFM must be used. This resolution is very difficult to achieve, because PDMS is a sticky, soft polymer which will contaminate the measuring tip. Raman spectroscopy might be able to measure in pores of a thin membrane, but it has only been done on a flat substrate before [55].

Integration membrane in microfluidic device   The integration in a microfludic device has some risk, since the azobenzene-grafted PDMS membrane might be difficult to adhere to pristine PDMS parts. The easiest method to try first is by placing uncured PDMS on the edges to be connected and cure the PDMS for a secure bond. Another way is to prevent grafting at the edges of the membrane. A sacrificial layer is probably the most straightforward solution. Before grafting the sacrificial layer is placed along the edges of the membrane. After grafting that layer can be removed revealing the PDMS surface underneath.

<div align="right">

5

</div>

Wettability-controlled permeability of porous PDMS membranes on agar and mouse brain

5.1. Abstract

Local drug administration is a critical feature of a drug delivery device in the brain. This feature can potentially be realized with an impermeable membrane that can be locally stimulated to become permeable. Porous PDMS membranes were fabricated by replica molding in a 3D-printed mold. The smallest pore diameter was 105±8 μm and the thinnest membrane thickness was 161±7 μm. The permeability of such a membrane is tested by a dye which must go through the membrane in order to observe staining in 0.6% agarose gel to simulate diffusion of brain tissue. No staining was detected using pristine PDMS membranes. However, a fast flow from hydrophobic to hydrophilic side was observed in a PDMS membrane recently plasma-treated on a single side. Furthermore, slow diffusion of the dye was present in a less hydrophilic, dextran-modfied membrane that received plasma treatment on one side as well. Thus, the permeability was controlled by the wettability of the membrane surface without modification of the entire inner pore. The same experiments were performed on a mouse brain to be compared to the results on agarose gel. The brain phantom is useful for further investigation of a local drug delivery device, but a few improvements are required to better correspond to the brain.

5.2. Introduction

Administration of drugs can help in the recovery of the brain for example after a stroke. There are many available delivery routes such as intravenous injection or local injection in the brain [104]. Whereas, the former encounters problems with systemic side effects, the latter requires multiple invasive brain surgery. Alternative methods such as drug-loaded hydrogel [23] or intranasal delivery [61] are being implemented as a compromise. Ideally, a brain implant, that can administer drugs locally with the added benefit of integrating electrodes for neural monitoring, could optimize the recovery. However, before such an implant can be fabricated, a drug delivery system must be designed. A crucial part of such system is a impermeable membrane which can locally become permeable by a remote stimulant.

Polydimethylsiloxane (PDMS) is a popular materials used in microfluidic applications and has been used before in flexible brain monitoring implants, called electrocorticograms (ECoG) [96]. The main advantages of PDMS for a brain implant is biocompatibility [6] and low Young's modulus to reduce mechanical strain on the brain [107]. For research purposes, this material is also great for prototyping, especially since molds can be 3D-printed. A thin, porous PDMS membrane can be fabricated spin coating uncured PDMS and imprinting with a mask with pillar structures as described by Huh et al. [49]. They achieved a pore size of 10 μm. An easier and faster method is replica molding, but membranes will be relatively thick and will have larger pores.

Stimuli-responsive materials have been of great interest in the last decade. Smart gating mechanisms can make use of environmental stimuli, such as temperature [90, 133] and pH [131], that react to changes in the environment. Light can be used to remotely and locally to activate a mechanism that is useful for controlled

drug delivery. In particular, azobenzene is well known for its photoisomerization from trans to cis isomer under the influence of UV-light and can be integrated in different ways to make a material photoresponsive. Since its trans isomer has a longer effective length than its cis isomer, azobenzene can grafted in mesoporous silica to change the pore size with UV and visible light [75]. However, the pore size of PDMS membranes will be much larger than in mesoporous silica making the effective size change of 3.4 Å redundant in a PDMS membrane made with the current fabrication methods [72]. Furthermore, when azobenzene is integrated in a hydrogel, the polymer network will expand and shrink [106]. The implementation of a hydrogel is relatively complicated, because it requires optimization of the chemical composition, and the layer thickness. Hydrogels and PDMS differ in mechanical properties, thus the adhesion is also an important consideration [16]. Moreover, azobenzene with a hydrophilic or hydrophobic end group grafted on a surface has the ability to switch its wettability [99]. Integrating azobenzene on the surface of PDMS membrane with microscale pores can potentially allow for light-controlled permeability for local drug delivery.

In this work, the fabrication of a porous PDMS membrane and its permeability on agar and mouse brains are presented. The membrane was fabricated by mold casting in a high-resolution 3D-printed mold. The limitations of the pore size and the membrane thickness were determined. The interaction and permeability of unmodified PDMS membranes were evaluated on agarose gel. Surface modifications were applied on the PDMS membranes to obtain different degrees of hydrophilicity and its effect on the permeability. An attempt was made to introduce azobenzene on a PDMS surface to obtain light induced switchable wettability. Lastly, preliminary tests are done ex vivo on mouse brains to evaluate the feasibility of PDMS membranes and to compare the results to the permeability experiments on agar.

5.3. Materials and method

5.3.1. Materials

The PDMS used was Sylgard 184 by Dow Corning. (3-Aminopropyl)triethoxysilane (APTES), dextran (M_r = 70,000), sodium (meta)periodate, sodium borohydride, N,N-dimethyl-4,4'-azodianiline (DMADA), potassium permanganate, agar, hydrochloric acid (36.5-38.0%), hydrogen peroxide solution (30%), and dimethyl sulfoxide (DMSO) are purchased at Sigma-Aldrich. Phosphate-buffered saline (PBS) solution (0.2 M, pH 8) is made by adding 47.35 mL of 0.2 M sodium phosphate dibasic and 2.65 mL of 0.2 M sodium phosphate monobasic dihydrate (Sigma-Aldrich). Deionized water was produced by PURELAB flex 3, Elga (18.2 mΩ cm).

5.3.2. Fabrication of porous PDMS membrane

Porous PDMS membranes are fabricated by means of replica molding. The mold was 3D-printed out of a material called HTM140 using EnvisionTEC, Micro Plus Hi-Res. The mold design is shown in Figure 5.1. It features a support on opposite ends to aid the removal of the PDMS from the mold. The pillars are one layer (25 µm) taller than the surrounding wall to ensure through pores. Much taller pillars are not recommended, because of strong capillary effects of PDMS and HTM140.

PDMS monomer and curing agent were mixed thoroughly in a 10 (monomer) to 1 (curing agent) ratio by hand for 5 minutes and poured into the mold. The excess PDMS is removed using a glass microscope slide. The PDMS is degassed in a desiccator for 30 minutes. A small amount of PDMS is added to the supports to fill the volume of the air bubbles. The membranes are cured in an oven at 80 °C for 2 hours. The membrane is removed by cutting along the sides of the mold using a scalpel. The membrane is lifted out of the mold using tweezers and droplets of ethanol to reduce the adhesion of the PDMS to the mold.

5.3.3. PDMS surface modification

A global overview of the surface modification process is illustrated in Figure 5.2. First, partially oxidized dextran was prepared by dissolving 0.333 g of dextran and 0.197 g of sodium periodate. The solution was mixed for at least 4 hours wrapped in aluminum foil at room temperature on a rocking platform. The solution was used within 24 hours kept in dark at all times.

Before the PDMS surface was oxidized, the sample was cleaned in ethanol for 5 minutes by sonication and air dried for at least 30 minutes. After the PDMS had dried, it was placed in the plasma cleaner (Diener Femto) for an air plasma treatment of 2 minutes at 40 W and 4 mbar. In the case of solution-based oxidation, PDMS was submerged in a beaker with $H_2O/HCl/H_2O_2$ in 5:1:1 volume ratio for 15 minutes on a rocking platform. The other tested oxidizing solution is known as piranha solution which is a mixture of H_2SO_4 and H_2O_2 in 3:1 volume ratio.

After the PDMS surface was oxidized, APTES could be bonded. A solution was prepared in ethanol con-
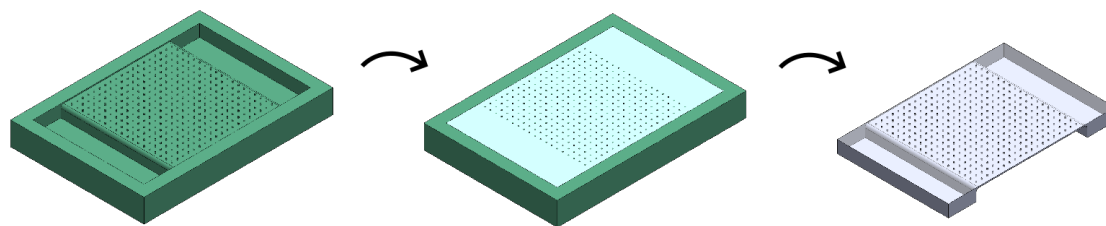
Figure 5.1: Replica molding of porous PDMS membranes. The mold was filled with uncured PDMS and the excess was removed with a microscope glass. After curing the membrane is lifted out of the mold at the supports.

taining 5% volume DI water and the pH was adjusted to 4.5-5.5 with acetic acid. Next, 5% volume APTES was added to mixture, which was left for 5 minutes to form silanols by hydrolysis of APTES. Oxidized PDMS was left in the mixture for 30 minutes on a rocking platform. Next, the sample was rinsed with several washes of ethanol, followed by DI water and dried in the oven at $110\,°C$ for 30 minutes.

The partially oxidized dextran solution was added to 0.2 M $NaHPO_4$ buffer at pH 8 in a 1:1 volume ratio. Amine-functionalized PDMS was submerged in the mixture for 18 hours on an orbital shaker at room temperature wrapped in aluminum foil. Next, the mixture was decanted and the modified PDMS was added to a solution of 0.1 M $NaBH_4$ for 2 hours at room temperature. The sample was rinsed with several washes of DI water.

For the grafting of azobenzene on dextran modified samples, dextran was first further oxidized in 0.1 M $NaIO_4$ for 4 hours wrapped in aluminum foil. N,N-dimethyl-4,4'-azodianiline (DMADA) was dissolved in DMSO to 0.1 M. The 3 or $30\,\mu L$ (samples denoted as Azo3 and Azo30) of dissolved DMADA was added 3 mL of PBS. The PDMS with oxidized dextran was exposed to the solution overnight on a rocking platform at room temperature. The Schiff bases were reduced with 0.1 M $NaBH_4$ for 2 hours again a moving platform at room temperature. Finally, the samples were rinsed and sonicated in DI water for 2 minutes.

5.3.4. Pore size
The porous PDMS membranes were characterized by their pore size which were acquired by SEM (Jeol, JSM-6010LA) using an acceleration voltage of 10 kV. PDMS membranes were made conductive by sputtering Au/Pd (2 min, 10 mA). The images were processed by image analysis in ImageJ. First, the image was converted to 8-bit and the threshold was manually adjusted to the best fit of the pore. Ferret and MinFeret, which are the maximum and minimum caliper values, were measured to find the average diameter.

5.3.5. Membrane thickness
Membrane thickness was determined white light interferometry (Bruker, ContourGT-K1) and data was processed using Vision64. The software features multiple-region analysis in which a top and bottom interface can be selected. The difference between these interfaces was calculated to find the average membrane thickness in that location. This procedure was repeated four times at different locations on a single membrane. The membrane thickness was obtained from a total of two membranes.

5.3.6. Water contact angle
The contact angle was measured using Krüss, DSA100 on a flat substrate. For every measurement $1\,\mu L$ of DI water was dispensed from which the static contact angle was extracted using the software called DSA provided by Krüss. For each sample at least 5 measurements were made at different locations. Samples were cleaned before the measurement with an air gun.

For water contact angle measurements with UV-light, visible light needs to be blocked. However, visible light is still needed for images after UV irradiation, thus a specific setup is used to ensure a quick measurement. The sample was put in position in a humidity box with its windows blocked with blackout plastic-coated cardboard. The light guide connected to Honle Bluepoint 4 Ecocure equipped with a 320-390 nm was secured in the hole of the drop dispenser. The aperture was set to 100% for an intensity of $14.000\,mW^2\,cm^{-1}$. The sample was set at a distance of about 1.5 cm from the end of the light guide.
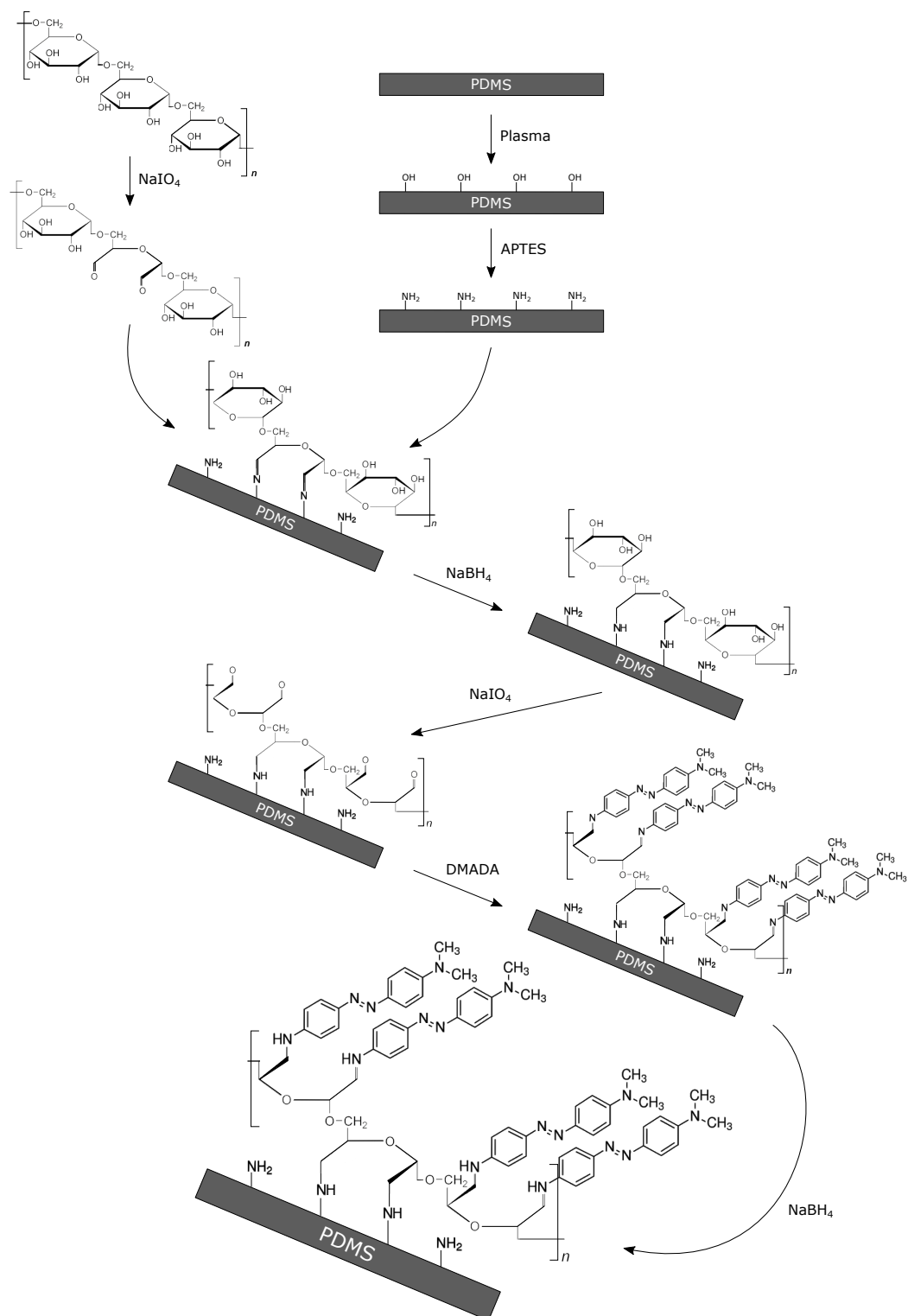
Figure 5.2: Schematic of the grafting procedure. Dextran is first partially oxidized by NaIO$_4$. Meanwhile, PDMS is oxidized to form OH-groups at the surface for bonding with APTES. Next, oxidized dextran is reacted with amine-functionalized PDMS to form Schiff bases which are then reduced with NaBH$_4$. Dextran is further oxidized for DMADA to be bonded.

5.3.7. Raman and FTIR

Raman spectra were obtained with Horiba Scientific Raman Spectroscope fitted with a tunable Argon-ion laser set to 514 nm. The CCD detector was cooled with liquid nitrogen. The software used to control the measurement parameters was LabSpec 6 (Horiba). Spectra were obtained from a range of 100 to 4000 cm^{-1}. Acquisition time was set to 5 seconds and data was accumulated over 5 measurements to remove spikes. A 50× objective was used and the ND filter was set to 25% to prevent damage from the high laser power. The laser was manually focused on the top surface.

FTIR spectra were measured using Nicolet 6700 FTIR Spectrometer (Thermo Scientific) fitted with a single-reflection accessory for attenuated total reflection (ATR) measurements. The software used to control the measurement parameters was OMNIC. A background scan was performed without a loaded sample and this spectrum was subtracted from all measured spectra with samples. A total of 128 scans were performed to reduce the noise. The crystal was cleaned with ethanol before each measurement.

5.3.8. Permeability on agar

0.6% agarose gel was prepared by adding 0.3 g of agar to 50 ml of DI water. This mixture was boiled for 2 minutes and cooked for another 5 minutes at low heat. The liquid agar mixture was transferred into a disposable Petri dish and was left to cool down. Displacement of the Petri dish before solidification is best to be prevented as this results in the flattest possible agar surface. When a gel was formed, the Petri dish could be moved for storage in a fridge at 4 °C.

The permeability was tested by putting a droplet of water-based dye on the membrane. For best contrast with imaging, 0.1 M potassium permanganate was used. The diffusion of dye into the agar was imaged by tilting the digital microscope (Keyence VHX-6000) to a 90° angle. Ring light mode was selected for the most accurate color representation. Membranes were rinsed with DI water and dried with a cleanroom cloth between measurements.

The images were transformed from RGB to HSV. Saturation was found to contain the most information on the color change in agar. The saturation values of the images were extracted over several lines that start at the pore opening at the agar side and going radially outward. These saturation values were averaged for each distance from the pore which could then be used to create a saturation profile graph. The saturation values were normalized by the agar as zero. The maximum value was set to the average of a line near the top interface of the agar after a droplet of dye placed directly onto agar.

5.3.9. Permeability on ex vivo brain

A mouse brain was extracted using the protocol as described by Gage et al. [35] without fixating the brain pumping with paraformaldehyde by perfusion. After extraction the brain's position was fixed in place at the bottom of a Petri dish with a 2-3 mm thick layer of 0.6% agarose gel which was prepared similarly as described above, but DI water was substituted with PBS. After the agarose gel had solidified, the membrane was placed on the brain by placing one side of the membrane on the agar before the rest of the membrane to prevent air bubbles. The membrane was pushed in place carefully by pressing it down with tweezers around the perimeter of the brain. One droplet of 2 μL dye was pipetted on each hemisphere. An example of the setup can be seen in Figure 5.12a. After 10 minutes the membrane and the remaining droplet was removed. The brain was placed in fixation solution for 5 days before slicing.

Image analysis was performed using ImageJ. The image was changed to 8-bit and the threshold is manually adjusted to the size of the stained area to select the area for measurements. The build-in analysis option was used to measure the mean gray value and Feret's diameter. MinFeret is equal to the smallest caliper value which is the distance from the point at the brain interface where the pore is located to the edge of the stain perpendicular to the former point.

5.4. Results and discussion

5.4.1. Characterization of porous PDMS membrane

Membranes will be referred to by their respective mold's CAD model measurements. Their names are abbreviated to dXXXhXXX where 'd' is the diameter of the modeled pillar, 'h' is the modeled height of the membrane, and XXX is the respective value in microns.

The geometry of the porous PDMS membrane was determined by the limitations in the mechanical strength of PDMS, and the 3D-printed mold. For replica molding, the thinnest membrane that could be removed from the mold without breaking was a modeled height of 200 μm. This could only be achieved by
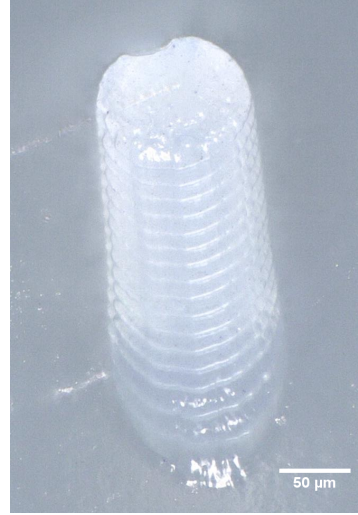
Figure 5.3: Side view of a pillar d200h200. Tilt: 30° (Keyence VHX-6000: full coaxial light)

Table 5.1: Comparison of the bottom and top diameters (d_{bot}, d_{top}) of the pillar and the membrane for a constant modeled diameter of 200 μm where d_{CAD} is the diameter of the CAD model, and $d_\mu = \frac{d_{bot}+d_{top}}{2}$ in μm

| h_{CAD} | Mold | | | Membrane | | | |
	d_{bot}	d_{top}	$d_{\mu 1}$	d_{bot}	d_{top}	$d_{\mu 2}$	$d_{\mu 2}/d_{\mu 1}$
200	133 ± 4	123 ± 3	128	105 ± 8	106 ± 7	105	82%
300	127 ± 3	115 ± 6	121	119 ± 11	98 ± 13	109	90%
400	137 ± 8	124 ± 6	130	117 ± 10	105 ± 5	111	85%
500	136 ± 6	125 ± 6	130	105 ± 8	100 ± 8	102	79%

adding features in the design of the mold to aid the removal of the membrane from the mold. Supports were implemented at opposite sides of the membrane to lift off one side instead of one corner to decrease the chance of breaking. Furthermore, the edges of the plateau were rounded to smoothen the transition between the support and the membrane. The smallest pillar diameters that could be reliably fabricated was 200 μm with a height of 200 μm. The 3D-printer could print layers about 25 μm thick. These layers resulted in defined lines that gave the pillars their ribbed structure as seen in Figure 5.3. Towards the top of the pillar the layers become slightly smaller in diameter than the layers closer to the base.

The diameters of the pillars were measured at the top and at the base for different heights and are summarized in Table 5.1. The deviation between top and bottom diameter was about 10%. This difference was more or less equal as the height of the pillar increases. The resulting pores in PDMS were 10-20% smaller in diameter than those of the pillars with a relatively large variation. From a study by Madsen et al. [78], it was found that PDMS has a shrinkage of about 2% at a curing temperature of 80 °C for 2 hours for structures of 3 and 10 μm wide. They used a chromium and platinum coating for the mold, while this study uses HTM140 cleaned in ethanol. The use of different materials for PDMS molding is likely the main reason for the different amount of shrinkage. Another cause can be the method of curing which in the case of Madsen et al. was by hot plate, while the membranes were cured in a oven. The mold is heated first, when a hot plate is used, thereby curing the PDMS adjacent to the mold faster. This effect is encouraged by the difference in material properties. Even though, the heat conductivity of HTM140 is not officially stated by the distributor, the mica mold used by Madsen's group is likely a better heat conductor than HTM140 which is a resin. The fact that the pores shrink more using 3D-printed molds is actually an advantage for the fabrication of smaller pores, since this is limited by smallest printable pillar size. The only difficulty would be to take shrinkage into account for a particular pore size.

Similarly, the diameter of the pillars were varied and measured for the mold and the membrane listed in Table 5.2. The pillars that were modeled to be 200 μm in diameter were printed considerably smaller by 36%. As the modeled diameter increased, the difference between the modeled and printed diameter decreased. Furthermore, the amount of shrinkage in the pore size decreased as the diameter of the mold is increased.

Table 5.2: Comparison of the bottom and top diameters (d_{bot}, d_{top}) of the pillar and the membrane for a constant modeled height of 200 µm where d_{CAD} is the diameter of the CAD model, and $d_\mu = \frac{d_{bot}+d_{top}}{2}$ in µm

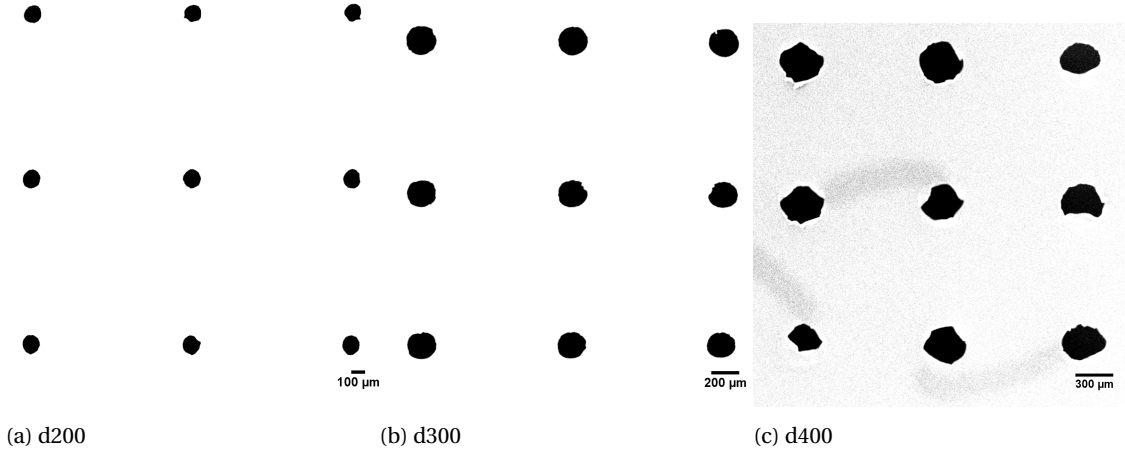|	Mold				Membrane			
d_{CAD}	d_{bot}	d_{top}	$d_{\mu 1}$	$d_{\mu 1}/d_{CAD}$	d_{bot}	d_{top}	$d_{\mu 2}$	$d_{\mu 2}/d_{\mu 1}$
200	133 ± 4	123 ± 3	128	64%	105 ± 8	106 ± 7	105	82%
300	243 ± 16	212 ± 7	227	76%	217 ± 10	203 ± 16	210	92%
400	337 ± 5	320 ± 6	329	82%	320 ± 12	321 ± 41	320	97%

(a) d200   (b) d300   (c) d400

Figure 5.4: SEM images of the top side of the membrane

Notably, the deviation of the diameter at the top side of the membrane increased as the diameter increased. The shape became less circular for larger pores as seen in Figure 5.4. The surface on top of the pillar was increased making PDMS remains more likely.

Lastly, the modeled height is compared to the membrane thickness in Table 5.3. The height of the mold was only about 5% smaller than the modeled height and was relatively constant as the height was increased. Moreover, the membrane thickness became very close to the height from the mold as the height was increased. The standard deviation of the membrane thickness was also much smaller than with the diameter of the pores. Thus, membrane thickness was better reproducible than the pore diameter. These findings are useful, when optimizing the performance of a permeability switching membrane by the two of the main parameters pore size and membrane thickness.

The amount of through-holes varied per batch. This was mainly due to molds being slightly tilted during the fabrication. Transporting the PDMS-filled mold from the desiccator to the oven could result in unevenness in the membrane, especially at higher temperatures. Moreover, the mold itself is not completely flat. After curing the mold with UV-light, some bending was visible at the corners of the mold. The design could be made smaller, but this would decrease throughput. Further optimizations are possible by adjusting the thicknesses of the base plate and walls, however these were not further explored within this research. Molds fabricated by SU-8 using photolithography on silicon wafers are flat by default. This feature and the availabiltiy of larger wafers, makes this mold fabrication method feasible for upscaled production of these mem-

Table 5.3: Comparison of the printed height of the mold to the thickness of the PDMS membrane where the modeled CAD height is h_{CAD}, mold height is h_{mold}, and membrane thickness is t in µm.

h_{CAD}	h_{mold}	h_{mold}/h_{CAD}	t	h_{mold}/t
200	188 ± 4	94%	161 ± 7	85%
300	291 ± 3	97%	268 ± 8	92%
400	384 ± 5	96%	353 ± 9	92%
500	484 ± 3	97%	480 ± 5	99%

Table 5.4: Comparison of the water contact angle for different oxidation treatments on PDMS

Sample	Water contact angle
Air plasma	<10°
H_2O/HCl/H_2O_2 5 min	108±3°
H_2O/HCl/H_2O_2 10 min	100±3°
H_2O/HCl/H_2O_2 30 min	108±4°
Piranha 45 sec	99±1°
Piranha 5 min	84±5°
Piranha 10 min	76±3°

branes. Furthermore, after the mold was used, some PDMS remains on the pillar, especially for larger pores. When the mold was reused, uncured PDMS would bond to the PDMS remains resulting in a thicker layer that would stay intact after the membrane was removed from the mold and close off the pore. This was partially remedied by scraping a glass microscope slide over the PDMS membrane before removing it from the mold. This was however not possible for pillars with aspect ratio larger than (height/diameter=1), because the pillars would easily break.

5.4.2. Water contact angle
The water contact angle is one of the important parameters that determines the capillary rise in microchannels or, this case, pores in a membrane. A hydrophilic surface will have a positive capillary height, whereas this value is negative for hydrophobic surfaces. Pristine PDMS is known to be hydrophobic with a water contact angle of 107± 2°. Plasma treatment is a fast and effective method to form OH-groups at the surface. Water will form hydrogen bonds with these group, so as a result PDMS becomes hydrophilic. In the case of a membrane, the plasma cannot reach inside relatively narrow pores. It was therefore attempted to make PDMS hydrophilic using solution-based oxidation methods. The water contact angle was measured within 30 minutes after each treatment and summarized in Table 5.4. The plasma treatment was considerably more effective than its solution-based counterparts in generating a hydrophilic surface. Even though, the HCl/H_2O_2 solution had been used as oxidation step in other protocols before [49], the surface did not become hydrophilic. This could indicate that there was no formation of hydroxyl groups at the surface, but there was the possibility that the amount of formed hydroxyl groups was too low to affect the water contact angle as also observed by Hoek et al. using another oxidation solution 1 M NaOH for 24h [48]. Piranha solution was able to make the surface hydrophilic, however the PDMS surface was severely damaged by the solution's etching properties for treatments longer than 5 minutes. The lowered contact angle was partially the result of the increased surface roughness, and therefore, was not a true representation for the formation of hydroxyl groups. Plasma treatment was the most effective for a flat surface, however in a PDMS membrane plasma would not effectively oxidize the inside of the pores. A flow-through process using an oxidizing solution would be needed to modify the inner pores in a PDMS membrane.

PDMS was oxidized by either air plasma or a mixture of HCl/H_2O_2 and was subsequently modified with APTES, dextran and azobenzene. The water contact angle was measured for each step and listed in Table 5.5. All plasma-treated samples were more hydrophilic than samples oxidized by HCl/H_2O_2. This was to be expected, since air plasma generates a more hydrophilic surface than the other oxidation solutions. Plasma-treated PDMS surfaces returned to their hydrophobic characteristic within a day, but since the grafting procedure was in aqueous solution the induced hydrophilic property was better retained. The contact angle for PDMS-APTES in HCl/H_2O_2 was close to the value of pristine PDMS. A more hydrophilic surface was expected for the modification with APTES, since primary amine groups are able to form hydrogen bonds. This suggests that either the APTES was not silanized to the PDMS surface or that the grafting density was insufficient to decrease the contact angle. Farrell et al. also found a hydrophobic contact angle slightly smaller than pristine PDMS [32]. A decrease in the contact angle was observed after dextran was grafted with both oxidation methods. This confirms the presence of dextran on the surface, since it is a hydrophilic substance. The contact angle was increased after grafting of azobenzene. This shows that the surface was changed and could be an indication for the presence of azobenzene which is hydrophobic due to its methyl end groups.

The contact angle of PDMS-APTES-dextran with plasma treatment was measured over a period of time stored in air as seen in Figure 5.5. Since the PDMS substrate was only plasma-treated on one side only, the contact angle was also measured of the non-plasma side. The contact angle of the dextran-functionalized

Table 5.5: Water contact angle measurements 1 hour after each grafting step using air plasma or HCl/H$_2$O$_2$

Oxidation	Sample	Water contact angle
	Pristine PDMS	107±2°
Air plasma	PDMS-APTES	87±5°
	PDMS-APTES-dextran	62±4°
	PDMS-APTES-dextran-azobenzene	82±2°
HCl/H$_2$O$_2$	PDMS-APTES	105±2°
	PDMS-APTES-dextran	80±4°
	PDMS-APTES-dextran-azobenzene	107±2°

PDMS surface was observed to be increasing to a value of pristine PDMS after only four days storage in air. This was in contrast with the results found by Farrell et al. [32]. They measured a water contact angle of about 80° after two weeks. These contradictory results suggested that the grafting of dextran on PDMS was unreliable as minor changes in the method resulted in major different results. Furthermore, the rate of hydrophobic recovery in air was slower than plasma-treated PDMS without further surface modifications. The standard deviation was too large to find a trend for the side that was not treated with plasma. Notably, the value of the standard deviation was decreasing over time suggesting that some dextran adhered to the PDMS surface without covalently bonding with APTES generating small, more hydrophilic patches. Between measurements, samples were blow-dried with an air gun which slowly removed adhered dextran making the PDMS surface more uniform, and thus decrease the deviation. A reason for the non-covalent bonding of dextran might be formaldehyde which is a reaction product formed for each oxidized dextran unit. The aldehyde in formaldehyde can form a Schiff base instead of the aldehyde in dextran. However, dextran should have a larger influence the surface wettability than formaldehyde, since dextran is much larger in size than formaldehyde. Another reason might be the use of sodium borohydride instead of sodium cyanoborohydride. Both chemicals should be able to reduce Schiff bases, however sodium cyanoborohydride is more effective [45]. All in all, the method for grafting dextran to PDMS is not recommended for implant applications based on the long-term stability indicated by the hydrophobic recovery.
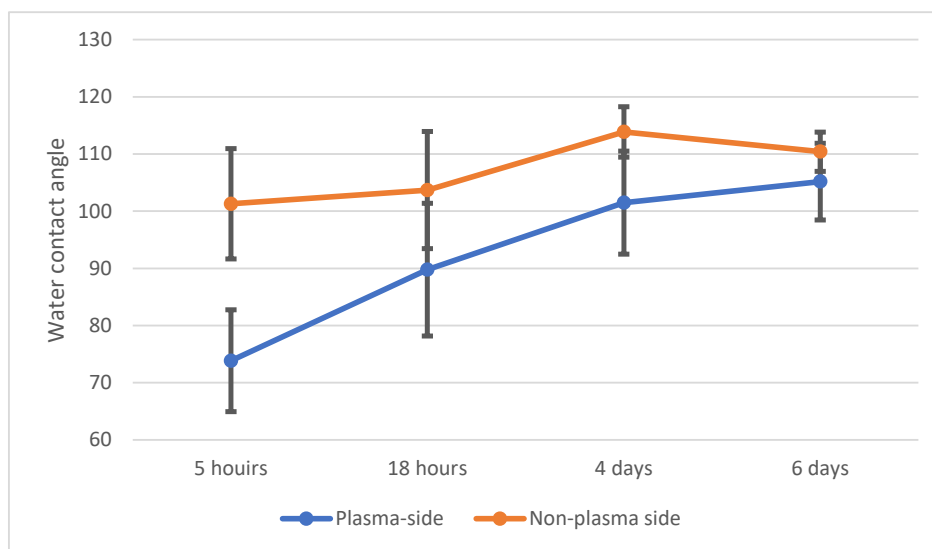

Figure 5.5: Evolution of the water contact angle on PDMS-APTES-dextran oxidized by plasma treatment on one side, stored in air.

Even though, hydrophobic recovery was found in dextran-grafted PDMS samples, azobenzene was still present on the surface as indicated by the orange color of the modified PDMS and water contact angle compared to the sample before contact with DMADA. The sample with azobenzene was irradiated with UV-light for 30 minutes after which immediately the water contact angle was measured and compiled in Table 5.6. There was no significant change in the contact angle after exposure to UV-light. If azobenzene were to tran-

Table 5.6: Water contact angle measurements before and after 30 minutes of UV irradiation

	Visible light	After UV-light
Azo3	113±2°	112±3°
Azo30	109±3°	110±1°

sition from its trans to cis isomer, the surface was expected to become more hydrophilic, since the methyl groups would move to the toward the surface instead of facing outward. However, since the hydrophilic nature of dextran disappeared over time adhered azobenzene would not have the correct orientation, which is perpendicular to the surface, or azobenzene was absorbed rather than adsorbed in the PDMS. Moreover, UV treatment is a known method to oxidize PDMS, but this is usually done using shorter wavelengths at around 200 nm and is combined with ozone for increased oxidation [30]. The range of the filter used was 320-390 nm and no ozone was applied, so oxidation effects on PDMS should be minimal. These results verified that this grafting method was not effective in achieving light-switchable wettability on PDMS.

5.4.3. Raman and FTIR

The surface chemical composition of the modified PDMS samples with APTES, dextran, and azobenzene were verified using Raman and FTIR. Raman spectra are obtained from flat PDMS substrates modified with APTES and dextran using both air plasma and HCl/H_2O_2 solution and shown in Figure 5.6. Small peaks were observed in the 3580-3700 cm^{-1} region. One of these peaks could be associated with amine-groups. Furthermore, a sharp peak was found at 1124 cm^{-1} which was characteristic for in-phase stretch in alkoxysilanes (Si-O-R) [62]. A peak couple was observed at 2104 and 2167 cm^{-1} and there was a distinct peak at 3080 cm^{-1} in the samples oxidized by air plasma. These peaks were however not associated with the spectrum of pure APTES [13], so the peaks were related to other molecular bonds of reacted APTES that was not the covalent Si-O-Si bond which is also present in pristine PDMS. The peak at 2167 cm^{-1} could be Si-H stretching [15]. Fluorescence background was slightly increased with both APTES and dextran modified PDMS compared to pristine PDMS. No new peaks were observed after grafting of dextran. There were a few differences between the spectra of samples oxidized by air plasma and the solution-based method. The intensity of peaks 1124, 2104 and 2167 cm^{-1} were much higher in plasma-treated samples than with the oxidation solution. Peaks at 3080 and 3580 cm^{-1} were only present in samples treated with plasma and not visible at all in samples oxidized in solution. This indicates that there was more APTES present on plasma-treated than on oxidative solution-treated samples.

The ATR-FTIR spectra were obtained using the same samples as with the Raman spectroscopy and are displayed in Figure 5.7. The presence of APTES on the PDMS surface was verified by the characteristic peaks of primary amines of which a weak broadband was visible at 3200-3460 cm^{-1} and a peak at 1655 cm^{-1} was found representing the in-plane deformation of primary amines [33]. Contrastingly, a more distinctive peak at 1655 cm^{-1} was observed with the sample modified by solution-based oxidation, whereas the band in 3200-3460 cm^{-1} region was stronger with the plasma-treated sample. The absence of the peak at 1655 cm^{-1} in samples with dextran indicated the lack of primary amines, and likely the formation of secondary amines. Dextran was characterized by its OH-groups and C-O-C bonds. A moderate peak was found at 3550 cm^{-1} which could be associated with O-H stretching vibrations. C-O-C stretching might overlap with Si related vibrations from the PDMS, but no new strong peaks were found in the region of 1050-1250 cm^{-1}. Aldehydes (C=O) were formed in dextran due to oxidation, but should have reacted to bond to amine-groups. The presence of aldehydes should give a peak at around 1650-1700 and 2730 cm^{-1} [62]. However, no significant peaks were found in these regions. So, there was no or only a very small amount of aldehydes after the functionalization protocol and storage in air for a few days.

The Raman spectra were measured of azobenzene bonded to dextran-modified PDMS samples and are displayed in Figure 5.8. The following findings were similar for both samples oxidized by plasma and $H_2O/HCl/H_2O_2$ solution. Azobenzene caused fluorescence background which increased with the amount azobenzene added in the grafting solution. This problem could have masked some interesting peaks. However, a small peak could still be detected at 1145 cm^{-1} which was assigned to symmetric stretching of C-N [116]. Another peak was found at about 1450 cm^{-1} which could be assigned to Azo N=N stretching known for its strong intensity in Raman occurring between 1400-1580 cm^{-1} [62]. Thus, the presence of the azobenzene molecule on PDMS was chemically verified. ATR-FTIR did not provide further information cause the covalent bond formed between the amine-containing azobenzene and oxidized dextran was the same as the bond formed between
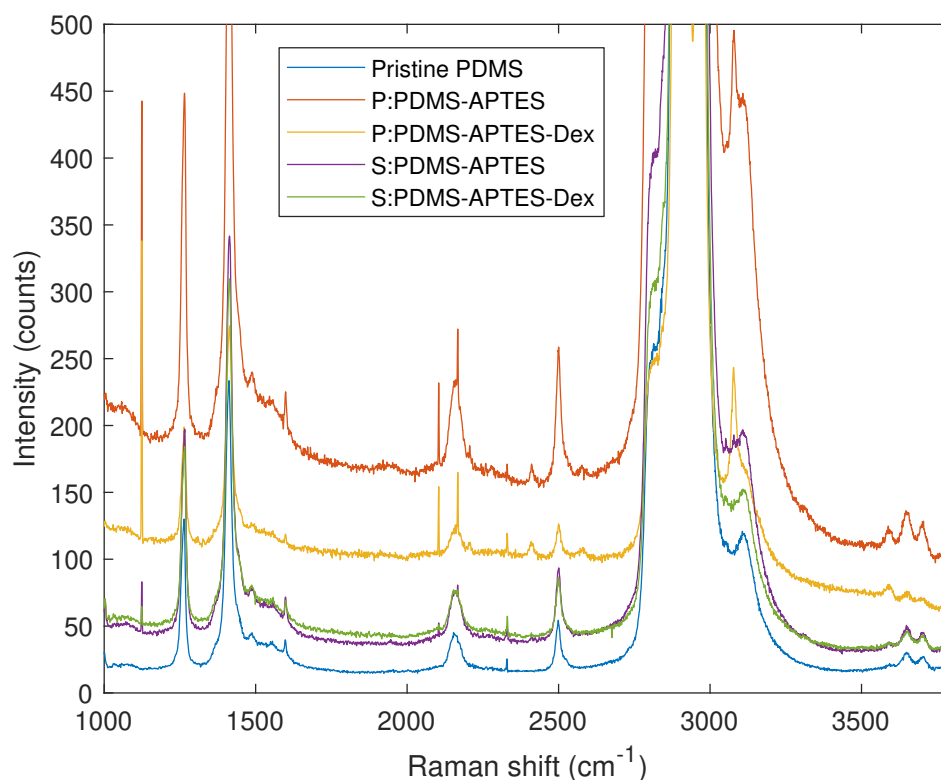
Figure 5.6: Raman spectra of pristine PDMS compared with APTES and dextran (Dex) modified PDMS by air plasma (P) and HCl/H$_2$O$_2$ solution (S)

APTES and oxidized dextran. When combined with the findings from the water contact angle measurement after UV irradiation, these result suggested that the grafting density of azobenzene was insufficient which could be expected from the hydrophobic recovery of PDMS grafted with dextran. The PDMS did experience an overall change in color from translucent to yellow-orange. Azobenzene was likely absorbed in the PDMS, because it is not soluble in water. This was partially prevented by using DMSO instead of ethanol as the solvent [64].

5.4.4. Permeability on agar

Real-time permeability measurements have been done before in a two-channel microfluidic system by fluorescent detection [134]. However, this method would be unsuitable for testing local permeability as required for a drug delivery device. Agarose gel (0.6%) has been used as a diffusion medium to substitute brain tissue [17]. A membrane can be placed on top of the agar interface, similarly as a drug delivery implant would be placed on the brain. When a vibrant dye is dispensed on the membrane, the agar is stained where the dye goes through the pore. The gel is reasonably transparent allowing for real-time measurements. The first series of membranes to be tested on agar were pristine, porous PDMS membranes. A dye was dispensed on membrane placed on agar, but no discoloration could be perceived in the agar after 24 hours in membranes d200h200 and d400h200. When viewed from the side, the water-based dye in the pore did not touch the inner pore wall and does not connect to the agar side without the help of applied pressure as seen in Figure 5.9. A solution of food dye in DMSO showed that polar solvent touched the pore wall. Potentially, hydrophilic inner pores in PDMS membranes should be permeable for water-based liquids. However, from the water contact angle measurements it was found that solution-based oxidation did not result in a hydrophilic surface without damaging the surface.

The experiment on agar with a PDMS membrane oxidized on one side only with air plasma resulted in the dye flowing instantaneously through the membrane (d200h200) and spreading between the PDMS membrane and agar interface before diffusing into the agar itself in the case, when the hydrophilic side was facing the agar. When the membrane was reversed, the dye would only spread over the hydrophilic surface without going through the membrane. This showed that the wettability of the surface could play an important role
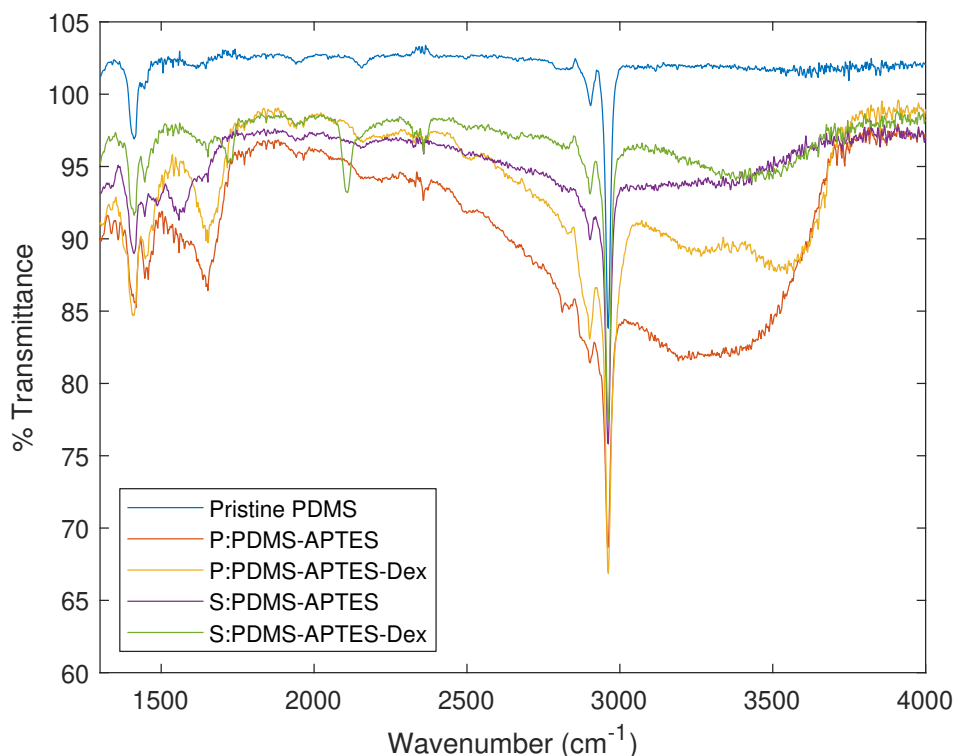
Figure 5.7: ATR-FTIR spectra of pristine PDMS compared with APTES and dextran (Dex) modified PDMS by air plasma (P) and HCl/H_2O_2 solution (S).

in the permeability of a membrane without the need of altering the inner pore surface, since plasma cannot reach far inside a pore at this aspect ratio. The thickness of the membrane was the largest limiting factor, because increasing the thickness to 300 μm did not induce a flow through the pores.

To find the effect of a slightly more hydrophilic surface than pristine PDMS, dextran was grafted onto the porous PDMS membranes. While the dye would go immediately to through the membrane, in the case with the dextran-modified membranes dye slowly stained the agar without spreading between the membrane and agar interface. Since the measured water contact angle of dextran-modified PDMS was much higher than recently plasma-oxidized PDMS, this showed that the permeability of the membrane could be controlled with the wettability. This gave defined diffusion patterns that were complementary to the pore spacing as seen in Figure 5.10. Agar was decently translucent, thus the diffusion in agar was examined over time at the cost of some accuracy in color intensity of the dye, even though the membrane was placed as closely to the edge closest to the microscope. Furthermore, the agar interface at the rim of a Petri dish was not flat, so the diffusion was not truly perpendicular to the plane of the membrane.

A series of measurements was performed one day after the procedure for dextran-modified PDMS membranes d200-d400h200, while stored in air. For membranes d200h200, the staining was very minimal and the contrast was too low for image analysis. Increasing the pore size to membrane d300h200, increased the amount of visible staining in agar. The diffusion of dye in agar was quantified by image analysis and its saturation values were determined for the distance from a pore shown in Figure 5.11. No staining was found, when the more hydrophobic side was facing the agar for d300h200. The results of this membrane would be most suited for local drug delivery, because the staining of the dye was pore controlled. This validated that the rate of the flow is controllable by the wettability for this geometry. An additional 100 μm in pore size resulted in fast spreading of dye between the membrane and agar interface similar to the recently plasma-treated membranes with the hydrophilic side facing the agar. However, when the membrane was flipped, the staining in agar was similar to membrane d300h200 with its hydrophilic side on agar. Thus, the diameter should be modeled smaller than 400 μm in a 200 μm-thick membrane to be able to control the permeability by the wettability.

The same series of experiments were performed on the dextran-modified membranes d200-d400h200 after being stored for one week in air. The water contact angle of dextran-modified flat PDMS slabs returned
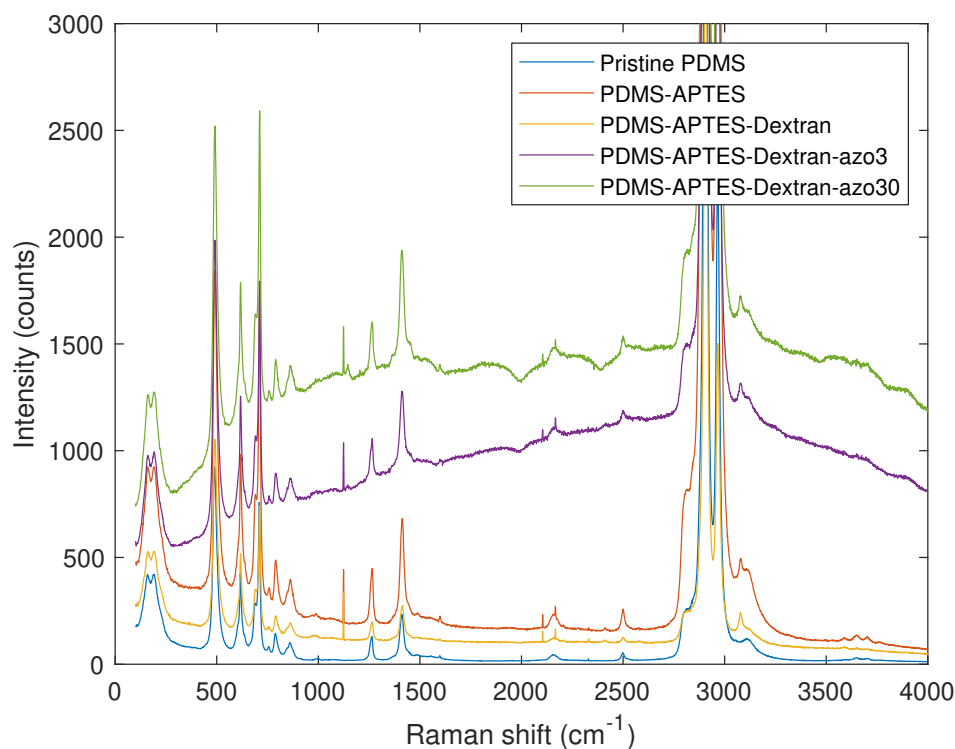
Figure 5.8: Raman spectra of azobenzene-grafted samples using air plasma to oxidize surface.
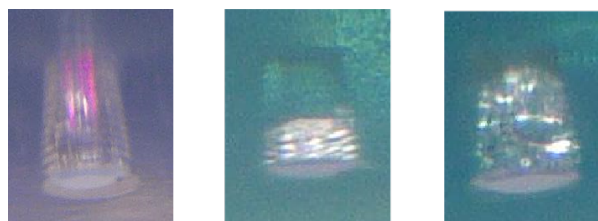

Figure 5.9: Side view of pristine PDMS membrane on agar. A droplet is pipetted on top with a solution of concentrated KMnO$_4$ in DI water (left) and blue food dye in DMSO (middle, right). Magnification: 150×. Tilt:90° (Keyence VHX-6000: ring light)

to the value of pristine PDMS over time. Membrane d200h200 did not have any staining on the agar no matter which side was facing the agar, however d300h200 did have very little staining, but not enough for proper image analysis. Increasing the pore size further to 400 µm did have a medium amount of staining independent of which side was on the agar similar to d300h200 with dextran after one day. This showed that the dextran surface after one week was still different than pristine PDMS, even though this result was not supported by the increased water contact angle of dextran-modified PDMS. A small amount of dextran could still be present inside the pore rather than the membrane surface, since the ridges of the 3D-printed layers can trap particles. This would explain why there was no difference in permeability when the membrane was flipped.

The experiments on agar showed that wettability could control the permeability in a porous PDMS membrane. Above all, the inner pore was not required to be modified using a flow-through process for solution-based oxidation and the grafting of dextran. Plasma treatment of a single side of the PDMS membrane (d200h200) was sufficient to induce fast flow from hydrophobic to hydrophilic side given that the membrane was not too thick. Whereas, pristine PDMS membranes did not stain the agarose gel at all. The rate of flow was also influenced by the degree of hydrophilicity as demonstrated by dextran-modified PDMS membranes on agar. On the one hand, the liquid at the hydrophobic side could be attracted to the hydrophilic side causing it to go through the pore. This seemed more the case with recently plasma-treated membranes, since the dispensed droplet disappeared to the hydrophilic side of the membrane. On the other hand, capillary rise of the water from the agar may have occurred in the pore. When water from the agar connects with the liquid from

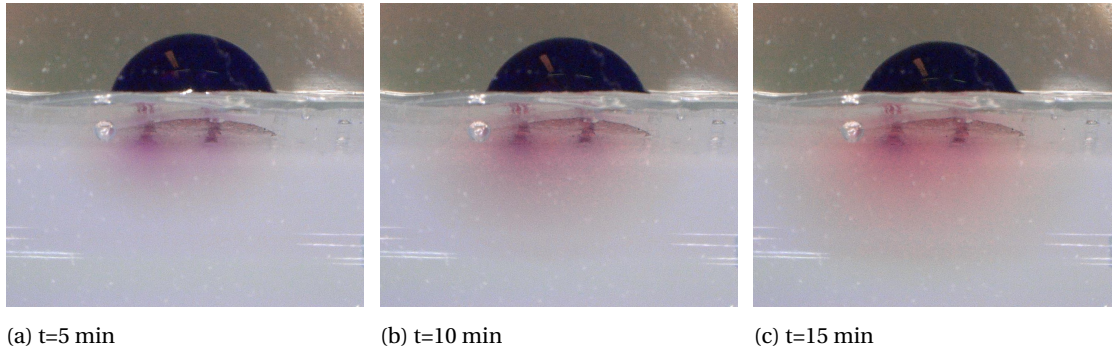(a) t=5 min   (b) t=10 min   (c) t=15 min

Figure 5.10: Time series of diffusion through PDMS membrane d300h200 functionalized with APTES and dextran. Tilt:90° (Keyence VHX-6000: ring light)
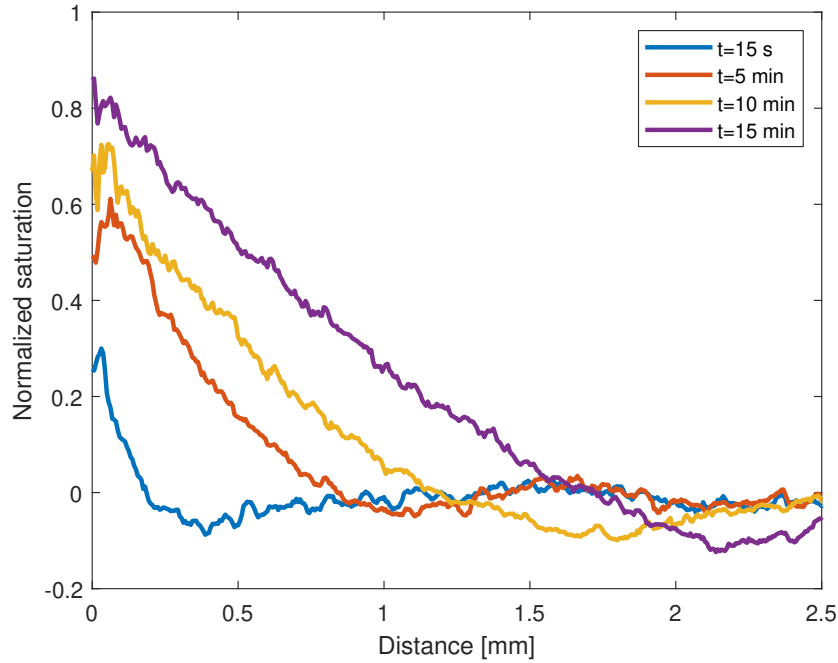

Figure 5.11: Normalized saturation values for a distance from the pore of a PDMS membrane d300h200 diffusion in agar, hydrophilic side facing agar, stored in air for 1 day.

the hydrophobic side, particles may diffuse to the agarose gel. This effect was more prominent with dextran-modified membranes. After 15 minutes, the dispensed droplet was still on the membrane, even though there was some staining of the agar. Introducing switchable wettability to the membrane would have been interesting to test whether permeability can be actively controlled. However, the water contact angle did not change after UV irradiation of a azobenzene-modified PDMS substrate, so azobenzene-modified membranes were not tested.

5.4.5. Permeability on ex vivo brain
The permeability of porous PDMS membranes is validated on ex vivo mouse brains similarly to the setup on agar for comparison. The setup of the experiment is displayed in Figure 5.12a. The initial impression was that the membrane adheres for the largest part to the relatively flat cortex surface of the mouse brain. The membrane did not fold into corner that the brain makes with the agar. This was especially visible at the side of the brain stem where the membrane was detached from the brain even after pushing it down.

Due to the limited amount of available brains, membranes d300h200 in the variations pristine, plasma-treated which were stored in water for one day, and PDMS-APTES-dextran which were stored in water for one day, were selected. Membranes were dried, before the dye was dispensed on top. After the membrane was removed from the brain, staining was clearly visible. There were dark brown marks present for each

(a) Experimental setup

(b) Brain with staining after removal of remaining dye and membrane

(c) Cross-sectional view of light staining

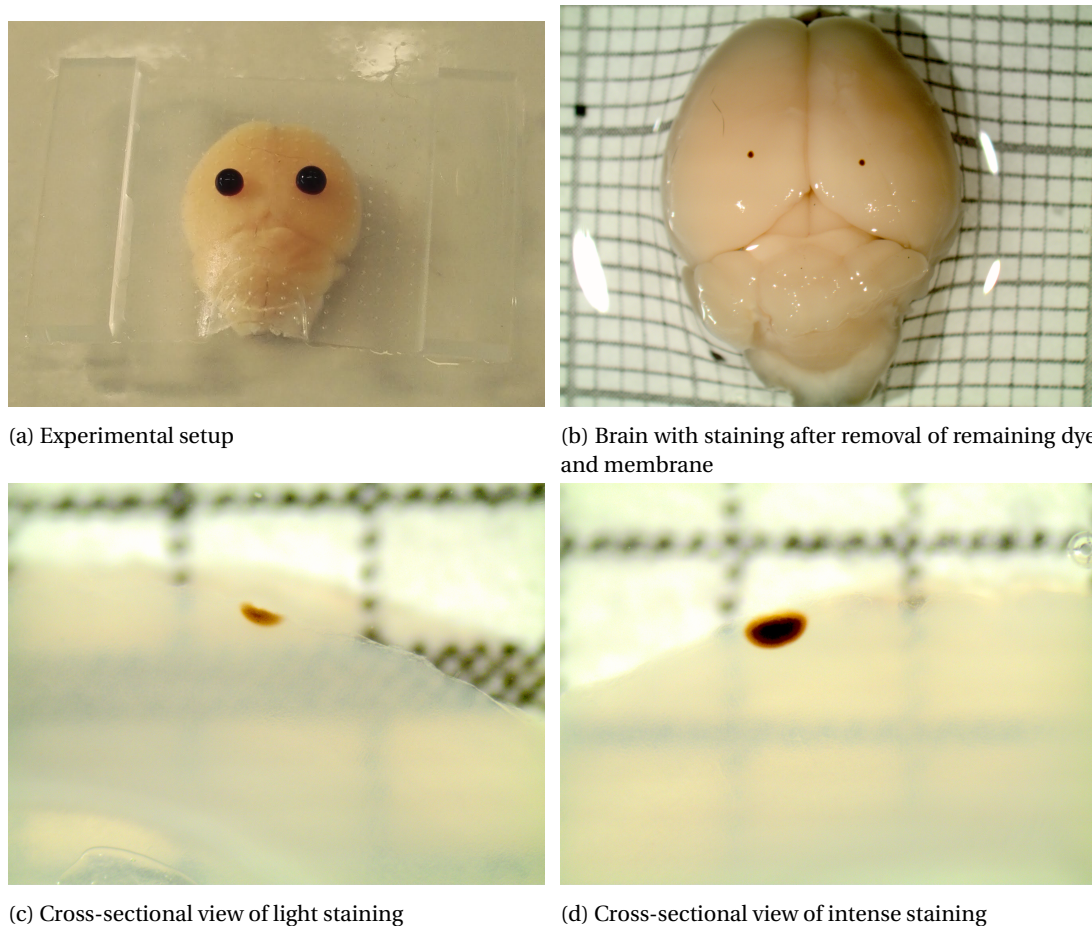(d) Cross-sectional view of intense staining

Figure 5.12: Images of the experiments with porous PDMS membranes on mouse brains

membrane including the pristine PDMS membrane which did not show staining in the experiment on agar. When the membrane modified with dextran was used, one side did not have any mark and the other side had two marks about 1 mm apart equal to the space between two pores.

Images were taken after slicing of the brain at the staining mark as seen in Figure 5.12. From these images the amount of diffusion can be quantified by image analysis in ImageJ. The browned dye and the slicing helped in defining the diffusion distance, which was less distinct in agar. Moreover, from the stained area the mean gray values were determined. These results are put in perspective in graphs in Figure 5.13. Diffusion distance with both modified PDMS membranes was larger than with pristine PDMS, however the deviation was also very large. The mean gray value was the largest in pristine PDMS which means that the stained area had the lightest color. A darker color represents a higher concentration of brown particles. In contrast with the agar experiments, pristine PDMS showed permeability, but at a slightly lesser degree to the modified PDMS membranes. The diffusion distance in the brain was less then one tenth of the distance in agar, due to fast oxidation of the dye in the brain. The diffusion distance and the gray value are both evidence that the plasma-treated and dextran-modified PDMS membranes were slightly more permeable than pristine membranes, but not as convincingly as with the experiment on agar.

Comparison brain vs. agar   Agarose gel has been used as a phantom material for the brain in particular in infusion studies [17]. This model was found to mimic the poroelasticity of the brain, but it has a few short-comings. In regards to the structure, agarose model is more homogeneous and isotropic, whereas the brain is inhomogeneous and anisotropic. Long fibers in white matter and blood vessels promote directional flow along their tracts in infusion experiments [39]. The diffusion of a dye is expected to travel faster along these tracts. The novelty compared to previous infusion studies is the interaction of a membrane at the agar or brain interface. Agar is a tight network of hydrophilic polymer chains that holds water, similar to extra cellular matrix in the brain. However, cell and blood vessels are separated from the matrix by a membrane. Water
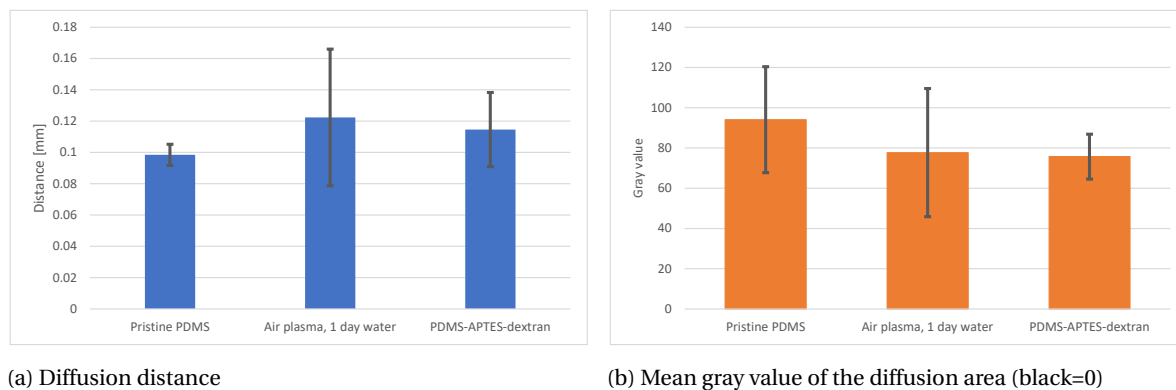
(a) Diffusion distance

(b) Mean gray value of the diffusion area (black=0)

Figure 5.13: Results of KMnO$_4$ on PDMS membrane on mouse brains for 10 minutes

can traverse these membranes freely by osmosis, however water-soluble substances cannot.

On agar, it was observed that when the dye passed through the membrane fast, the dye would spread between the membrane and the agar interface before diffusing into the agar. Furthermore, when removing the membrane from the agar, a watery layer with diluted dye could be observed. In contrast, these results did not occur in the experiment on the brain. Thus, there was no watery layer between the membrane and the brain. A possible explanation is that agar was saturated with DI water and had no tendency to absorb any more water. The brain, however, seemed to absorb water by the fact that there was staining with the pristine PDMS membrane on the brain and no staining with agar. This effect was enhanced by osmosis, since the dye was only diluted in DI water. The effect of osmosis can be excluded, when PBS is used instead of DI water in the future.

Another important difference between the experiment in agarose gel and the brain was the reaction with the dye. The color transition from purple to brown marks the oxidation reaction of potassium permanganate with various organic molecules. Upon reacting, a brown, suspended particle is formed. The mobility of this particle is, thereby, greatly reduced. It was thought to be used as an advantage, since the brain needs to be suspended in fixation fluid for a few days. However, the rate at which the reaction occurs is much faster in the brain than in agar. In agar, the color first transitions to a yellow and orange after 30 minutes. Whereas, on the brain a brown colored stain was visible within 10 minutes. As a consequence, the radial diffusion length after 10 minutes is much shorter in the brain than in agar. To improve the model in agar using this dye, the agar should be modified to have the same oxidation rate as in the brain. However, it is easier to use a dye, such as Monastral blue, that does not react. In this case it is needed to observe the diffusion in agar after dye is removed from the membrane until diffusion has visibly stopped.

5.5. Conclusions

Porous PDMS membranes were fabricated by replica molding. Molds were 3D-printed to make PDMS membranes with smallest pore diameter of 105±8 µm and a minimum thickness 161±7 µm. The amount of shrinkage PDMS features was found to be larger than literature. When the pristine membrane was placed on agar and a dye was dispensed on the membrane, the dye would not stain the agar for the aforementioned geometric characteristics. When the membrane was plasma-treated on one side, the dye would pass quickly from the hydrophobic to the hydrophilic side. Therefore, the permeability could be controlled by the wettability of the surface with air plasma without modifying the inside of the pore. Modified PDMS with dextran was only slightly more hydrophilic than pristine PDMS, and permeability was decreased compared to recently plasma-treated membranes. Agar (0.6%) can potentially be used as model for analyses of membranes on brains, but it needs some adjustments to get comparable results with ex vivo mouse brains.

Grafted dextran did not retain its hydrophilic character over a period of two weeks as reported in literature. Hydrophobic recovery was found within 4 days. Moreover, azobenzene was found to be present on the PDMS surface. However, when irradiated by UV-light for 30 minutes, azobenzene did not change the water contact angle. Even though, the grafting procedures to fabricate a light-responsive PDMS surface was insufficient, this has created a larger interest for switchable wettable surfaces for the application in porous membranes.

When combined with a remote-controlled stimuli such as light to activate the switch in wettability, this can change the local permeability of a membrane which can ultimately be integrated in applications such as drug delivery implants and lab-on-chip.

5.6. Recommendations

The agarose model should be adapted to better predict the interaction of a membrane on a brain. For the simple model used in this research, the agar interface should be dried to prevent the dye from first spreading on the the agar before diffusing in the agar. Secondly, the agarose gel should be made with PBS replacing DI water to simulate the effect of the ionic gradient on the diffusion. A dye should be used that does not oxidate with brain tissue and agar to be able to compare the results properly. These changes can improve the simplest agarose model, however the brain is more complex. The model can be adapted to more accurately represent the brain in terms of shape. Mouse brains have relatively smooth surface, thus a flat agar surface should be sufficient. In contrast, the cortex of human brains have ridges which will form a gap, if the PDMS membrane does not fully conform to the shape. Expanding the agarose model to represent human brains, the model should be adapted to mimic ridges in the cortex. This would require a more complex mold design which can, for example, be 3D-printed.

Concerning the attempt to fabricate a PDMS surface with switchable wettability, grafting methods seem to be insufficient for this application. Coatings of ZnO or TiO$_2$ might be attractive especially, because the surface of the membrane can determine the permeability without the necessity of modifying the inner pore surface. The change in water contact angle of these coatings are also much larger than with grafted azobenzene on silicon wafers. Another approach might be to integrate azobenzene directly into the PDMS matrix, although the change in wettability is expected to be small without other modifications.

Hydrogels are also be interesting to look into, because hydrogels can control the diffusion of particles rather than the flow. The dosing would be much slower, but hydrogels allow for better control and easier 'on-off'-switching. The performance would mostly be tweaked by the chemical composition rather than pore size. The difficulty would be the integration in a drug delivery device.

For the realization of a drug delivery implant for the brain, the next challenge will be the integration of the functional membrane with controllable permeability in a microfluidic system for the drug supply. The inclusion of an external source would allow for administration of multiple drugs which is an advantage over a drug-loaded hydrogel. Finally, electrodes can be integrated for brain activity measurements to monitor the drug efficacy.

Appendices

A
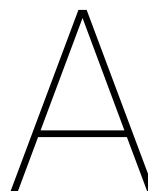
Protocols

In this chapter the protocols for the fabrication of porous PDMS membranes and the functionalization of PDMS are described step by step in detail.

A.1. Fabrication of porous PDMS membrane

This protocol is mainly similar to other protocols for PDMS replica molding. Some points of attention are added.

A.1.1. Materials
- Poly(dimethylsiloxane) (PDMS; Sylgard 184 Silicone Elastomer Kit; Dow Corning)
- Mold
- Dessicator
- Oven

A.1.2. Method
1. Clean the mold in the sonicator for 5 minutes with ethanol.

2. PDMS monomer and curing agent are mixed in 10 (base):1 (curing agent) ratio by weight for 5 minutes. After mixing the PDMS should be cloudy and contain many bubbles.

3. The mixed PDMS is poured into the mold and the excess PDMS is removed with a glass microscope slide, while making sure that the mold is filled to the rim with PDMS and the pillars are visible. Be careful not to break the pillars.

4. Degass the molds with PDMS and the remaining PDMS in a desiccator for 30 minutes to remove the trapped air bubbles. Preheat the oven to 80 °C. Check if the oven rack is horizontal.

5. When the air bubbles are removed, check if the mold is still filled to the rim with PDMS and leveled. Add some more PDMS and remove excess with the glass slide, when necessary. Put the molds in the oven for at least 2 hours.

6. Take the molds out of the oven and let them cool down for 10 minutes. Using a scalpel cut along all edges and lift the PDMS support out of the mold. A few droplets of ethanol can be added, when the PDMS adhesion to the mold is large. With tweezers carefully remove the porous PDMS membrane from the mold. Additionally, remove the excess PDMS from the side walls to ensure the same membrane thickness, when the mold is reused.

A.2. PDMS modification
A.2.1. Materials
- (3-Aminopropyl)triethoxysilane (Sigma-Aldrich, cat. no. 440140)

Table A.1: Troubleshooting

Step	Problem	Possible reason	Solution
1	Pillars break off	The materials become more brittle, when reused many times	Increase the diameter or decrease the height of the pillar
6	Membrane breaks	Mold was not kept leveled, when transferred to the oven or oven rack was slanted. Or not enough PDMS in the mold. Or too much force was applied, during removal	Keep the mold leveled. Or mold should be filled with PDMS to the rim. Or add a few droplets of ethanol and remove the membrane very slowly from the mold.

- Dextran (Sigma-Aldrich, cat. no. 31390)
- Sodium (meta) periodate (Sigma-Aldrich, cat. no. 71859)
- Sodium borohydride (Sigma-Aldrich, cat. no. 71320)
- N,N-dimethyl-4,4'-azodianiline (Sigma-Aldrich, cat. no. 379298)
- Phosphate buffer pH 8 (PBS)
- Dimethyl sulfoxide (DMSO) (Sigma-Aldrich, cat. no. D4540)
- DI water (18.2 MΩ cm, Purelab Flex 3, Elga)
- Ethanol (Sigma-Aldrich, cat. no. 32221)
- Aluminium foil
- Falcon tube
- Parafilm
- Scalpel

A.2.2. Equipment
- Plasma cleaner, Diener Femto
- Orbital shaker
- Oven

A.2.3. Method
Partial oxidation of dextran

1. Add 0.333 g of dextran to 10 ml of DI water in a Falcon tube and close off with the lid. Dissolve dextran completely with the orbital shaker at 2600 RPM for 20 seconds.

2. Add 0.197 g of sodium periodate to the dextran solution and shake again until completely dissolved.

3. Wrap the tube in aluminium foil to protect it from light and let it react by gently mixing at around 100 RPM for at least 4 hours.

The solution was made fresh every time, but it can be stored in the fridge up to 2-3 days. For increased storage time, the solution can be lyophilized and stored at $-20\,°C$.

PDMS-APTES Adapted from Hermanson [45].

1. Samples are cut to smaller sizes at about 1×2 cm. When working with multiple samples, the PDMS is marked with shallow cuts with a scalpel.

2. Clean the PDMS with tape and sonicate it for 5 minutes in ethanol. Remove excess ethanol by blow drying and let it air dry for 30 minutes.

3. Oxidize the surface with air plasma for 2 minutes at 40 W. Alternatively, solution-based oxidation is achieved by immersing the PDMS in a solution of $H_2O/HCl/H_2O_2$ in 5:1:1 volume ratio for 15 minutes in ambient conditions under the fume hood.

4. Prepare a solution containing 3-5% water in ethanol (v/v) and adjust pH to 4.5-5.5 with acetic acid.

5. Under a fume hood add 2-5% (v/v) APTES solution to the water/ethanol mixture. After stirring let the mixture sit for 5 minutes in ambient conditions to allow hydrolysis to occur for 5 minutes to form reactive silanols. Close off the beaker with parafilm.

6. Submerge the oxidized PDMS in the APTES-containing mixture and again close the beaker off with parafilm. Secure the beaker with tape to the orbital shaker platform and set it to a gentle rocking motion at about 100 RPM for 30 minutes at ambient conditions.

7. Set the oven to 110 °C. Rinse the PDMS with several washings of ethanol, followed by DI water and remove excess liquid on the PDMS with an air gun.

8. Place the PDMS in the oven in a glass petridish lined with baking paper for 30 minutes.

PDMS-APTES-dextran

1. Add oxidized dextran solution to 0.2 M $NaHPO_4$ buffer at pH 8 (v/v=1:1).

2. Incubate APTES-functionalized PDMS on the orbital shaker secured by tape at room temperature overnight with parafilm and in aluminium foil for 18h.

3. Decant dextran solution and immerse the modified PDMS in 0.1 $NaBH_4$ solution for 2 hours at room temperature in the fume hood.

4. Decant the solution and rinse the sample with DI water and blow dry.

PDMS-APTES-dextran-azodianiline

1. The dextran-functionalized PDMS is further oxidized in a solution of 0.1 M $NaIO_4$ for 4 hours, while protected from light.

2. N,N-dimethyl-4,4'-azodianiline is dissolved in DMSO 4 mg in 2 mL. The oxidized dextran-functionalized PDMS is added to a mixture of PBS and diluted N,N-dimethyl-4,4'-azodianiline in 10:1 volume ratio left overnight on the orbital shaker at room temperature protected from light.

3. The sample is transferred to a solution of 0.1 M $NaBH_4$ on the orbital shaker for 2 hours at room temperature in the fume hood.

4. The solution is decanted and the sample is rinsed several times with DI water and air dried.

B

Porous PDMS membrane

This chapter describes the process and its findings to make a porous PDMS membrane in a chronological order. This chapter and the following chapters are mostly meant for people who are interested in all the explored methods during the project time including the results that were not used in the report. The pore size is determined by the limitations in the mold fabrication. These limitations were first characterized for molds made by 3D printing. There are two different procedures that determine the thickness of the membrane. The first method uses spin coating to obtain a 'thin' membrane thickness of about $20\,\mu m$. The second method is by casting which gives membranes thicker than $200\,\mu m$.

B.1. Mold

For the fabrication of the mold a high resolution 3D printer (Envisiontec, Micro Plus Hi-Res) is used, because it can print at a small resolution ($\sim 30\,\mu m$) using the resin HTM-140. The innate high heat deflection temperature ($140\,°C$) allows PDMS curing in the oven without losing the accuracy of the dimensions, while decreasing the curing time. The printer can be conveniently used to prototype molds for PDMS microstructures without the use of more expensive equipment for photolithography and a clean room. The 3D CAD models are build in the recommended software, Perfactory RP, by Envisiontec. In the buildstyle settings the smallest layer thickness of $25\,\mu m$ was chosen. Post-treatment consists of removing the excess resin with an airgun, sonication for two minutes in isopropanol, drying with an airgun and two min UV-light treatment.

B.1.1. Pillar diameter

It is expected that the pillar diameter of the 3D-printed mold would be the limiting factor, therefore the smallest possible pillars are tried first to be used to create these pores. Different pillar diameters of 50, 100, 150 and $200\,\mu m$ are modeled in a 3D CAD program (Solidworks) to find the smallest diameter pillars that can be printed reliably on the Envisiontec printer. All pillars are $100\,\mu m$ high.

It was found that no pillars of 50 and $100\,\mu m$ diameter could not be printed or are washed away immediately, when removing the excess resin. Pillars of $150\,\mu m$ in diameter could printed, but the quality was heavily dependent on the quality of the membrane used in the Envisiontec printer. When printed with a new membrane, all pillars could be printed. However, as the membrane started to show signs of wear, the amount of printed pillars decreased with more pillars printed in the center and none in the outer region. This effect was not found, when printing pillars of $200\,\mu m$ diameter. The quality was consistent after multiple uses of the printer's membrane. Therefore, for the rest of this work it was chosen to fabricate molds with pillars of $200\,\mu m$ diameter.

B.1.2. Pillar characterization

The printed pillars are characterized optically. At first sight it can be seen, whether the printer could successfully print pillars. When the pillars are printed on a base plate of 3 mm thick, it can be seen that the corners of the base plate bend upwards. Ideally, this surface should be as flat as possible for uniform fabrication of the porous PDMS membrane.

To assess the quality of the 3D printed structures, it is observed with a digital microscope (Keyence VHX-6000). From the first look, the shape is of pillar is not perfectly cylindrical. The pillar shape could be described

as a rough cylinder with a bulge at the side and an uneven top as can be seen in Figure B.1. All pillars have roughly a similar shape, but with variations in the size of the bulge and the uneven top surface. The pillars are not smooth, because of the printed layers as seen in Figure B.2. The pillars look like a tall, tiered cake which becomes slightly more tapered towards the top.
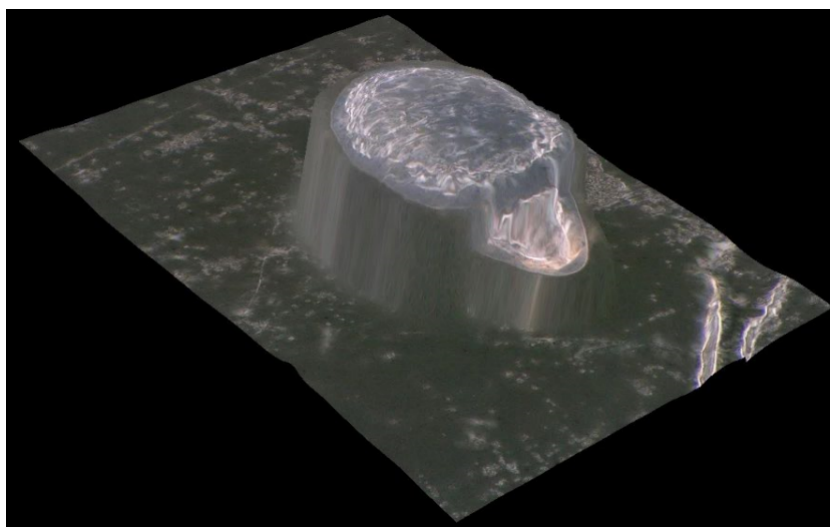

Figure B.1: Examples of a pillar with an 'odd' shape. 3D reconstruction from top (Keyence VHX-6000: ring light mode)

B.1.3. Post-treatment

When the structure is done with printing, it can be cut off from the stage. Excess liquid HTM-140 is removed, followed by a 2 min sonication in isopropanol and 2 min UV-light treatment. After sonication tiny white crystals have formed on the surface of the 3D-printed structure.

For the curing of PDMS on HTM-140 it is important the clean the surface extensively, because otherwise curing agent in the PDMS is inhibited. Molds with pillars are cleaned with acetone, ethanol, and isopropanol, individually. There was no significant change in pillar size after 10 minutes of sonication using these chemicals.

B.2. Thin film porous membrane

The fabrication of thin film porous PDMS membranes has been reported by Huh et al. [49]. They made their mold by spin-coating SU-8 and photolithography to create pillars of 10 µm in diameter. This mold is then used to imprint a thin layer of spin-coated uncured PDMS on a silanized PDMS support. This method was first adapted to facilitate the available equipment. Initially, the only change was that the SU-8 mold is replaced with the 3D-printed mold. However, more changes were made as problems occurred with the curing and the release of the membrane from the support.

B.2.1. Curing

The protocol by Huh et al. [49] left the PDMS to cure overnight followed by curing in the oven at 60 °C for one hour. This resulted in uncured PDMS in the fabrication method that uses a HTM-140 instead of SU-8 as the mold. Therefore, the curing time in the oven was increased to 70 °C. The PDMS membrane was cured most of the time, but some membranes would still be partially uncured for unknown reasons. Molds could only be used once, because after one use small patches of PDMS would be left behind on the mold. These PDMS patches could not be easily removed without destruction of the pillars. Removal of these patches was tried by sonication in ethanol or isopropanol for 10 up to 30 minutes, but was found to be unsuccessful.

B.2.2. Release membrane from support

For the release of the thin PDMS membrane from the thick PDMS support, the protocol developed by Huh et al. [49] uses an anti-stiction layer by silanization of the PDMS support. The exact procedure described in the protocol for this silanization cannot be reproduced, because a silanization trap is not available in the
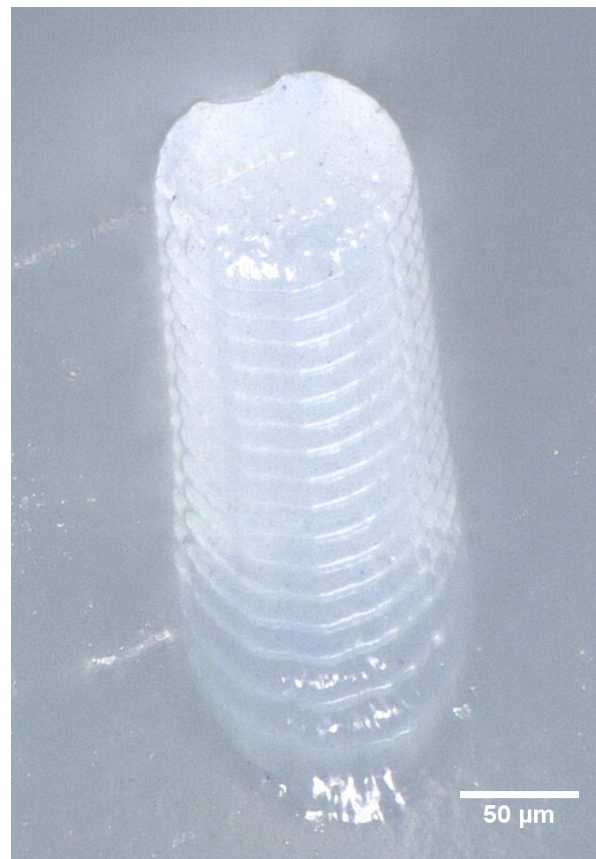
Figure B.2: Side view of a pillar. Tilt: 30° (Keyence VHX-6000: full coaxial)

lab. It is first tried to silanize the surface by putting the PDMS support in a Petri dish and pipette 35 mL of 3-aminopropyltrimethoxysilane (APTMS) on a piece of glass or cotton pad with and without pretreatment with air plasma. However, it was found that breakage of the membrane occurs, when trying to remove the membrane by attaching it to another PDMS structure using air plasma. Therefore, a sacrificial layer was introduced in the protocol to release the membrane. The main advantage is that no physical force is required to release the membrane lowering the chance of breaking the membrane.

Water-soluble sacrificial layers are useful, because water is a gentle solvent compared to for example acetone. The etching rates are also generally fast. Polyacrylic acid (PAA) and dextran can both be used as sacrificial layers, but PAA has some advantages over dextran. The PAA viscosity can be more easily adapted for different film thicknesses and solubility can be controlled by Ca^{2+} or Cu^{2+} [69].

Solutions of PAA in DI water can be made at different weight to volume ratios. The more PAA is dissolved, the thicker the layer will be after spin coating. The relation between the layer thickness and the rotational speed is documented by Linder et al. [69]. Provided that the membrane will be relatively large (>1 cm^2), a thicker sacrificial layer will be required to reliably etch the layer.

A layer of 30 w/v % PAA is spin coated (500, 1000, 2000, and 3000 RPM) on PDMS slab attached to a glass cover slip and heated at 90°C for 2 min on a hot plate as suggested by Linder et al. [69]. This resulted in cracking of the PAA-layers and the formation of ripples and cracks in thinner layers as shown in Figure B.3 and B.4. Furthermore, the PAA residue from spin coating on the glass turned into a burned brown-black color.

Concluding that the temperature was too high, the drying process is altered to 60°C for 5 min as described by Guo and DeWeerth [41]. This improved the quality of the membrane tremendously, since in none of the samples cracks were formed. Slight differences can be seen between the PAA-layers spin coated at different rotational speeds as seen in Figure B.5. The layer spin coated at 500 and 1000 RPM are free of ripples, but higher rotational speeds (2000 and 3000 RPM) still induces these ripples. For these thin layers a shorter drying time or lower drying temperature will likely increase the quality.

After drying, the PDMS slabs with a PAA-layer are than spin coated with uncured PDMS as described by Huh et al. [49]. For this first test, no 3D-printed master is used to make pores. The PDMS is cured overnight,
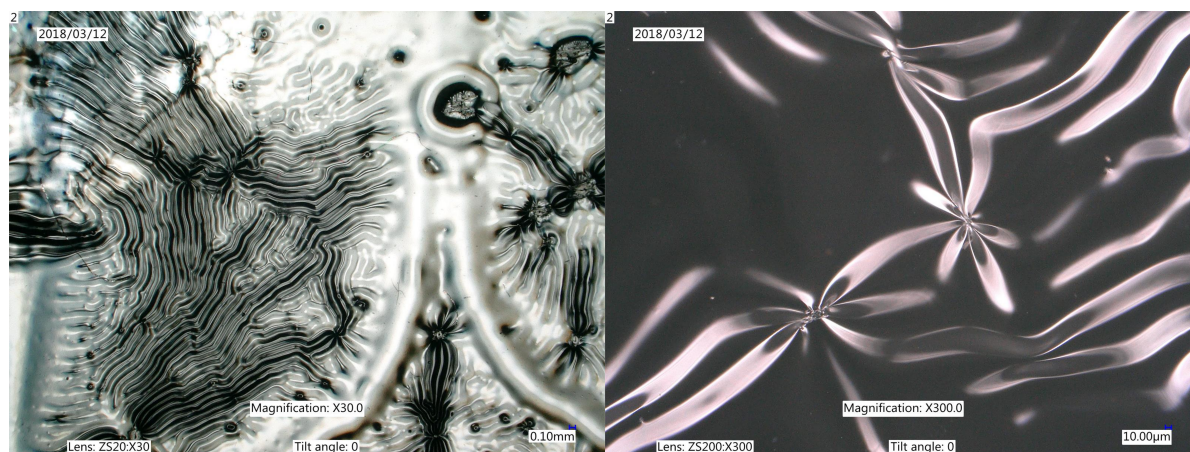
Figure B.3: Examples of ripples in the PAA-layer spin coated at 500 RPM after heating at 90°C for 2 min on a hot plate at different magnifications (Keyence VHX-6000: full coaxial light mode)
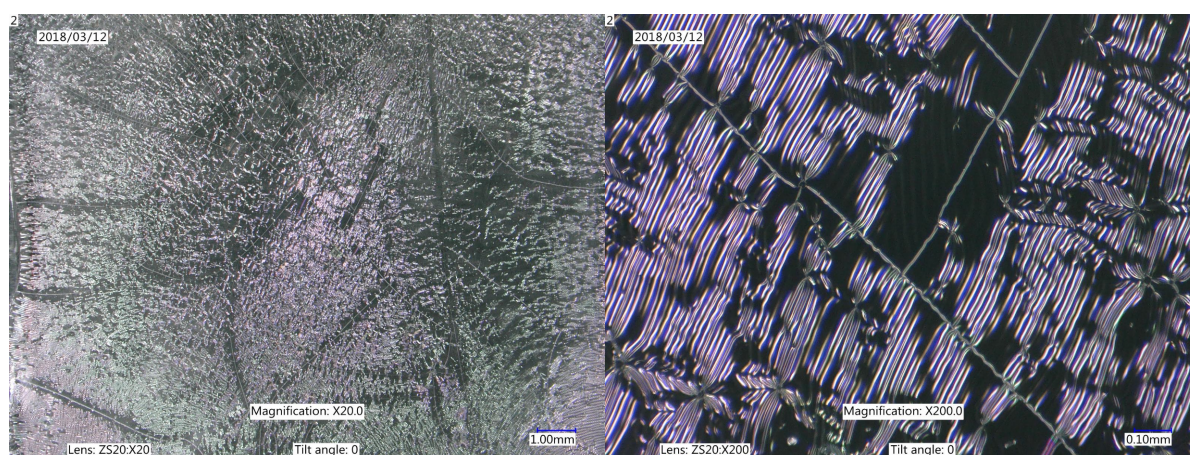

Figure B.4: Examples of cracking and ripples in the PAA-layer spin coated at 3000 RPM after heating at 90°C for 2 min on a hot plate at different magnifications (Keyence VHX-6000: full coaxial light mode)

followed by baking in the oven at 60°C for 1 hour. After the curing process, it could be seen that cracks have formed in all the PAA-layers as seen in Figure B.6. Even though, the curing temperature is the same as the drying temperature of the PAA-layer, the formation of cracks will occur, because the PDMS support is allowed to expand during baking for 1 hour. To prevent cracking one can let it cure at room temperature for another day or cure at a lower temperature. However, for the fabrication for the PDMS porous membrane using a 3D printed mold out of HTM-140, the PDMS will not cure at room temperature for at least 3 days, even though PDMS is normally cured in less 48 hours at room temperature in for example a Petri dish. So, curing the PDMS would be too time-consuming.

For the release of the PDMS thin film from the PDMS support, the PAA layer is dissolved in a bath filled with DI water on a hot plate at about 80-90°C. After a few minutes the edges of the PDMS films begin to separate from the support and curl upwards. After 30 minutes the films with PAA-layers spin coated with 1000 and 2000 RPM can be removed by sticking it on a glass plate. PAA-layers made with 500 and 3000 RPM needed a bit more help to be removed. It was observed that the cracks formed in the PAA-layer during the curing of the PDMS membrane are also visible in the membrane after release from the support as seen in Figure B.7.

The procedure was repeated using a PAA-layer spin coated at 1000 RPM, but with the 3D-printed master to form the pores in the membrane. Two out of three membranes were properly cured after curing overnight at room temperature and 60°C for 3 hours. When put into a hot water bath, even after two hours there were no signs of release of the membrane from the support. The edges were still securely attached to the support, while the edges of the PDMS membrane without the holes came lose after a few minutes.
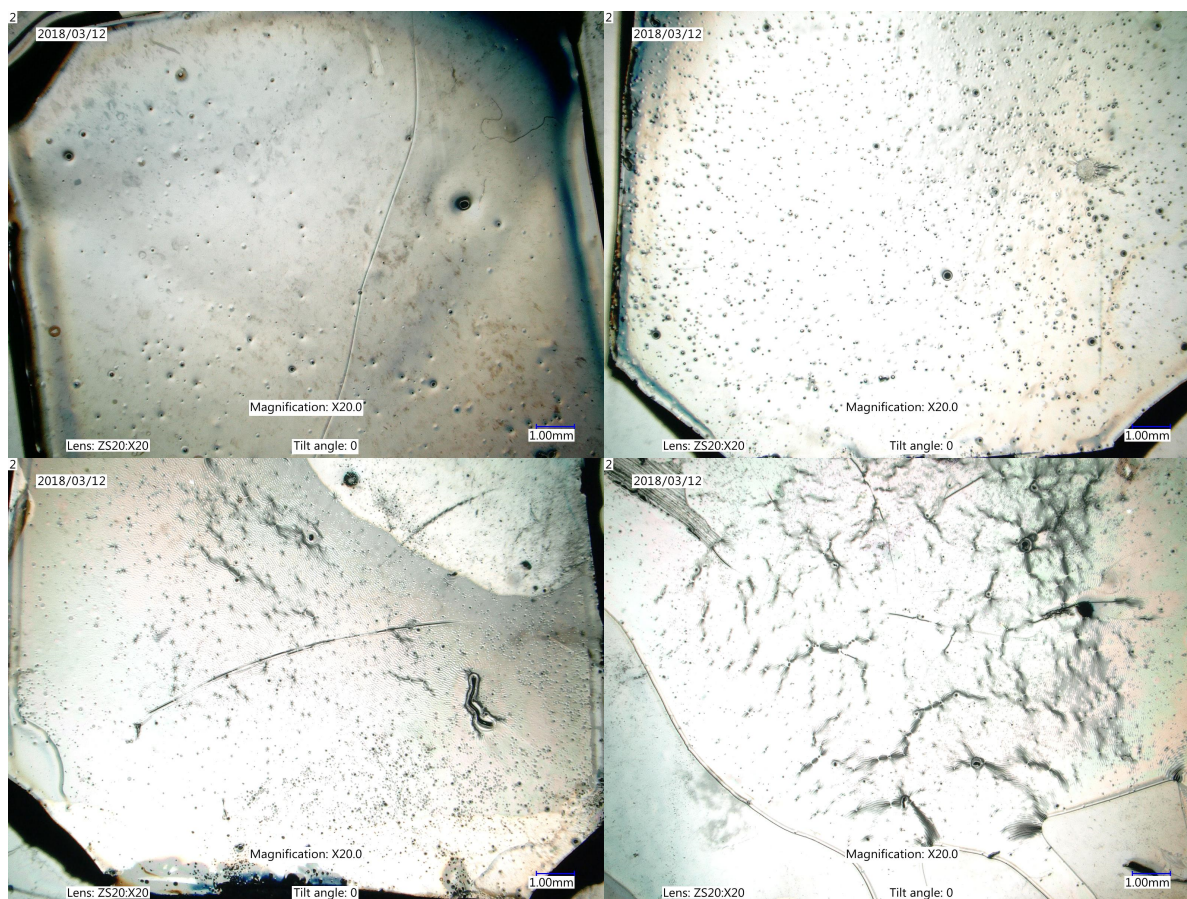
Figure B.5: Comparison of 30 w/v% PAA spin coated on PDMS and dried at 60°C in the oven. From left to right: (top) 500, 1000, (bottom) 2000, 3000 RPM (Keyence VHX-6000: full coaxial light mode)

From this it was concluded that PAA and uncured PDMS might have mixed preventing the PDMS from curing, even though the curing temperature (60 °C) is much lower than the glass transition temperature 106 °C [108]. The only difference from the reported method was the material of the mold. Since the HTM-140 mold has been successfully used as a casting mold for larger structures, the fabrication of the porous membrane is altered to a casting method.

B.3. Thick porous membrane

The fabrication method to make a porous membrane was changed to be better suit the materials of the mold and the capabilities of the used 3D printer, Envisiontec. The resulting thick porous membrane has a few advantages compared to the thin film porous membrane. First of all, it is easier to handle and is less fragile. Secondly, the fabrication process is simpler and faster. Furthermore, molds can be reused multiple times, since the PDMS was always fully cured after for 3 hours in the oven at 70 °C and no uncured PDMS was left behind. The advantage of the thin film porous membrane is that there is a potential for making smaller pores (10 μm), but this was not possible to be achieved with the Envisiontec 3D-printer.

B.3.1. Design of the mold

Uncured PDMS was poured over the pillar structures and cured to create a porous membrane. The mold was further adapted to accommodate membranes with different thicknesses and supports are added for easy removal of the membrane from the mold. Molds were designed to fabricate membranes from 200 to 500 μm thick. An example of a mold is shown in Figure B.8. All pillars were modeled to have a diameter of 200 μm, since these could be printed reliably as concluded previously. Two supports at opposite sides of the membrane's edge add an extra thickness to the membrane of 2 mm to easily remove the membrane from the mold and to handle it with a tweezer. The height of the walls determine the membrane thickness. The pillars were
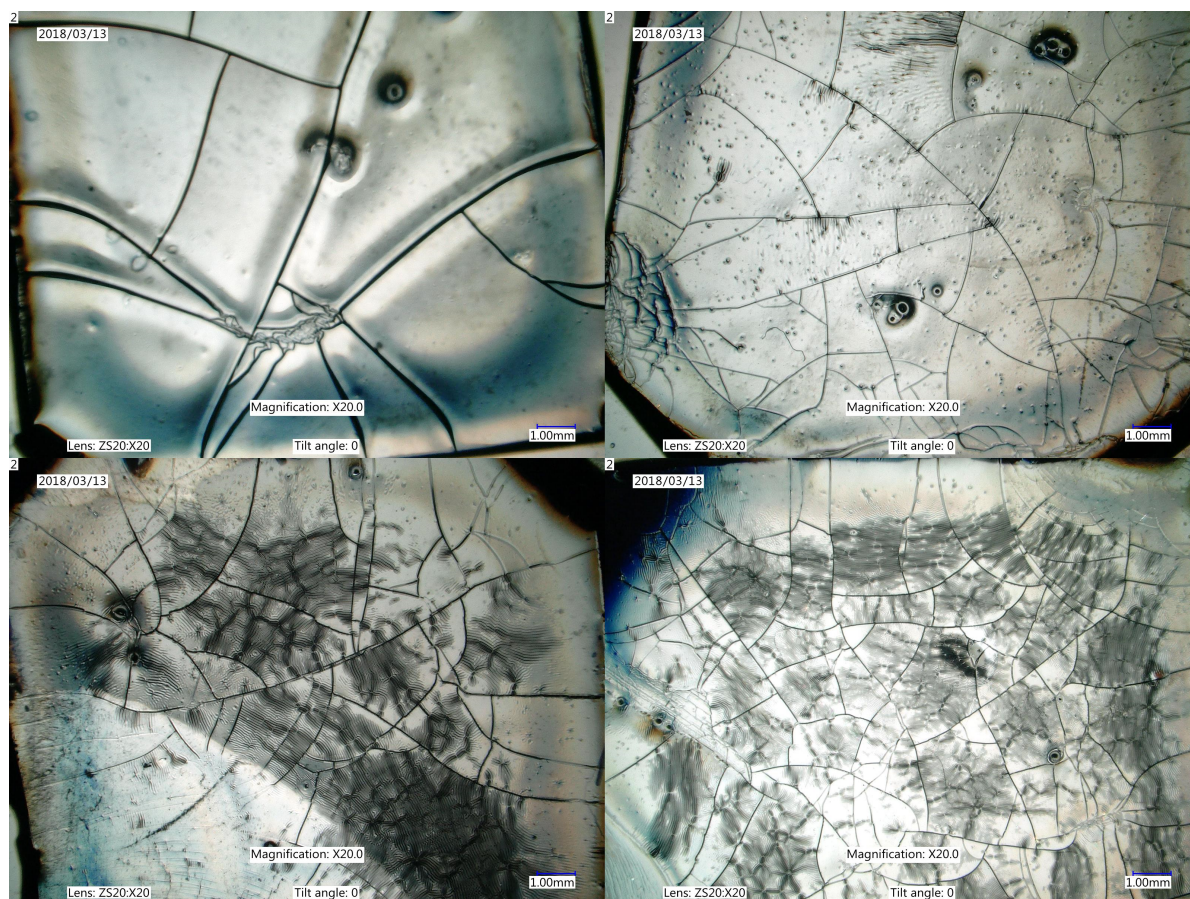
Figure B.6: Comparison of 30 w/v% PAA spin coated on PDMS support, dried at 60°C in the oven, a spin coated layer of PDMS is cured overnight and 1 hour in the oven at 60°C. From left to right: (top) 500, 1000, (bottom) 2000, 3000 RPM (Keyence VHX-6000: full coaxial light mode)

made at the same height as the walls and an additional 25 µm, which resulted in one layer more than te walls to be printed on the Envisiontec set on HTM140M 25 µm for 'Ultra'. This was done to ensure the formation of open pores. Taller pillars will result in concave menisci of PDMS around the pillars. This is the reason why the pillar's height is not further increased. The transition between support and membrane was made more gradual by fillets, because this was found to be a fragile point during removal of the membrane from the mold.

B.3.2. Membrane thickness
The actual membrane thickness was measured using a white light interferometer by Bruker. The data was processed using Vision64 which allowed for multi-region analysis to separate the data in two groups top and lower level. The membrane thickness was determined by taking the difference between the PDMS (top) and glass (bottom) interface.

B.3.3. Pore size
The diameter of the pores was determined for the front and back side. An optical microscope can visualize these pores, however the pore has a thick black outline, because PDMS is translucent, which makes it difficult to see what the actual pore size is at the top interface. An easier way to visualize the pore is with the scanning electron microscope (SEM). To make the sample conductive, the top and back side of the membrane is sputtered (2 min, 10 mA) using a Au/Pd target. The images that are obtained with SEM have a higher contrast than images taken with the optical microscope. This is useful for automatized image analysis. Images are taken of an array of pores. The pores are measured by binarization in ImageJ and analyzed. The analysis function automatically measures the diameter.
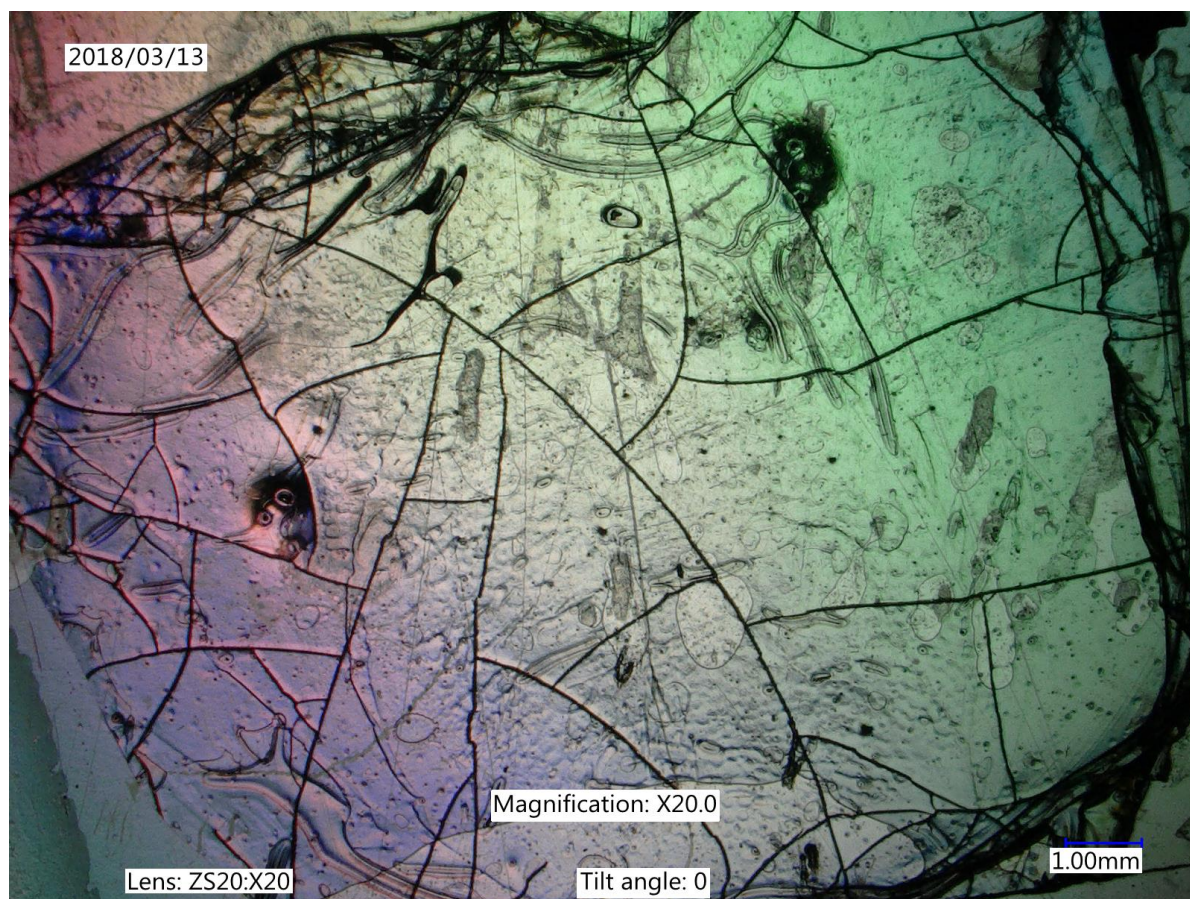
Figure B.7: PDMS membrane without holes after release from support with PAA-layer (1000 RPM) (Keyence VHX-6000: full coaxial light mode)
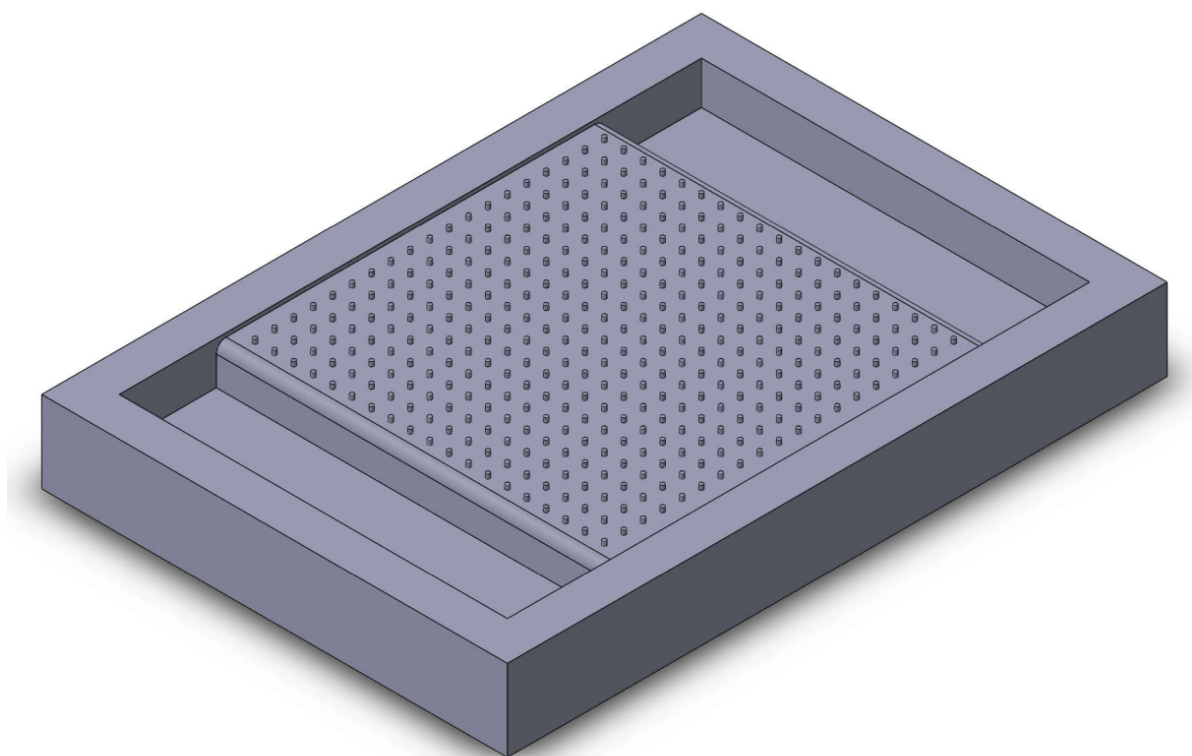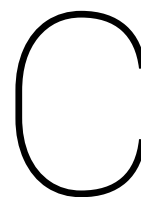
Figure B.8: 3D CAD model of the mold to make a porous PDMS membrane

C

PDMS functionalization

C.1. Protocol development

Azobenzene has been grafted mostly on mesoporous silica by silanization for covalent bonding. However, it is desired to use PDMS as the substrate. Grafting azobenzene to PDMS has never been reported before, so existing fabrication methods should be adapted. When a PDMS surface is oxidized, a similar silanization technique can be used. The difficulty is however that advanced chemical techniques and dangerous chemicals are used. Fortunately, azobenzene can be purchased with amine or carboxyl end-group, therefore well-known conjugation protocols can be used. The functionalization of PDMS is most commonly done by adding amine groups to the surface by silanization of APTES.

C.1.1. Initial protocol

The initial protocol was based on the method used by Yu et al. [135]. Yu et al. first formed hydroxyl-groups to the PDMS surface by chemical oxidation with a mixture of $H_2O/HCl/H_2O_2$ in 5:1:1 volume ratio. Beforehand, dextran is oxidized using sodium periodate overnight. The amine end groups are used as anchor points for partially oxidized dextran to bond with. Dextran is then further oxidized to provide more attachment points for the amine-containing azobenzene.

The protocol is the same as presented by Yu et al. [135], except for the oxidation of PDMS air plasma and the $H_2O/HCl/H_2O_2$ mixture are both tested and a azobenzene with amine end group is used instead of an antibody. The reported method is originally designed for a flow-through process in a microfluidic channel which should also be useful for surface modification of pores in a PDMS membrane. However, the protocol is first tested on flat PDMS substrate which is easy to handle and can be used for contact angle measurements. First, 0.475 g of dextran in dissolved in 10 mL DI water after which 0.232 g sodium periodate ($NaIO_4$) is added as an oxidant. The mixture is stirred in a disposable Falcon tube. The tube is closed and placed under the fume hood for 5-7 hours instead of overnight as suggested in the reported method. Cured PDMS slabs are cleaned by sonication in ethanol for 5 minutes after which PDMS was oxidized. The first oxidation method was with air plasma for 2 minutes at 40 W at 4 mbar. The second oxidation method is by submergence in a mixture of hydrochloric acid (37%) and hydrogen peroxide (30%) with DI water in $H_2O/HCl/H_2O_2 = 5:1:1$ volume ratio. After 15 minutes in the oxidative solution, PDMS is rinsed 5 times with DI water and put in ethanol for 5 minutes. Next, the oxidized PDMS is suspended in 3-aminopropyltriethoxylsilane (APTES)/ethanol (1:1, v/v) solution for 30 minutes covered with Parafilm under the fume hood. The excess APTES remaining on the surface by several washed in ethanol followed by rinsing with DI water for several times. Amine-modified PDMS is bathed in the fleshly prepared dextran solution for 1 hour. Excess dextran is removed by multiple washings with DI water. Dextran-modified PDMS is further oxidized in $NaIO_4$ (0.1 M) for 2 hours. N,N-Dimethyl-4,4'-azodianiline (DMADA) is dissolved DMSO to make a stock solution. The added amount of the stock solution diluted in DMSO and exposure time of the PDMS in the mixture should be optimized.

The initial observations are to be shortly described. After adding the PDMS slab to the oxidized dextran solution, the PDMS changed from a translucent to a milky white color. The Raman spectrum showed new peaks compared to the spectrum of pristine PDMS after silanization with APTES. However, the same peaks are also observed, when grafting dextran to PDMS without silanizing the surface with APTES first. Thus, dextran can be easily adsorbed and probably absorbed. Moreover, the water contact angle has not significantly

changed indicating that the functionalization method should be reviewed. PDMS-APTES-dextran was found to have a contact angle of 97± 5°, while pristine PDMS would have a contact angle of 107± 2°. The contact angle was expected to be much lower, since dextran introduces many -OH groups to the PDMS surface to form hydrogen bonds with water. The small change in contact angle indicates that the presence of dextran at the surface is low, thus most dextran is absorbed into the PDMS.

This instigated a more detailed research on the chemical side of the method. It was found that de aldehyde of oxidized dextran and an amine can form a Schiff bond which is easily hydrolyzed and is therefore an unstable bond. This bond must be reduced to form a covalent bond [45]. The protocol was altered to include reductive amination for bonding amines to aldehydes.

C.1.2. Improved protocol

The initial protocol was found to be insufficient leading to an altered procedure. The final protocol is described step by step in Appendix A.2. The following paragraph mentions the differences compared to the first method. The described methods are adapted from Hermanson et al. [45].

The silanization process was changed to a mixture of ethanol (90%), APTES (5%), and DI water (5%). The pH is also adapted to 4.5-5 with acetic acid, since it was proven to enhance the reaction. The bath of PDMS in the APTES mixture was followed by curing or drying in the oven at 110 °C.

Sodium phosphate or phosphate-buffered saline (PBS) is used as a buffer and the pH is increased to 8, since higher pH increase the conjugation yield. A stock solution is prepared and stored in the fridge for about a month. PBS is usually used in combination with proteins as it mimics the natural osmolarity and ion concentration of a human body. Here, it is mainly used for the pH and buffering property.

Reductive amination is the process of reducing the Schiff base to a strong secondary amine linkage. This process must thus be utilized after adding dextran to bond with APTES and after further oxidation of dextran to bond with DMADA. Sodium borohydride was used for initiation of the reaction, because it was readily available in the lab. However, sodium cyanoborohydride is preferred, since borohydride converts the aldehydes (=O) into hydroxyls (-OH) much quicker than sodium cyanoborohydride, ultimately reducing the amount of available bonds [45]. The protocol described by Greg T. Hermanson [45] suggested combining the formation of Schiff bases and their reduction in a single step. This method uses sodium cyanoborohydride, instead of sodium borohydride, therefore these steps are separated.

All reactions involving sodium periodate are protected from light using aluminum foil. The initial protocol did not consider the degradation of sodium periodate in light at all. In their defense, the visible effect of light is not visible in few days time. The solution has clearly degraded after a week, because the solution becomes a light pink which turns into a darker pink over a longer time. This degradation also occurs, when stored in aluminum foil in the fridge. This is why oxidized dextran is usually lyophilized and stored in the freezer.

The initial observation with the revised protocol was that adding the reduction step did not make the PDMS milky white. Only a small change was observed with Raman spectroscopy, but was not very convincing, because the layer thickness is very thin making it difficult to detect with Raman spectroscopy. However, a significant change could be observed in the contact angle after grafting dextran and DMADA. The addition of DMADA changed the color to an orange (Figure C.1a). The color was darker, when more DMADA was used, but the color became lighter when kept in DI water (Figure C.1b).

C.2. Characterization

The characterization is performed on a flat PDMS surface which for the most part is representative for the surface of a pore in a membrane. The difference is mainly found in the surface roughness formed by the layered structure of the 3D-printed mold. Furthermore, the grafting efficiency inside a pore is expected to be less compared a flat surface. This decrease in efficiency should not be large, since the pores are still relatively large (200 μm) and the membrane is thin.

The grafted chemicals are written in the order they were added to the PDMS. For example, PDMS-APTES is APTES grafted on PDMS. Also, PDMS-dextran is a sample in which the silanization step with APTES is skipped and the dextran is grafted using the same method as described in the protocol.

C.2.1. Raman

The Raman spectrum of various samples is measured to verify the presence of chemical bonds characteristic for the grafted molecule. The spectra of the samples fabricated with protocol as described in Appendix A.2 and air plasma to oxidize the PDMS surface is shown in Figure C.2. The functionalization of APTES on
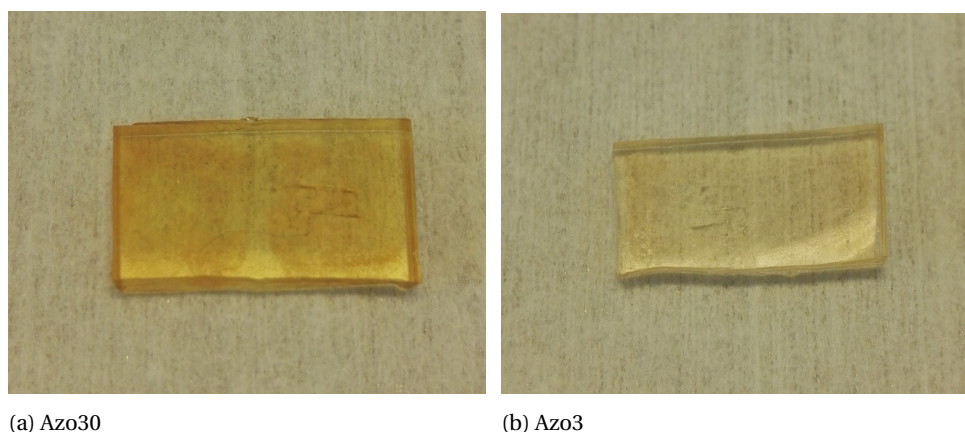
(a) Azo30   (b) Azo3

Figure C.1: PDMS samples with DMADA using the improved protocol where AzoX refers to XµL added from the stock solution. The samples were photographed with a white background.

PDMS is difficult to verify. Small peaks are observed in the 3600-3700 cm^{-1}. One of these peaks can be associated with amine-groups and the other peak with hydroxy-groups formed after oxidation of the PDMS surface. Furthermore, a sharp peak can be found 1124 cm^{-1} which is characteristic for in-phase stretch in alkoxysilanes (Si-O-R) [62]. A peak couple is observed at 2104 and 2167 cm^{-1} and there is a distinct peak at 3080 cm^{-1}. Fluorescence background is slightly increased compared to pristine PDMS. No new peaks are observed after grafting of dextran. The peaks in 3600-3700 cm^{-1} found on PDMS-APTES have mostly disappeared. The overal intensity has also been decreased compared to PDMS-APTES. High intensity peaks of only N,N-dimethyl-4,4'-azodianiline (DMADA) are found at around 1150 and 1390 cm^{-1} [109]. In the Raman spectrum of PDMS-APTES-dextran-azo there is a lot of fluorescence background which hides the smaller characteristic peaks of DMADA. A peak can be detected at 1145 cm^{-1} which becomes more intense the higher the concentration of DMADA used. This peak can be assigned to symmetric stretching of C-N [116]. The peak of the trans azo compound that is supposed to be around 1390 cm^{-1} is indiscernible from the fluorescent interference and the peak at 1410 cm^{-1} present in PDMS.

The Raman spectrum is measured for the same series displayed in Figure C.3, but oxidized with a solution of H$_2$O/HCl/H$_2$O$_2$. The new peaks were also visible, but the intensity was much smaller compared to samples oxidized with air plasma. It was an indication to believe that the amount of grafting was better with air plasma than with the oxidative solution.

The aforementioned measurements were done before finding that sodium borohydride converts aldehydes to hydroxyls more quickly than sodium cyanoborohydride used in the prescribed protocol. The Raman spectra is measured of samples that were fabricated by the formation of Schiff bases between DMADA and oxidized dextran, before adding sodium borohydride as shown in Figure C.4. New peaks indicative for azobenzene were more clearly visible, but the fluorescence made it difficult to compare the effect of the updated surface modification method.

As a result of the increasing water contact angle (discussed in more detail later) over time of dextran-modified PDMS samples, the Raman spectra is compared in Figure C.5. It was observed that the peaks, that were present with PDMS-APTES-Dextran and not in pristine PDMS, have disappeared after 2 months. This was in agreement with the results of the contact angle. Therefore, dextran was not covalently bonded to PDMS, but it only temporarily changed the surface chemistry. Furthermore, there was a difference in the Raman spectra between the first batches in April/May and later batches in July, even though the executed protocol was the same. Even samples that have recently been modified with dextran did not show the peaks from the first batch. This suggests that the difference is caused during the fabrication before storage methods matter. The exact reason for this result is unknown. It was first thought that an old PBS solution could affect the reaction, because crystals were formed in the stock solution. However, this did not change the result.

C.2.2. FTIR

The FTIR spectrum is obtained using the same samples as with the Raman spectroscopy as shown in Figure C.6. The presence of APTES on the PDMS surface is verified by the characteristic peaks of primary amines of which a weak broadband is visible at 3200-3460 cm^{-1} and a peak at 1655 cm^{-1} is found representing the in-
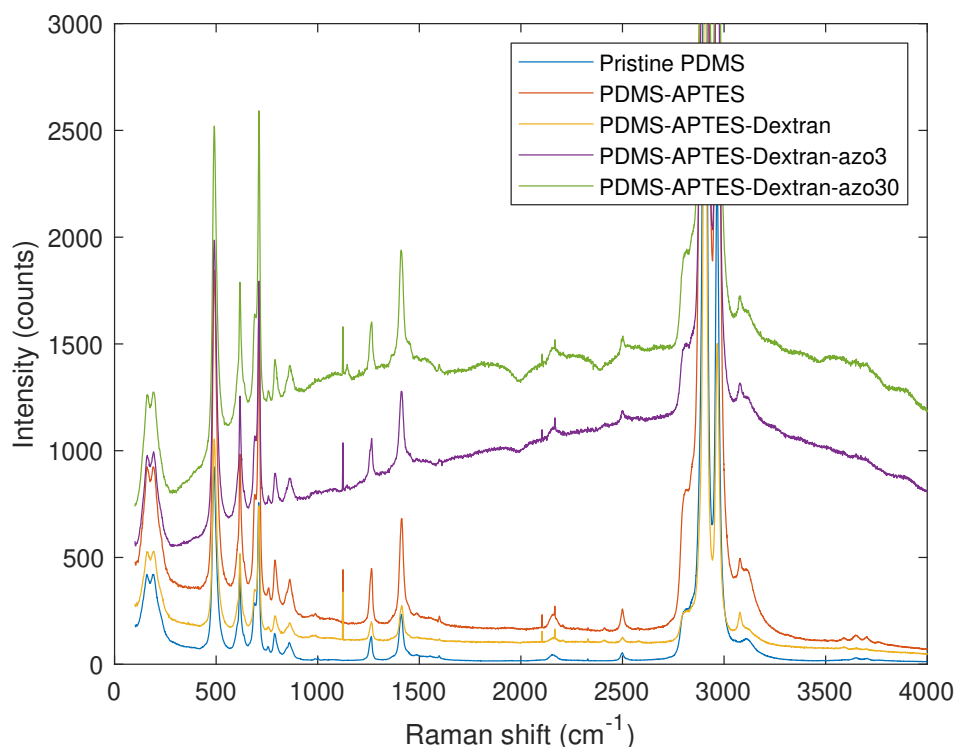
Figure C.2: Raman spectrum of samples oxidized by air plasma. Raman laser: 514 nm, ND: 25%

plane deformation of primary amines. Dextran is characterized by its OH-groups and C-O-C bonds. A moderate peak is found at $3550\,cm^{-1}$ which can be associated with O-H stretching vibrations. C-O-C stretching overlaps with Si related vibrations from the PDMS. Aldehydes (C=O) are formed in dextran due to oxidation, but are used to bond to amine-groups. The presence of aldehydes should give a peak at around 1600 and $2730\,cm^{-1}$. The peak at $1600\,cm^{-1}$ overlaps with the amine deformation. However, at $2730\,cm^{-1}$ no significant peak is found. So there are no remaining aldehydes after the functionalization protocol and storage in air.

The FTIR spectrum of the samples oxidized by oxidative solution had two different peaks compared to the samples oxidized by air plasma as seen in Figure C.7. There is a defined peak at $1600\,cm^{-1}$ with PDMS-APTES indicating the amine component. There is also a peak at around $2000\,cm^{-1}$ with PDMS-APTES-Dextran, but it does not represent a bond of dextran. The broad bands in the region of $3200\text{-}3500\,cm^{-1}$ are indicative for O-H and N-H stretching. In contrast, these bands seems to be less intense with the oxidative solution than with air plasma.

FTIR measurements are also performed one month later displayed in Figure C.8. The peaks for N-H and O-H stretching have disappeared over time. The FTIR spectrum of PDMS-APTES-Dextran became the same as pristine PDMS confirming the results found with Raman spectroscopy and water contact angle measurements.
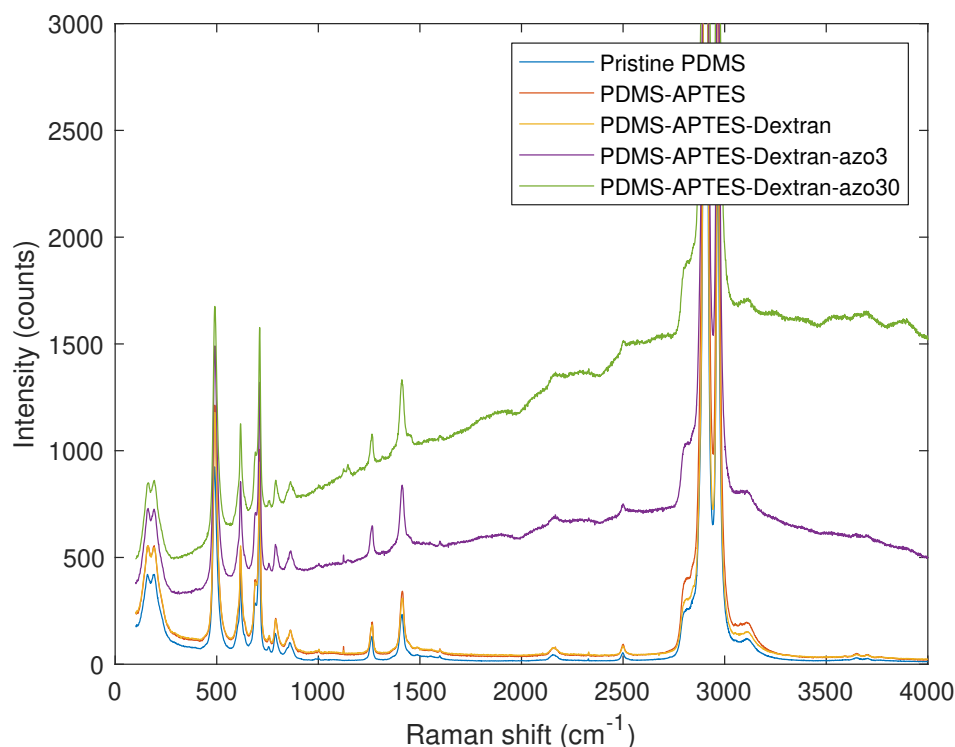
Figure C.3: Raman spectrum of samples oxidized by liquid oxidation solution. Raman laser: 514 nm, ND: 25%

C.2.3. Contact angle

A change in the water contact angle is an indication for a change of the surface. Pristine PDMS is known to be hydrophobic. When oxidized by for example oxygen plasma, -OH groups are introduced to the surface making the PDMS hydrophilic. The contact angle is measured for the various steps of the functionalization.

For quick and convenient measurements in the PME department, the Keyence VHX-6000 digital microscope can be used. This microscope can be tilted to 90° to obtain an image from the side. A white background is created with a sheet of regular printing paper. The images are taken using the full coaxial light mode. Droplets of 2 µL are dispensed using a micropipette. Images are processed using ImageJ and a plugin: contact angle. The image is rotated such that the drop is upside down and the interface should be as horizontal as possible. After starting the plugin, one point is first added to the most left drop-interface contact point, then the most right. Then, 5 points are added to along the contour of the drop. The contact angle is calculated using the option 'Manual Points Procedure'.

The water contact angle measurements using Keyence VHX-6000 are performed to detect changes in the surface. PDMS-APTES-dextran was found to have a contact angle of 97± 5°, while pristine PDMS would have a contact angle of 107± 2°. The contact angle was expected to be much lower, since dextran introduces many -OH groups to the PDMS surface to form hydrogen bonds with water. The small change in contact angle indicates that the presence of dextran at the surface is low, thus most dextran is absorbed into the PDMS. Since the water contact angle has not significantly changed indicating that the functionalization method should be reviewed. A significant change in water contact was measured using the impvoed protocol. The results are summarized in Table C.1. The grafting protocol is performed with two different oxidation methods: a mixture of $H_2O/HCl/H_2O_2$ and air plasma. The improved protocol resulted in a significant change in the contact angle. For PDMS-APTES-dextran the PDMS has become more hydrophilic using both methods. It indicates that the dextran has been sufficiently grafted to the PDMS surface to make hydrophobic PDMS more hydrophilic. The use of borohydride also aided the conversion of remaining aldehydes not used to bond with APTES to hydroxyls.

The switching of the azobenzene molecule has the potential to change the water contact angle, when exposed to only UV light (~360 nm). The difficulty is that visible light is required to obtain an image for the measurement of the angle. Thus, it was of importance to keep the time between exposure to UV light and the imaging of the water droplet as short as possible. Instead of the Keyence VHX-6000 for the imaging, it
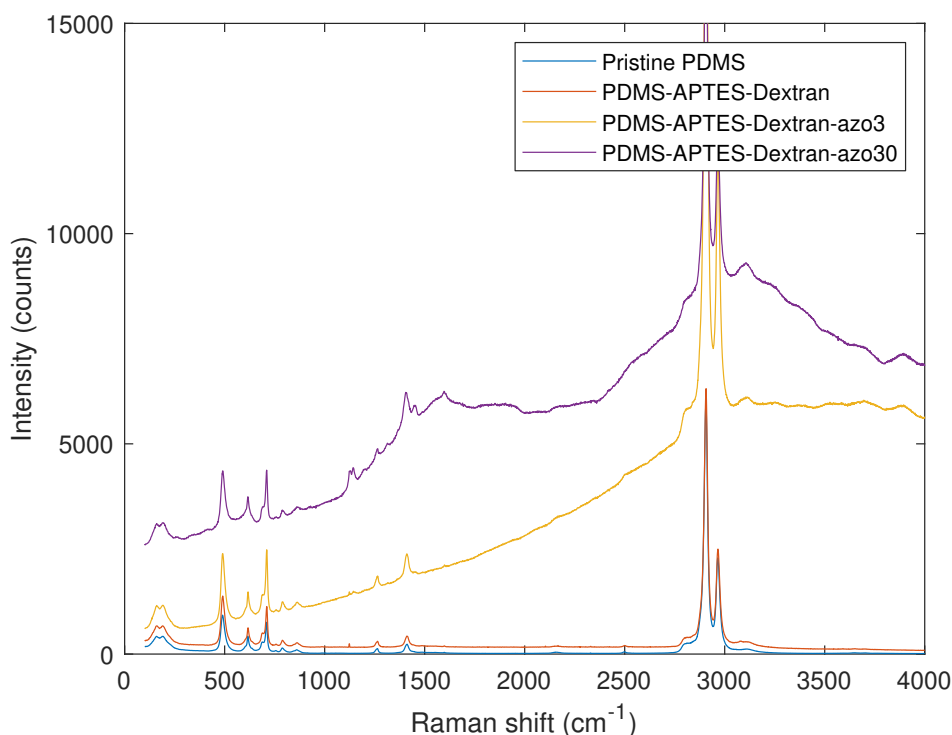
Figure C.4: Raman spectrum of samples oxidized by air plasma after separating the formation of Schiff bases and reductive amination. Raman laser: 514 nm, ND: 25%

Table C.1: Water contact angle measurements 1 hour after each grafting step using air plasma or HCl/H$_2$O$_2$

Oxidation	Sample	Water contact angle
	Pristine PDMS	107± 2°
Air plasma	PDMS-APTES	87± 5°
	PDMS-APTES-dextran	62± 4°
	PDMS-APTES-dextran-azobenzene	82± 2°
HCl/H$_2$O$_2$	PDMS-APTES	105± 2°
	PDMS-APTES-dextran	80± 4°
	PDMS-APTES-dextran-azobenzene	107± 2°

was chosen to use the drop shape analyser, Kruss DSA100 to achieve a faster workflow. An overview of this setup is given in Figure C.9 The windows of the chamber that holds the sample are blocked with plastic-coated blackout cardboard secured with tape. The light guide that connects the UV source (Honle, Bluepoint 4 Ecocure) is fixed with two layers of black duct tape in the hole for the droplet dispenser which is moved up. The UV source is equipped with a filter that has a radiation permeability range of 320 – 390 nm. After the set exposure time with UV-light, the light guide and window blockers are quickly removed and the dispenser is moved in position for the water contact angle measurement.

The UV source has a time limit of 15 minutes. The water contact angle is measured after 15 minutes of UV-light and after two sessions of 15 minutes, but no significant change in the water contact angle was measured. This was expected, because water contact angle would increase over time with dextran-modified PDMS indicating that there was no covalent bonding, thus DMADA would also not be covalently bonded to dextran. PDMS with DMADA was orange of color indicating that some azobenzene was present, either absorbed and/or adsorbed. The water contact angle measurement after UV proved that either adsorbed azobenzene do not affect the contact angle, because there would be no alignment of the molecule relative the substrate, or that the amount of azobenzene present at the surface was too small to influence the wettability.
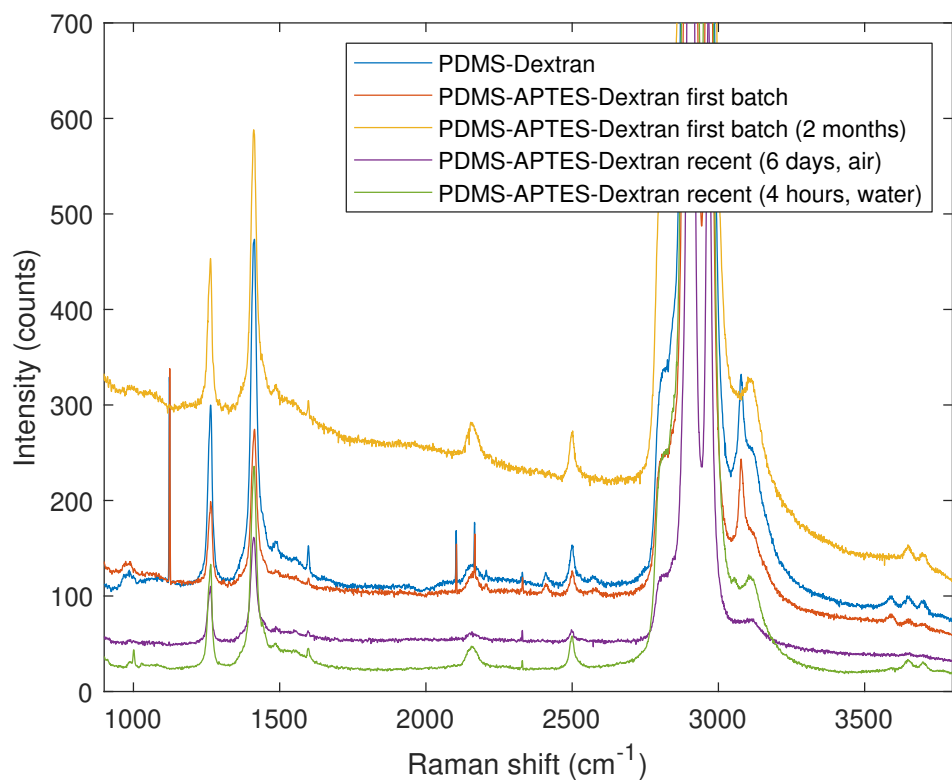
Figure C.5: Comparison of Raman spectrum from old batch versus recent batch using air plasma to oxidize surface. Raman laser: 514 nm, ND: 25%
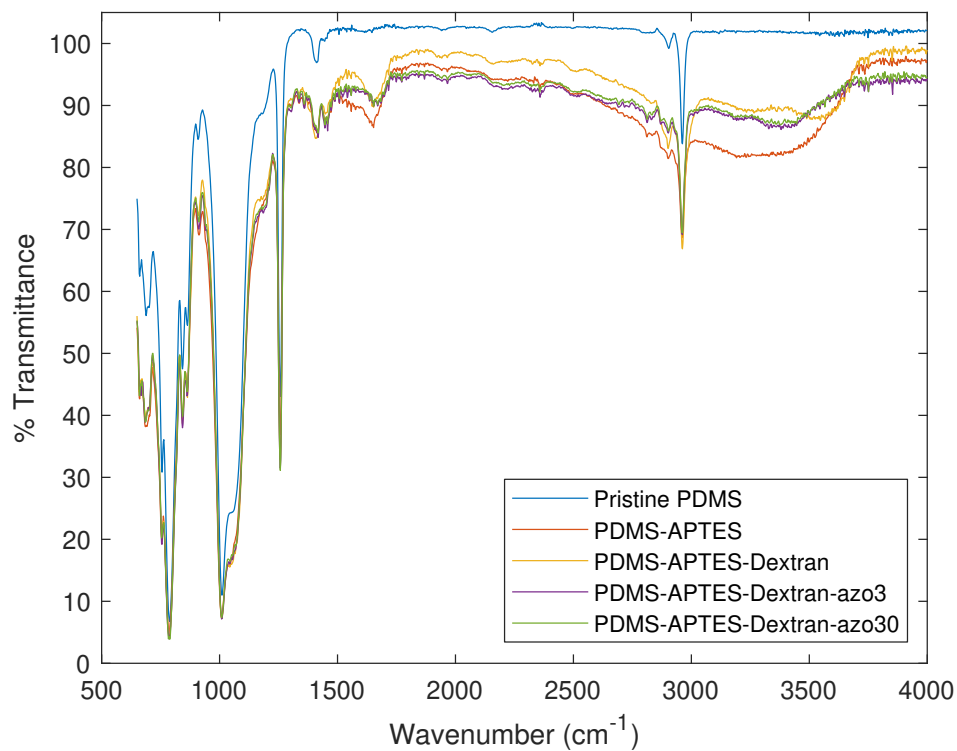
Figure C.6: FTIR spectrum using air plasma to oxidize surface

Figure C.7: FTIR spectrum using oxidation solution to oxidize surface

Figure C.8: FTIR spectrum using air plasma to oxidize surface measured after 1 month.

(a) Overview

(b) Closeup

Figure C.9: Setup overview of Kruss DSA100 for water contact measurements after UV irradiation.

D

Membrane permeability on agar

The diffusion through the PDMS membrane is a feature that should be ultimately controlled. This is first characterized for a pristine PDMS membrane. Sequentially, the PDMS surface is altered based on the obtained results. A description of the method and series of experiments are explained below.
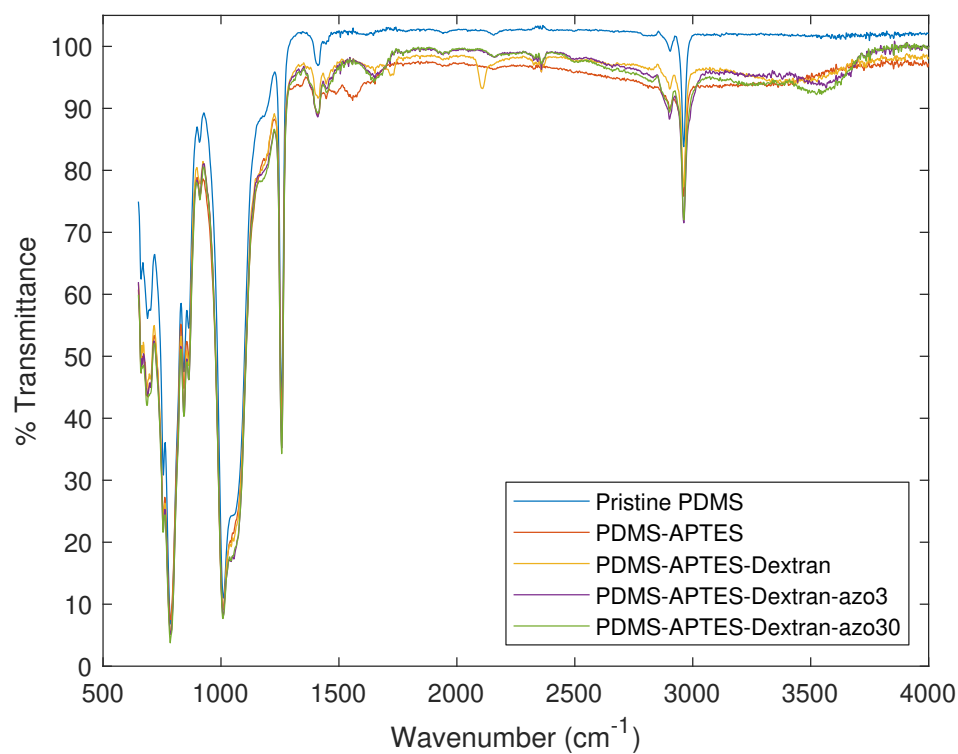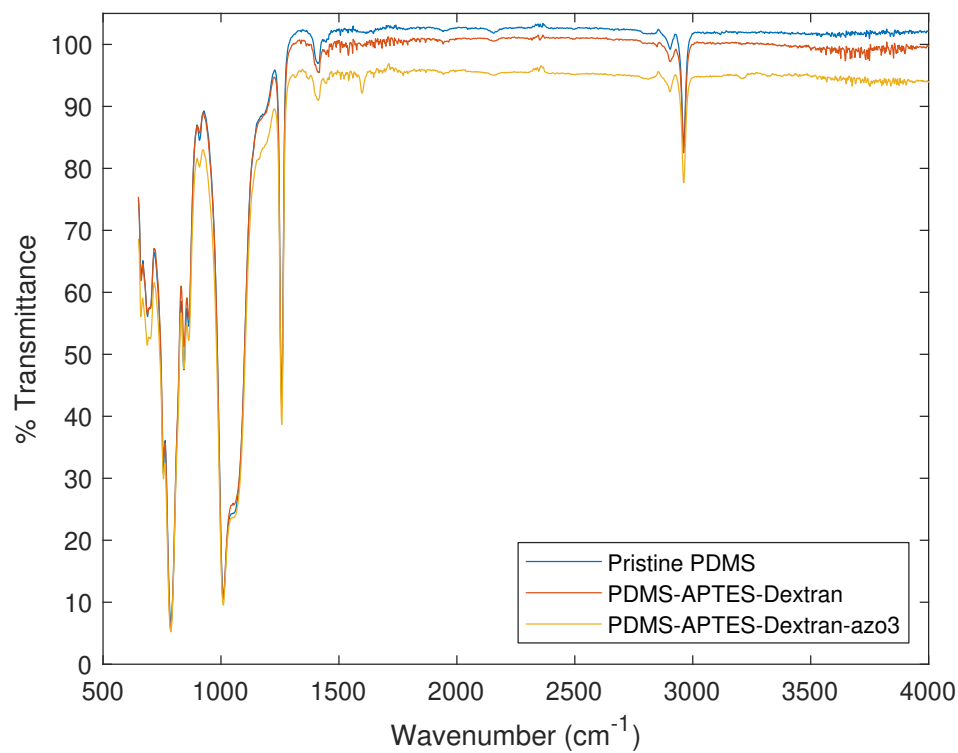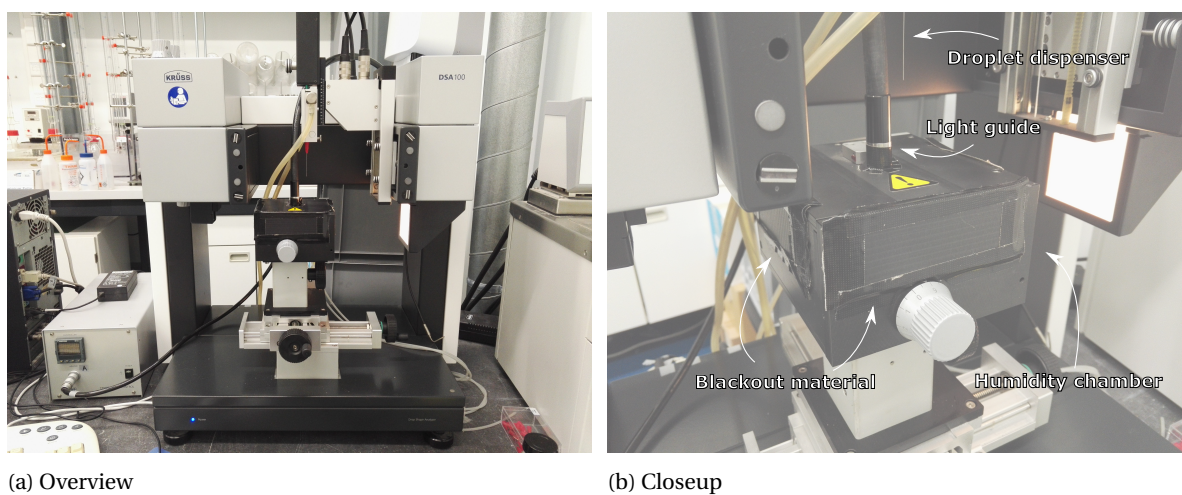
To characterize the diffusion through pristine PDMS membrane, a diffusion medium is required. For the ultimate goal this is a human brain, but before that it should first be tested using a cheap and readily available medium. Agarose gels have been used for in vitro models of the human brain. The most used variant is the 0.6% agarose gel, which was also chosen as the diffusion medium to be used in the experiments.

D.1. Method

The setup of the experiment is displayed in Figure D.1. The agarose gel is made by adding 0.3 g of agar (Sigma-Aldrich, ash 2.0-4.5%) to 50 ml of DI water. The mixture is boiled for 2 minutes followed by cooking at medium heat for 5 minutes. The mixture then transferred to clean petri dishes and left to cool down until solid. The agar-filled petri dishes are stored in the fridge kept at 4 °C. The agar gel is taken out of the fridge 15 minutes before the measurements and kept at room temperature. A membrane is placed on top of the agar gel near the edge of the petri dish. The micrscope is tilted to about a 90° angle to obtain a side view of the agarose gel. A droplet of colored water-based solution is pipetted on the surface making sure the droplet does not touch the side of the membrane. At first, the solution used was a blue food dye dissolved in a bit of water. The contrast in the images was not sufficient, thus a concentrated solution of potassium permanganate 1 M in water was used.

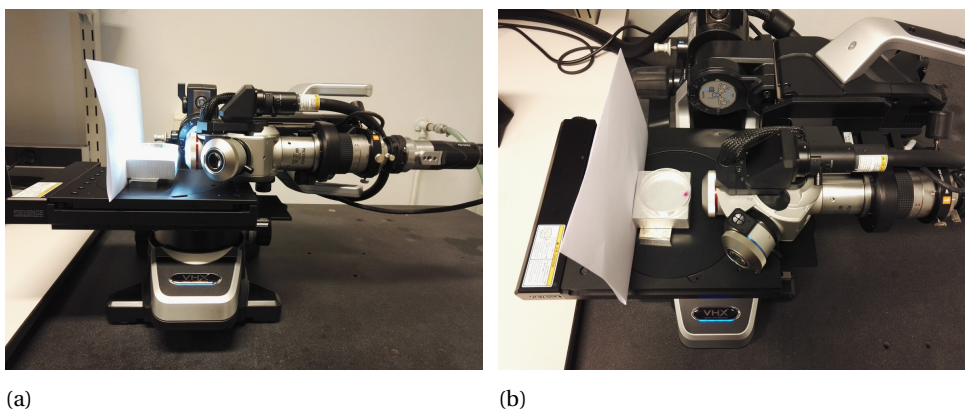(a)   (b)

Figure D.1: Setup overview of the Keyence VHX-6000 to image the side view of a PDMS membrane on agar.

The image is taken from the side to visualize the diffusion in z-direction. The membrane itself does not sit completely flat, because the liquid agar is affected by capillary forces to the edge of the petri dish forming
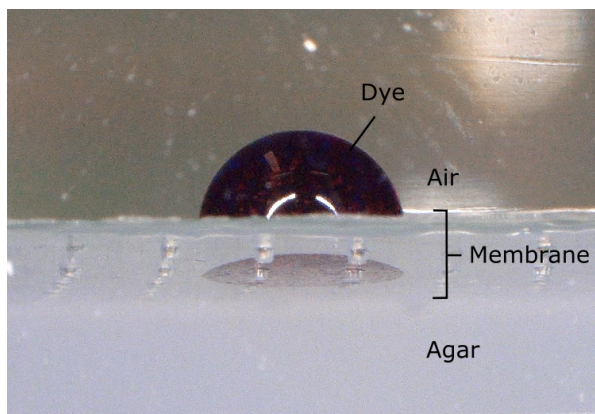
Figure D.2: Overview of the side view with PDMS membrane on agar using the explained setup. A droplet is pipetted on top with a solution of concentrated $KMnO_4$ in DI water. Magnification: 30x

a meniscus before solidifying. The images have to be taken with the membrane near the edge to obtain the highest quality image of the diffusion, for agar is only partially transparent.

D.2. Results

The first tests were performed using a passive PDMS membrane d200h200. No visible results could be obtained within a time frame of a few hours. Leaving the droplet on the membrane overnight did not obtain visible results either, even after removing the membrane of the agar. Thus, there is no flow through the pores for this geometry and surface characteristic of pristine PDMS. Increasing the pore diameter without increasing the membrane thickness to d300 and d400 gave the same results.

Some images of the side view of pores are taken. In Figure D.3 a comparison can be made of the behavior between a water-based solution and a polar aprotic solvent in the pore. The water-based solution goes partially inside the pore, but without touching the inner pore wall. When a polar aprotic solvent, like DMSO, is used, the liquid touches the inner pore wall. After about 10 minutes the liquid moves towards the agarose gel side. However, the liquid looks diluted and there is still a lot of air in the pore. When left overnight a small amount of dye was visible on the agar surface. From this comparison it can be seen that surface interactions have a larger influence than the geometry. Therefore, the next experiment is to test a hydrophilic PDMS membrane.
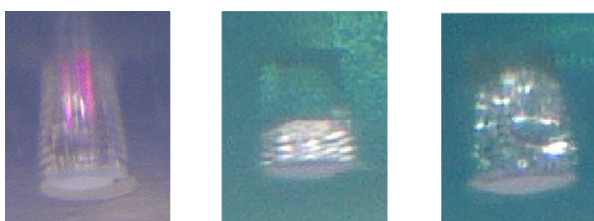
Figure D.3: Side view of pristine PDMS membrane on agar. A droplet is pipetted on top with a solution of concentrated $KMnO_4$ in DI water (left) and blue food dye in DMSO (middle, right). Magnification: 150x

D.2.1. Oxidizing inner pore

Oxidizing the flat PDMS surface is not difficult using air plasma, however the plasma cannot reach inside the pore. Therefore, a solution-based oxidation technique can be used to oxidize the inner pore surface and to make the PDMS surface more hydrophilic. There are two variants of oxidizing solutions used, but they have never been compared before, so both solutions are tested on a flat PDMS substrate and the water contact angle is measured.

Table D.1: Water contact angle measurements on flat PDMS substrates for various oxidation times in $H_2O : H_2O_2 : HCl = 5 : 1 : 1$ (v/v/v)

Oxidation time	Water contact angle
5 min	108.4 ± 2.8
10 min	99.9 ± 3.7
15 min	102.2 ± 9.9
30 min	108.6 ± 3.6
1 h	102.1 ± 4.6

Table D.2: Water contact angle measurements on flat PDMS substrates for various oxidation times in piranha solution ($H_2SO_4 : H_2O_2 = 3 : 1$)

Oxidation time	Water contact angle
45 sec	99.3 ± 1.3
5 min	84.1 ± 4.4
10 min	75.7 ± 3.5

The first solution is a mixture of $H_2O : H_2O_2 : HCl = 5 : 1 : 1$ (v/v/v) as reported by . They oxidized the PDMS for 5 minutes. The effect of the oxidation time is tested by measuring the water contact angle for different oxidation times. The results are displayed in Table D.1. There was no significant change in the contact angle and the PDMS did not become hydrophilic. Therefore, $H_2O : H_2O_2 : HCl$ will not render the inside of a pore in a PDMS membrane hydrophilic.

The following solution to be tested is the so-called piranha solution, which is a mixture of an acid and hydrogen peroxide. Different acids and ratios can be used, but for this experiment the most used combination is used with sulfuric acid with volume ratio $H_2SO_4 : H_2O_2 = 3 : 1$. A hydrophilic surface can be obtained as suggested by the results displayed in Table D.2. However, the solution is also an etchant which makes the PDMS surface rougher and less transparent in 5 minutes (probably faster, but the experiment was not repeated for oxidation times 1-5 minutes). The lower contact angle was not only a result by the formation of -OH groups at the surface, but also the surface roughness. The geometry of the pores will also be altered. Thus, the hydrophilic effect inside a pore cannot be isolated for analysis. Since oxidizing solutions are not the perfect solution to making the inner pore surface hydrophilic, other methods should be considered.

D.2.2. Oxidizing one side of the membrane

Exposing one side of a PDMS membrane to air plasma results in one side being superhydrophilic for about one hour. The water contact angle will increase to its original value before plasma treatment in 24 hours. The other side of the membrane will remain hydrophobic. Using the same test setup as explained in Section D.1. The following results are measured as quickly as possible after plasma treatment and are summarized in Table D.3. Putting the hydrophobic side facing the agarose gel, resulted in the droplet spreading over the hydrophilic surface without flow through the pores. When the membrane is flipped such that the hydrophilic side is facing the agar, it resulted in a fast flow of the water-based solution. The flow through the pore is so high that the liquid spreads first outwards between the membrane and agar interface, before diffusing into gel. This result means that the flow through the pore can be controlled by the wettability of the large surface of the membrane with the condition that the thickness of the membrane is not too large. When the membrane is increased to a thickness of $300 \, \mu m$ the flow through the pore becomes very slow and without spreading on the agar surface first. Since $200 \, \mu m$ is the thinnest membrane that can be fabricated with replica molding and this membrane was the most affected by air plasma, only membranes of this thickness are used in the following experiments.

The next step is to test whether there is flow through the pore in the case when the hydrophilic side is not superhydrophilic. From the results of the grafting process it was found that the PDMS surface grafted with APTES and dextran has a water contact angle of $62 \pm 4°$ one day after the grafting procedure. The PDMS membrane was oxidized on one side only, so APTES would be bonded to that side, and consequently dextran. The results are summarized in Table D.4. Compared to membranes tested quickly after plasma treatment, membranes with dextran had generally a slower flow. For d200 the flow was very slow and diffusion in agar was barely visible. There was no significant spreading on the agar surface. Increasing the pore size to d300,

Table D.3: Diffusion through PDMS membrane oxidized on one side by air plasma. The time after air plasma is 30 minutes to 1 hour.

Geometry	Side facing up	Diffusion	Comment
h200d200	Hydrophobic	Yes	Fast, immediately
h200d200	Hydrophilic	No	Spreads over surface
h200d400	Hydrophilic	No	Spreads over surface
h300d200	Hydrophobic	Yes	Very slow

Table D.4: Summary of the results the diffusion in agarose gel for PDMS membranes of thickness 200 μm grafted with APTES and dextran. The measurements were made one day after functionalization and dried in air for 1 day.

Sample	Side facing up	Diffusion	Comment
d200	Hydrophobic	Yes	Very slow
d200	Hydrophilic	Yes	Very slow
d300	Hydrophobic	Yes	Faster than d200
d300	Hydrophilic	No	
d400	Hydrophobic	Yes	Fast, immediately
d400	Hydrophilic	Yes	Only 1/4 pores

the flow was faster than d200 with significant staining in the agar. The dye did not spread on the agar surface first and a droplet was still on top of the membrane after 15 minutes, whereas in recently plasma-treated membranes the dispensed droplet went through immediately. This result was the closest to the desired functionality for the intended application. The results with d400 was found to be similar to the plasma-treated samples. Generally, when the hydrophilic side was facing up of dextran-treated membranes the result would be less repeatable and consequent than with plasma-treated membranes. Some would have some staining in agar, but overall the permeability was lower when the hydrophilic side was facing up instead of down.

Images are taken at time intervals over 15 minutes. Using image analysis a relative diffusion rate can be estimated. An example is shown in Figure D.4. A pixel can be translated to values in grayscale, rgb or hsb that can be used to quantify the local concentration. The most appropriate method is chosen by comparing the individual images as shown in Figure D.5. In grayscale the color gradient is completely lost. In rgb the useful information is split between green and blue with green retaining more information of the higher concentration area and blue of the lower concentration area. For hsv, the saturation as shown in Figure D.5h displays the color gradient from high to low concentration close to the original. Therefore, the saturation values are used for the following analysis of the diffusion through the membrane into the agar.

The saturation values of the images are extracted over several lines that start at the pore opening at the agar side and going radially outward. These saturation values are averaged for each distance from the pore which can then be used to create a saturation profile graph. The saturation values are normalized by taking the average saturation value a line close to the interface for a droplet dispensed directly onto agar as one and
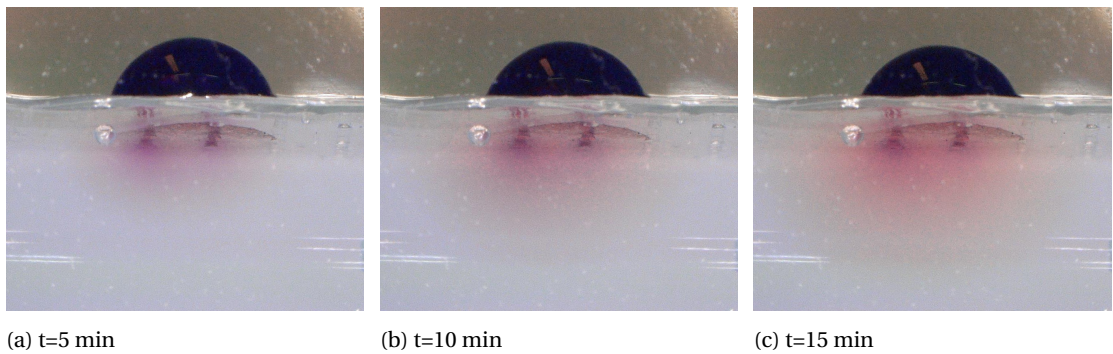
(a) t=5 min (b) t=10 min (c) t=15 min

Figure D.4: Eample of diffusion through PDMS membrane d300h200 functionalized with APTES and dextran.

(a) Original   (b) 16-bit   (c) 32-bit

(d) Red   (e) Green   (f) Blue
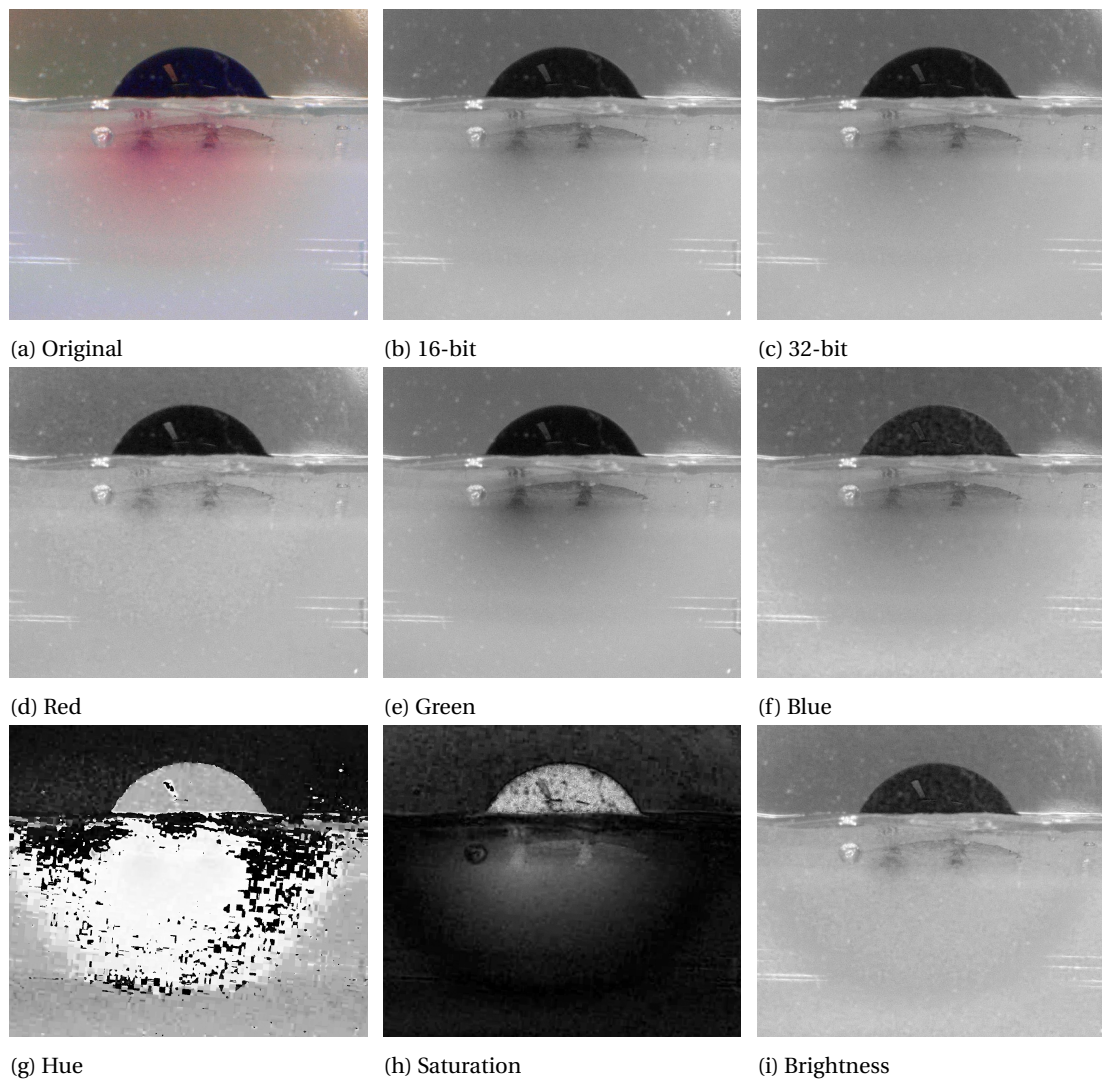
(g) Hue   (h) Saturation   (i) Brightness

Figure D.5: Comparison between different different strategies: grayscale, rgb, and hsb, to quantify pixels

Table D.5: Summary of the results the diffusion in agarose gel for PDMS membranes of thickness 200 μm grafted with APTES and dextran. The measurements were made 7 days after functionalization stored in air.

Geometry	Side facing up	Diffusion	Comment
h200d200	Hydrophobic	No	
h200d200	Hydrophilic	No	
h200d300	Hydrophobic	Yes	Very slow
h200d300	Hydrophilic	No	
h200d400	Hydrophobic	Yes	Medium fast
h200d400	Hydrophilic	Yes	Medium fast

the agar as zero. The calibration image is taken for every series in case of changes in the settings between sessions.

In Figure D.6 the change in the concentration is shown over distance from the pore opening and time. The concentration is the highest near the pore and it decreases below the agar base line after which it increases again to towards zero. As seen from Figure D.5h the lowest concentration area shows darker than the agar in terms of saturation. The dip below the zero base line depicts the edge of the diffusing dye. As time passes, the concentration near the pore increases, but slope representing the concentration gradient becomes less steep, since diffusion is driven by the concentration gradient.
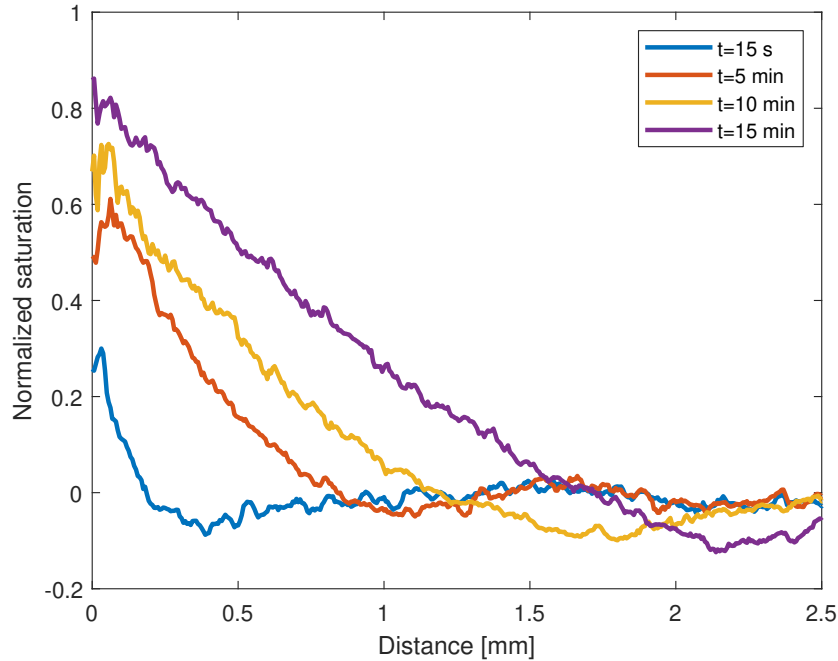

Figure D.6: PDMS membrane d300h200 diffusion in agar, hydrophilic side facing agar, stored in air for 1 day.

The same experiment is performed on the same samples 7 days after the grafting procedure stored in air. These results are summarized in Table D.5. The flow through the pores has decreased significantly. The flow through pores of diameter 300 μm is very little. In pores of 400 μm diameter there is a medium fast flow through the pore, but there is no difference between the hydrophobic and hydrophilic side. No staining in agar was expected, because the water contact angle was measured to return to a hydrophobic value within 4 days. This shows that the contact angle plays an important role, but there is another smaller factor that can influence the permeability. Maybe there is still some dextran left inside the pore, because the tiered structure inside the pore can enhance the retention of dextran. The fact that both sides of d400 had staining in agar can indicate that the difference was inside the pore. The amount of staining was similar for both sides as shown in Figures D.8 and D.9.
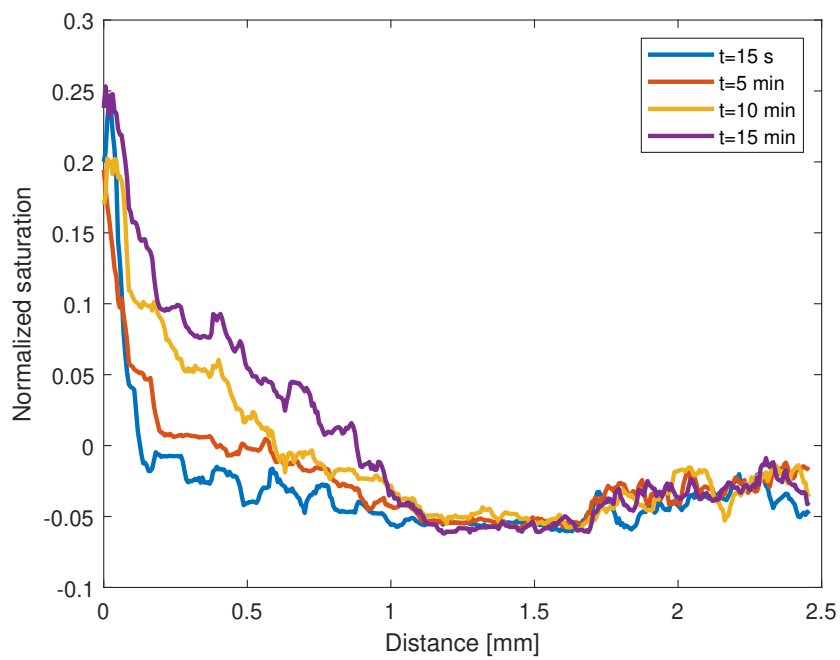
Figure D.7: PDMS membrane d300h200 diffusion in agar, hydrophilic side facing agar, stored in air for 7 days.
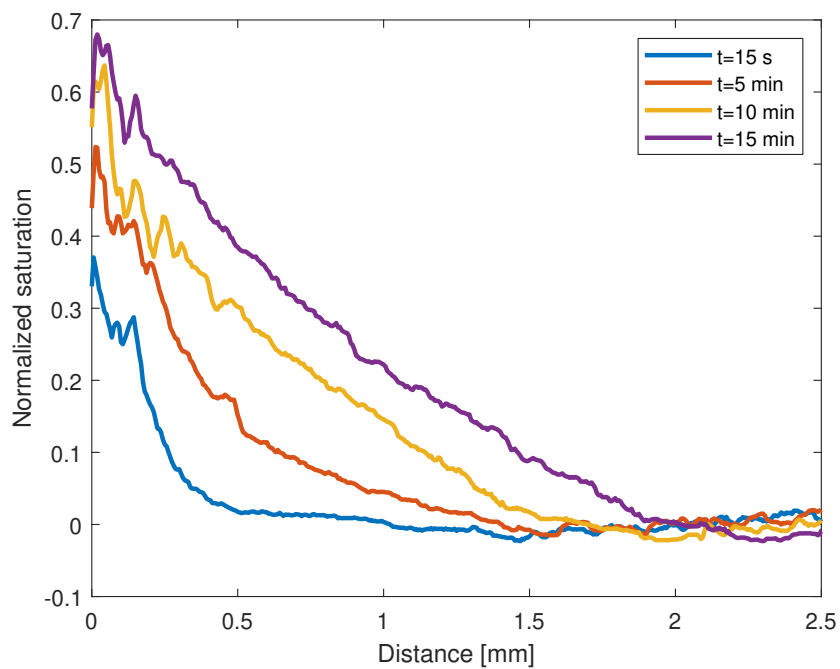

Figure D.8: PDMS membrane d400h200 diffusion in agar, hydrophilic side facing agar, stored in air for 7 days.
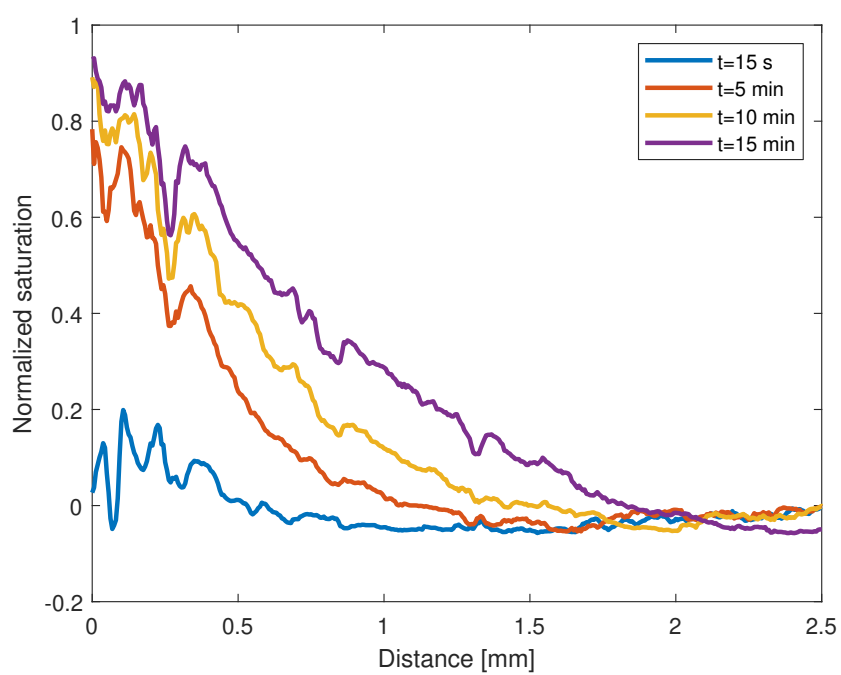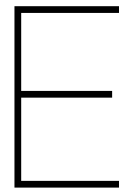
Figure D.9: PDMS membrane d400h200 diffusion in agar, hydrophobic side facing agar, stored in air for 7 days.

E

Membrane on ex vivo brain

This chapter includes the method for testing the permeability of the PDMS membranes on mouse brains. The experiments are performed at UVA so some slightly different chemicals may have been used. Furthermore, the brain extraction is briefly described, but keep in mind that this procedure was performed by a professional.

E.1. Materials

- IsoFlo (isoflurane) - inhalation anesthetic
- Injectable anesthetic
- 0.1 M phosphate buffer pH 7.2
- Agarose (Sigma-Aldrich, cat. no. A9793)
- Paraformaldehyde
- Potassium permanganate 0.1 M
- Pliers
- Tweezers
- Clippers
- Scalpel
- Pump + tubings
- Containers

E.2. Method

Preparation   Before the brain extraction a large batch of PBS is prepared. Next, agarose is weighed and heated in PBS until the boiling point by continuous stirring. The heating plate is set to low and stirring is continued until use. The tubings connected to a pump are filled with PBS in order to get rid of air bubbles.

Brain extraction   The mouse is first exposed to IsoFlo on a tissue in an enclosed box. It is then injected in the abdomen with a stronger anesthetic. Each limb is secured with tape and before moving on it is made sure that the anesthetic is working properly. The chest is cut and opened to reveal the heart. A hole is made in the jugular vein and connect the tubing filled with PBS with the left heart chamber to pump PBS through the body until all blood is removed. The brain is then extracted by removing the head first and carefully removing the surrounding tissue.

Permeability of membrane   The brain is placed in a Petri dish which is then partially filled with liquid agar using a disposable pipette, while making sure the temperature is not too hot (warm to the touch). It is left to solidify without moving the petri dish. After it has solidified, place it in the fridge for another few minutes to make sure the agarose has solidified. If the membrane is wet, it is dried using a cleanroom cloth. Using tweezers the membrane is carefully placed by resting one side on the agar before placing the rest of the membrane. The membrane is pressed down without pressing directly on the brain by pressing around the perimeter of the brain on the agar. One droplet of 2ul is pipetted on each hemisphere and left for 10 minutes. The excess

droplet is removed using a cleanroom cloth. The membrane is removed and the brain is placed in a fixation fluid for 5 days.

E.3. Results

There were only three mouse brains available, thus a selection had to be made. The series should include a pristine, dextran-modified and plasma-treated membrane. The chosen membranes were all d300h200, because the membrane with dextran gave the most desirable result in the case with agar. The plasma-treated membrane was treated the day before, because there was no plasma cleaner available at the location of the experiment. The membrane was transported in a bottle of DI water to prevent hydrophobic recovery.

Bibliography

[1] Guidelines for management of ischaemic stroke and transient ischaemic attack 2008. *Cerebrovascular Diseases*, 25(5):457–507, 2008. doi: 10.1159/000131083. URL https://doi.org/10.1159/000131083.

[2] Arthur W Adamson, Alice Petry Gast, et al. Physical chemistry of surfaces. 1967.

[3] Pejman Ahmadiannamini, Xianfeng Li, Ward Goyens, Nithya Joseph, Boudewijn Meesschaert, and Ivo FJ Vankelecom. Multilayered polyelectrolyte complex based solvent resistant nanofiltration membranes prepared from weak polyacids. *Journal of membrane science*, 394:98–106, 2012.

[4] Mercedes Alvaro, Miriam Benitez, Debashis Das, Hermenegildo Garcia, and Encarna Peris. Reversible porosity changes in photoresponsive azobenzene-containing periodic mesoporous silicas. *Chemistry of materials*, 17(20):4958–4964, 2005.

[5] Costas A Anastassiou, Sean M Montgomery, Mauricio Barahona, György Buzsáki, and Christof Koch. The effect of spatially inhomogeneous extracellular electric fields on neurons. *Journal of Neuroscience*, 30(5):1925–1936, 2010.

[6] M Andriot, SH Chao, AR Colas, SE Cray, F DeBuyl, JV DeGroot, A Dupont, T Easton, JL Garaud, E Gerlach, et al. Silicones in industrial applications. *Inorganic polymers*, pages 61–161, 2007.

[7] Emily Asenath Smith and Wei Chen. How to prevent the loss of surface functionality derived from aminosilanes. *Langmuir*, 24(21):12405–12409, 2008.

[8] Malar A Azagarsamy, Daniel L Alge, Srinidhi J Radhakrishnan, Mark W Tibbitt, and Kristi S Anseth. Photocontrolled nanoparticles for on-demand release of proteins. *Biomacromolecules*, 13(8):2219–2224, 2012.

[9] Elena Aznar, Rosa Casasús, Beatriz García-Acosta, M Dolores Marcos, Ramón Martínez-Máñez, Félix Sancenón, Juan Soto, and Pedro Amorós. Photochemical and chemical two-channel control of functional nanogated hybrid architectures. *Advanced Materials*, 19(17):2228–2231, 2007.

[10] Elena Aznar, Mar Oroval, Lluís Pascual, Jose Ramón Murguía, Ramón Martínez-Máñez, and Félix Sancenón. Gated materials for on-command release of guest molecules. *Chemical reviews*, 116(2):561–718, 2016.

[11] Andrew A Beharry and G Andrew Woolley. Azobenzene photoswitches for biomolecules. *Chemical Society Reviews*, 40(8):4422–4437, 2011.

[12] Yevgeny Berdichevsky, Julia Khandurina, András Guttman, and Y-H Lo. Uv/ozone modification of poly (dimethylsiloxane) microfluidic channels. *Sensors and Actuators B: Chemical*, 97(2):402–408, 2004.

[13] Inc. SpectraBase Bio-Rad Laboratories. Spectrabase compound id=epy2a0w01ql spectrabase spectrum id=jmprq97m1xu. http://spectrabase.com/spectrum/JMPrQ97M1xu?a=SPECTRUM_JMPrQ97M1xu. Accessed: Jul-29, 2018.

[14] SVG by Mysid. File:meninges-en.svg. https://commons.wikimedia.org/wiki/File:Meninges-en.svg. Accessed: 27-11-17.

[15] Dengke Cai, Andreas Neyer, Rüdiger Kuckuk, and H Michael Heise. Raman, mid-infrared, near-infrared and ultraviolet–visible spectroscopy of pdms silicone rubber for characterization of polymer optical waveguide materials. *Journal of Molecular Structure*, 976(1-3):274–281, 2010.

[16] Chaenyung Cha, Eleni Antoniadou, Minkyung Lee, Jae Hyun Jeong, Wylie W Ahmed, Taher A Saif, Stephen A Boppart, and Hyunjoon Kong. Tailoring hydrogel adhesion to polydimethylsiloxane substrates using polysaccharide glue. *Angewandte Chemie International Edition*, 52(27):6949–6952, 2013.

[17] Zhi-Jian Chen, George T Gillies, William C Broaddus, Sujit S Prabhu, Helen Fillmore, Ryan M Mitchell, Frank D Corwin, and Panos P Fatouros. A realistic brain tissue phantom for intraparenchymal infusion studies. *Journal of neurosurgery*, 101(2):314–322, 2004.

[18] Mengjiao Cheng, Feng Shi, Jianshu Li, Zaifu Lin, Chao Jiang, Meng Xiao, Liqun Zhang, Wantai Yang, and Toshio Nishi. Macroscopic supramolecular assembly of rigid building blocks through a flexible spacing coating. *Advanced Materials*, 26(19):3009–3013, 2014.

[19] Liang-Yin Chu, Yan Li, Jia-Hua Zhu, Hai-Dong Wang, and Yi-Jian Liang. Control of pore size and permeability of a glucose-responsive gating membrane for insulin delivery. *Journal of Controlled Release*, 97(1):43–53, 2004.

[20] Yon Jin Chuah, Shreyas Kuddannaya, Min Hui Adeline Lee, Yilei Zhang, and Yuejun Kang. The effects of poly (dimethylsiloxane) surface silanization on the mesenchymal stem cell fate. *Biomaterials science*, 3(2):383–390, 2015.

[21] Tai-Shung Chung. *Thermotropic Liquid Crystal Polymers: Thin-film Poly Chara Blends*. CRC Press, 2001.

[22] GT Clement and K Hynynen. A non-invasive method for focusing ultrasound through the human skull. *Physics in medicine and biology*, 47(8):1219, 2002.

[23] Michael J. Cooke, Yuanfei Wang, Cindi M. Morshead, and Molly S. Shoichet. Controlled epi-cortical delivery of epidermal growth factor for the stimulation of endogenous neural stem cell proliferation in stroke-injured brain. *Biomaterials*, 32(24):5688–5697, aug 2011. doi: 10.1016/j.biomaterials.2011.04. 032. URL https://doi.org/10.1016/j.biomaterials.2011.04.032.

[24] D Kacy Cullen, M Christian Lessing, and Michelle C LaPlaca. Collagen-dependent neurite outgrowth and response to dynamic deformation in three-dimensional neuronal cultures. *Annals of biomedical engineering*, 35(5):835–846, 2007.

[25] Kedar S Deshpande, Shreyas Kuddannaya, Judith Staginus, Peter C Thüne, Louis CPM de Smet, Joop H ter Horst, Luuk AM van der Wielen, and Marcel Ottens. Biofunctionalization and self-interaction chromatography in pdms microchannels. *Biochemical engineering journal*, 67:111–119, 2012.

[26] P Dietrich, F Michalik, R Schmidt, C Gahl, G Mao, M Breusing, MB Raschke, B Priewisch, T Elsässer, R Mendelsohn, et al. An anchoring strategy for photoswitchable biosensor technology: azobenzene-modified sams on si (111). *Applied Physics A*, 93(2):285–292, 2008.

[27] Ulrich Dirnagl, Costantino Iadecola, and Michael A Moskowitz. Pathobiology of ischaemic stroke: an integrated view. *Trends in neurosciences*, 22(9):391–397, 1999.

[28] Matthew J During, Andrew Freese, Bernhard A Sabel, W Mark Saltzman, Ariel Deutch, Robert H Roth, and Robert Langer. Controlled release of dopamine from a polymeric brain implant: in vivo characterization. *Annals of neurology*, 25(4):351–356, 1989.

[29] Aysan Durukan and Turgut Tatlisumak. Acute ischemic stroke: overview of major experimental rodent models, pathophysiology, and therapy of focal cerebral ischemia. *Pharmacology Biochemistry and Behavior*, 87(1):179–197, 2007.

[30] Kirill Efimenko, William E Wallace, and Jan Genzer. Surface modification of sylgard-184 poly (dimethyl siloxane) networks by ultraviolet and ultraviolet/ozone treatment. *Journal of colloid and interface science*, 254(2):306–315, 2002.

[31] Mohamed El Garah, Frank Palmino, and Frederic Cherioux. Reversible photoswitching of azobenzene-based monolayers physisorbed on a mica surface. *Langmuir*, 26(2):943–949, 2009.

[32] Megan Farrell and Stephen Beaudoin. Surface forces and protein adsorption on dextran-and polyethylene glycol-modified polydimethylsiloxane. *Colloids and Surfaces B: Biointerfaces*, 81(2):468–475, 2010.

[33] Jiu-Ju Feng, Ai-Jun Wang, Jing Fan, Jing-Juan Xu, and Hong-Yuan Chen. Hydrophilic biopolymer grafted on poly (dimethylsiloxane) surface for microchip electrophoresis. *Analytica chimica acta*, 658(1):75–80, 2010.

[34] Joseph T Francis, Bruce J Gluckman, and Steven J Schiff. Sensitivity of neurons to weak electric fields. *Journal of Neuroscience*, 23(19):7255–7261, 2003.

[35] Gregory J Gage, Daryl R Kipke, and William Shain. Whole animal perfusion fixation for rodents. *Journal of visualized experiments: JoVE*, (65), 2012.

[36] Aleksandra M Gajda and Mathias Ulbricht. Magnetic fe 3 o 4 nanoparticle heaters in smart porous membrane valves. *Journal of Materials Chemistry B*, 2(10):1317–1326, 2014.

[37] Mou Gao, Qin Dong, Hongtian Zhang, Yang Yang, Jianwei Zhu, Zhijun Yang, Minhui Xu, and Ruxiang Xu. Syringe needle skull penetration reduces brain injuries and secondary inflammation following intracerebral neural stem cell transplantation. *Experimental and Therapeutic Medicine*, 13(3):885–890, 2017.

[38] Aaron Gilletti and Jit Muthuswamy. Brain micromotion around implants in the rodent somatosensory cortex. *Journal of neural engineering*, 3(3):189, 2006.

[39] GT Gillies, TD Wilhelm, JAC Humphrey, HL Fillmore, KL Holloway, and WC Broaddus. A spinal cord surrogate with nanoscale porosity for in vitro simulations of restorative neurosurgical techniques. *Nanotechnology*, 13(5):587, 2002.

[40] Monika Gołda, Monika Brzychczy-Włoch, Marek Faryna, Klas Engvall, and Andrzej Kotarba. Oxygen plasma functionalization of parylene c coating for implants surface: nanotopography and active sites for drug anchoring. *Materials Science and Engineering: C*, 33(7):4221–4227, 2013.

[41] Liang Guo and Stephen P DeWeerth. An effective lift-off method for patterning high-density gold interconnects on an elastomeric substrate. *Small*, 6(24):2847–2852, 2010.

[42] Tae Mok Gwon, Chaebin Kim, Soowon Shin, Jeong Hoan Park, Jin Ho Kim, and Sung June Kim. Liquid crystal polymer (lcp)-based neural prosthetic devices. *Biomedical Engineering Letters*, 6(3):148–163, 2016.

[43] Dinggeng He, Xiaoxiao He, Kemin Wang, Jie Cao, and Yingxiang Zhao. A light-responsive reversible molecule-gated system using thymine-modified mesoporous silica nanoparticles. *Langmuir*, 28(8): 4003–4008, 2012.

[44] Dinggeng He, Xiaoxiao He, Kemin Wang, Jie Cao, and Yingxiang Zhao. A photon-fueled gate-like delivery system using i-motif dna functionalized mesoporous silica nanoparticles. *Advanced Functional Materials*, 22(22):4704–4710, 2012.

[45] Greg T Hermanson. *Bioconjugate techniques*. Academic press, 2013.

[46] Sophie Hernot and Alexander L Klibanov. Microbubbles in ultrasound-triggered drug and gene delivery. *Advanced drug delivery reviews*, 60(10):1153–1166, 2008.

[47] Todd Hoare, Brian P Timko, Jesus Santamaria, Gerardo F Goya, Silvia Irusta, Samantha Lau, Cristina F Stefanescu, Debora Lin, Robert Langer, and Daniel S Kohane. Magnetically triggered nanocomposite membranes: a versatile platform for triggered drug release. *Nano letters*, 11(3):1395–1400, 2011.

[48] Ingrid Hoek, Febly Tho, and W Mike Arnold. Sodium hydroxide treatment of pdms based microfluidic devices. *Lab on a Chip*, 10(17):2283–2285, 2010.

[49] Dongeun Huh, Hyun Jung Kim, Jacob P Fraser, Daniel E Shea, Mohammed Khan, Anthony Bahinski, Geraldine A Hamilton, and Donald E Ingber. Microfabrication of human organs-on-chips. *Nature protocols*, 8(11):2135–2157, 2013.

[50] Gh Iacob, Ovidiu Rotariu, Norval James Colin Strachan, and UO Häfeli. Magnetizable needles and wires–modeling an efficient way to target magnetic microspheres in vivo. *Biorheology*, 41(5):599–612, 2004.

[51] Costantino Iadecola. Bright and dark sides of nitric oxide in ischemic brain injury. *Trends in neurosciences*, 20(3):132–139, 1997.

[52] Boehringer Ingelheim. Pathophysiology. `http://actilyse.com/overview/pathophysiology`. Accessed: 27-11-17.

[53] American National Standards Institute. *American national standard for safe use of lasers*. Laser Institute of America, 2007.

[54] ID Johnston, DK McCluskey, CKL Tan, and MC Tracey. Mechanical characterization of bulk sylgard 184 for microfluidics and microengineering. *Journal of Micromechanics and Microengineering*, 24(3): 035017, 2014.

[55] Ulrich Jung, Mathias Müller, Norihiro Fujimoto, Katsuyoshi Ikeda, Kohei Uosaki, Ursula Cornelissen, Felix Tuczek, Claudia Bornholdt, Dordaneh Zargarani, Rainer Herges, et al. Gap-mode sers studies of azobenzene-containing self-assembled monolayers on au (111). *Journal of colloid and interface science*, 341(2):366–375, 2010.

[56] Kan Junwu, Yang Zhigang, Peng Taijiang, Cheng Guangming, and Wu Boda. Design and test of a high-performance piezoelectric micropump for drug delivery. *Sensors and Actuators A: Physical*, 121(1): 156–161, 2005.

[57] Daniel Kessler, Florian D Jochum, Jiyeon Choi, Kookheon Char, and Patrick Theato. Reactive surface coatings based on polysilsesquioxanes: universal method toward light-responsive surfaces. *ACS applied materials & interfaces*, 3(2):124–128, 2011.

[58] Marjo Kettunen, Riitta J Silvennoinen, Nikolay Houbenov, Antti Nykänen, Janne Ruokolainen, Jani Sainio, Viljami Pore, Marianna Kemell, Mikael Ankerfors, Tom Lindström, et al. Photoswitchable superabsorbency based on nanocellulose aerogels. *Advanced Functional Materials*, 21(3):510–517, 2011.

[59] Dion Khodagholy, Jennifer N Gelinas, Thomas Thesen, Werner Doyle, Orrin Devinsky, George G Malliaras, and György Buzsáki. Neurogrid: recording action potentials from the surface of the brain. *Nature neuroscience*, 18(2):310–315, 2015.

[60] H-J Kim, Hirofumi Matsuda, Haoshen Zhou, and Itaru Honma. Ultrasound-triggered smart drug release from a poly (dimethylsiloxane)–mesoporous silica composite. *Advanced Materials*, 18(23):3083–3088, 2006.

[61] Il-Doo Kim, Joo-Hyun Shin, Seung-Woo Kim, Sunghyun Choi, Junseong Ahn, Pyung-Lim Han, Jong-Sang Park, and Ja-Kyeong Lee. Intranasal delivery of hmgb1 sirna confers target gene knockdown and robust neuroprotection in the postischemic brain. *Molecular Therapy*, 20(4):829–839, 2012.

[62] Peter Larkin. Chapter 7 - general outline and strategies for {IR} and raman spectral interpretation. In *Infrared and Raman Spectroscopy*, pages 117 – 133. Elsevier, Oxford, 2011. ISBN 978-0-12-386984-5. doi: https://doi.org/10.1016/B978-0-12-386984-5.10007-2.

[63] Ilana Lavon and Joseph Kost. Mass transport enhancement by ultrasound in non-degradable polymeric controlled release systems. *Journal of controlled release*, 54(1):1–7, 1998.

[64] Jessamine Ng Lee, Cheolmin Park, and George M Whitesides. Solvent compatibility of poly (dimethylsiloxane)-based microfluidic devices. *Analytical chemistry*, 75(23):6544–6554, 2003.

[65] Guo Li, Guoxia Fei, Hesheng Xia, Jianjun Han, and Yue Zhao. Spatial and temporal control of shape memory polymers and simultaneous drug release using high intensity focused ultrasound. *Journal of materials chemistry*, 22(16):7692–7696, 2012.

[66] Po-Ying Li, Roya Sheybani, Christian A Gutierrez, Jonathan TW Kuo, and Ellis Meng. A parylene bellows electrochemical actuator. *Journal of Microelectromechanical Systems*, 19(1):215–228, 2010.

[67] Ho Sun Lim, Joong Tark Han, Donghoon Kwak, Meihua Jin, and Kilwon Cho. Photoreversibly switchable superhydrophobic surface with erasable and rewritable pattern. *Journal of the American Chemical Society*, 128(45):14458–14459, 2006.

[68] H-M Lin, W-K Wang, P-A Hsiung, and S-G Shyu. Light-sensitive intelligent drug delivery systems of coumarin-modified mesoporous bioactive glass. *Acta biomaterialia*, 6(8):3256–3263, 2010.

[69] Vincent Linder, Byron D Gates, Declan Ryan, Babak A Parviz, and George M Whitesides. Water-soluble sacrificial layers for surface micromachining. *Small*, 1(7):730–736, 2005.

[70] Jianan Liu, Wenbo Bu, Limin Pan, and Jianlin Shi. Nir-triggered anticancer drug delivery by upconverting nanoparticles with integrated azobenzene-modified mesoporous silica. *Angewandte Chemie International Edition*, 52(16):4375–4379, 2013.

[71] Nanguo Liu, Kui Yu, Bernd Smarsly, Darren R Dunphy, Ying-Bing Jiang, and C Jeffrey Brinker. Self-directed assembly of photoactive hybrid silicates derived from an azobenzene-bridged silsesquioxane. *Journal of the American Chemical Society*, 124(49):14540–14541, 2002.

[72] Nanguo Liu, Zhu Chen, Darren R Dunphy, Ying-Bing Jiang, Roger A Assink, and C Jeffrey Brinker. Photoresponsive nanocomposite formed by self-assembly of an azobenzene-modified silane. *Angewandte Chemie International Edition*, 42(15):1731–1734, 2003.

[73] Nanguo Liu, Darren R Dunphy, Plamen Atanassov, Scott D Bunge, Zhu Chen, Gabriel P López, Timothy J Boyle, and C Jeffrey Brinker. Photoregulation of mass transport through a photoresponsive azobenzene-modified nanoporous membrane. *Nano Letters*, 4(4):551–554, 2004.

[74] Eng H Lo, Aneesh B Singhal, Vladimir P Torchilin, and N Joan Abbott. Drug delivery to damaged brain. *Brain research reviews*, 38(1):140–148, 2001.

[75] Jie Lu, Eunshil Choi, Fuyuhiko Tamanoi, and Jeffrey I Zink. Light-activated nanoimpeller-controlled drug release in cancer cells. *Small*, 4(4):421–426, 2008.

[76] Dan Ma, Hengwu Chen, Dongyan Shi, Zhiming Li, and Jinfu Wang. Preparation and characterization of thermo-responsive pdms surfaces grafted with poly (n-isopropylacrylamide) by benzophenone-initiated photopolymerization. *Journal of colloid and interface science*, 332(1):85–90, 2009.

[77] Emilie Macé, Gabriel Montaldo, Ivan Cohen, Michel Baulac, Mathias Fink, and Mickael Tanter. Functional ultrasound imaging of the brain. *Nature methods*, 8(8):662, 2011.

[78] Morten Hannibal Madsen, Nikolaj A Feidenhans, Poul-Erik Hansen, Jørgen Garnæs, and Kai Dirscherl. Accounting for pdms shrinkage when replicating structures. *Journal of Micromechanics and Microengineering*, 24(12):127002, 2014.

[79] Honest Makamba, Ya-Yu Hsieh, Wang-Chou Sung, and Shu-Hui Chen. Stable permanently hydrophilic protein-resistant thin-film coatings on poly (dimethylsiloxane) substrates by electrostatic self-assembly and chemical cross-linking. *Analytical chemistry*, 77(13):3971–3978, 2005.

[80] P Mansky, Y Liu, E Huang, TP Russell, and C Hawker. Controlling polymer-surface interactions with random copolymer brushes. *Science*, 275(5305):1458–1460, 1997.

[81] JR Marier. The national institute of neurological disorders and stroke rt-pa stroke study group tissue plasminogen activator for acute ischemic stroke. *N Engl J Med*, 333(24):1581–1587, 1995.

[82] Surangkhana Martwiset, Anna E Koh, and Wei Chen. Nonfouling characteristics of dextran-containing surfaces. *Langmuir*, 22(19):8192–8196, 2006.

[83] MatWeb. Material property database: Parylene c. `http://www.matweb.com/search/DataSheet.aspx?MatGUID=32db38ac126141309a35849b7690452d`, . Accessed: 27-11-17.

[84] MatWeb. Material property data: Polyimide. `http://www.matweb.com/search/DataSheet.aspx?MatGUID=ab35b368ab9c40848f545c35bdf1a672&ckck=1`, . Accessed: 27-11-17.

[85] N. McDannold, C. D. Arvanitis, N. Vykhodtseva, and M. S. Livingstone. Temporary disruption of the blood-brain barrier by use of ultrasound and microbubbles: Safety and efficacy evaluation in rhesus macaques. *Cancer Research*, 72(14):3652–3663, may 2012. doi: 10.1158/0008-5472.can-12-0128. URL `https://doi.org/10.1158/0008-5472.can-12-0128`.

[86] Nathan McDannold, Costas D Arvanitis, Natalia Vykhodtseva, and Margaret S Livingstone. Temporary disruption of the blood–brain barrier by use of ultrasound and microbubbles: safety and efficacy evaluation in rhesus macaques. *Cancer research*, 72(14):3652–3663, 2012.

[87] Geeta Mehta, Mark J Kiel, Jung Woo Lee, Nicholas Kotov, Jennifer J Linderman, and Shuichi Takayama. Polyelectrolyte-clay-protein layer films on microfluidic pdms bioreactor surfaces for primary murine bone marrow culture. *Advanced Functional Materials*, 17(15):2701–2709, 2007.

[88] Fangang Meng, So-Ryong Chae, Anja Drews, Matthias Kraume, Hang-Sik Shin, and Fenglin Yang. Recent advances in membrane bioreactors (mbrs): membrane fouling and membrane material. *Water research*, 43(6):1489–1512, 2009.

[89] Philipp Mergenthaler, Ulrich Dirnagl, and Andreas Meisel. Pathophysiology of stroke: Lessons from animal models. *Metabolic Brain Disease*, 19(3/4):151–167, dec 2004. doi: 10.1023/b:mebr.0000043966. 46964.e6. URL https://doi.org/10.1023/b:mebr.0000043966.46964.e6.

[90] Dan E Meyer, BC Shin, GA Kong, MW Dewhirst, and A Chilkoti. Drug targeting using thermally responsive polymers and local hyperthermia. *Journal of controlled release*, 74(1):213–224, 2001.

[91] MIT. Material property database: Pdms. http://www.mit.edu/~6.777/matprops/pdms.htm, . Accessed: 27-11-17.

[92] MIT. Material property database: Polyimide. http://www.mit.edu/~6.777/matprops/polyimide.htm, . Accessed: 27-11-17.

[93] Raul-Augustin Mitran, Daniela Berger, Laura Băjenaru, Silviu Năstase, Cristian Andronescu, and Cristian Matei. Azobenzene functionalized mesoporous almcm-41-type support for drug release applications. *Open Chemistry*, 12(7):788–795, 2014.

[94] Matthew J Moorcroft, Wouter RA Meuleman, Steven G Latham, Thomas J Nicholls, Ryan D Egeland, and Edwin M Southern. In situ oligonucleotide synthesis on poly (dimethylsiloxane): a flexible substrate for microarray fabrication. *Nucleic acids research*, 33(8):e75–e75, 2005.

[95] KB Neeves, CT Lo, CP Foley, WM Saltzman, and WL Olbricht. Fabrication and characterization of microfluidic probes for convection enhanced drug delivery. *Journal of controlled release*, 111(3):252–262, 2006.

[96] Manuel Ochoa, Pinghung Wei, Andrew J Wolley, Kevin J Otto, and Babak Ziaie. A hybrid pdms-parylene subdural multi-electrode array. *Biomedical microdevices*, 15(3):437–443, 2013.

[97] Yu Pan, Sabine Neuss, Annika Leifert, Monika Fischler, Fei Wen, Ulrich Simon, Günter Schmid, Wolfgang Brandau, and Willi Jahnen-Dechent. Size-dependent cytotoxicity of gold nanoparticles. *Small*, 3 (11):1941–1949, 2007.

[98] Chiyoung Park, Jino Lim, Mikyoung Yun, and Chulhee Kim. Photoinduced release of guest molecules by supramolecular transformation of self-assembled aggregates derived from dendrons. *Angewandte Chemie*, 120(16):3001–3005, 2008.

[99] Xiaowei Pei, Antony Fernandes, Bertrand Mathy, Xavier Laloyaux, Bernard Nysten, Olivier Riant, and Alain M Jonas. Correlation between the structure and wettability of photoswitchable hydrophilic azobenzene monolayers on silicon. *Langmuir*, 27(15):9403–9412, 2011.

[100] Lu Peng, Mingxu You, Quan Yuan, Cuichen Wu, Da Han, Yan Chen, Zhihua Zhong, Jiangeng Xue, and Weihong Tan. Macroscopic volume change of dynamic hydrogels induced by reversible dna hybridization. *Journal of the American Chemical Society*, 134(29):12302–12307, 2012.

[101] Fatemeh Nazly Pirmoradi, John K Jackson, Helen M Burt, and Mu Chiao. A magnetically controlled mems device for drug delivery: design, fabrication, and testing. *Lab on a Chip*, 11(18):3072–3080, 2011.

[102] Boris Polyak and Gary Friedman. Magnetic targeting for site-specific drug delivery: applications and clinical potential. *Expert opinion on drug delivery*, 6(1):53–70, 2009.

[103] Keil J Regehr, Maribella Domenech, Justin T Koepsel, Kristopher C Carver, Stephanie J Ellison-Zelski, William L Murphy, Linda A Schuler, Elaine T Alarid, and David J Beebe. Biological implications of polydimethylsiloxane-based microfluidic cell culture. *Lab on a Chip*, 9(15):2132–2139, 2009.

[104] Taiyoun Rhim, Dong Yun Lee, and Minhyung Lee. Drug delivery systems for the treatment of ischemic stroke. *Pharmaceutical research*, 30(10):2429–2444, 2013.

[105] Birthe Rubehn, Conrado Bosman, Robert Oostenveld, Pascal Fries, and Thomas Stieglitz. A mems-based flexible multichannel ecog-electrode array. *Journal of neural engineering*, 6(3):036003, 2009.

[106] Taiga Sakai, Harumi Murayama, Shusaku Nagano, Yukikazu Takeoka, Masatoshi Kidowaki, Kohzo Ito, and Takahiro Seki. Photoresponsive slide-ring gel. *Advanced Materials*, 19(15):2023–2025, 2007.

[107] John P Seymour, Fan Wu, Kensall D Wise, and Euisik Yoon. State-of-the-art mems and microsystem tools for brain research. *Microsystems & Nanoengineering*, 3:16066, 2017.

[108] Sigma-Aldrich. Poly(acrylic acid), . URL https://www.sigmaaldrich.com/catalog/product/aldrich/323667?lang=en&region=NL. Accessed: 23-05-2018.

[109] Sigma-Aldrich. N,n-dimethyl-4,4-azodianiline raman ftir, . URL https://www.sigmaaldrich.com/spectra/rair/RAIR010479.pdf. Accessed: 22-05-2018.

[110] Benjamin E Slentz, Natalia A Penner, Emilia Lugowska, and Fred Regnier. Nanoliter capillary electrochromatography columns based on collocated monolithic support structures molded in poly (dimethyl siloxane). *Electrophoresis*, 22(17):3736–3743, 2001.

[111] Salah Sommakia, Heui C Lee, Janak Gaire, and Kevin J Otto. Materials approaches for modulating neural tissue responses to implanted microelectrodes through mechanical and biochemical means. *Current Opinion in Solid State and Materials Science*, 18(6):319–328, 2014.

[112] Guodong Sui, Jinyi Wang, Chung-Cheng Lee, Weixing Lu, Stephanie P Lee, Jeffrey V Leyton, Anna M Wu, and Hsian-Rong Tseng. Solution-phase surface modification in intact poly (dimethylsiloxane) microfluidic channels. *Analytical chemistry*, 78(15):5543–5551, 2006.

[113] Kimihiro Susumu, Eunkeu Oh, James B Delehanty, Juan B Blanco-Canosa, Brandy J Johnson, Vaibhav Jain, William Judson Hervey IV, W Russ Algar, Kelly Boeneman, Philip E Dawson, et al. Multifunctional compact zwitterionic ligands for preparing robust biocompatible semiconductor quantum dots and gold nanoparticles. *Journal of the American Chemical Society*, 133(24):9480–9496, 2011.

[114] Shingo Tamesue, Yoshinori Takashima, Hiroyasu Yamaguchi, Seiji Shinkai, and Akira Harada. Photoswitchable supramolecular hydrogels formed by cyclodextrins and azobenzene polymers. *Angewandte Chemie International Edition*, 49(41):7461–7464, 2010.

[115] Derrick Tarn, Daniel P Ferris, Jonathan C Barnes, Michael W Ambrogio, J Fraser Stoddart, and Jeffrey I Zink. A reversible light-operated nanovalve on mesoporous silica nanoparticles. *Nanoscale*, 6(6):3335–3343, 2014.

[116] Mary MJ Tecklenburg, Derek J Kosnak, Atul Bhatnagar, and Dillip K Mohanty. Vibrational characterization of azobenzenes, azoxybenzenes and azoaromatic and azoxyaromatic polyethers. *Journal of Raman spectroscopy*, 28(10):755–763, 1997.

[117] Gail Ter Haar. Therapeutic applications of ultrasound. *Progress in biophysics and molecular biology*, 93 (1):111–129, 2007.

[118] Dongliang Tian, Xiaofang Zhang, Jin Zhai, and Lei Jiang. Photocontrollable water permeation on the micro/nanoscale hierarchical structured zno mesh films. *Langmuir*, 27(7):4265–4270, 2011.

[119] Dongliang Tian, Xiaofang Zhang, Yu Tian, Yue Wu, Xiao Wang, Jin Zhai, and Lei Jiang. Photo-induced water–oil separation based on switchable superhydrophobicity–superhydrophilicity and underwater superoleophobicity of the aligned zno nanorod array-coated mesh films. *Journal of Materials Chemistry*, 22(37):19652–19657, 2012.

[120] Brian P Timko, Manuel Arruebo, Sahadev A Shankarappa, J Brian McAlvin, Obiajulu S Okonkwo, Boaz Mizrahi, Cristina F Stefanescu, Leyre Gomez, Jia Zhu, Angela Zhu, et al. Near-infrared–actuated devices for remotely controlled drug delivery. *Proceedings of the National Academy of Sciences*, 111(4):1349–1354, 2014.

[121] Jana Timm, Christian Stoltenberg, Jürgen Senker, and Wolfgang Bensch. Azobenzene-functionalized sba-15 material for application in selective separation. *Zeitschrift für anorganische und allgemeine Chemie*, 640(3-4):595–603, 2014.

[122] Jana Timm, Ulrich Schürmann, Lorenz Kienle, and Wolfgang Bensch. High azobenzene functionalization enhances stability of the cis isomer: Periodic mesoporous organosilica network on the way to new light triggered applicable materials. *Microporous and Mesoporous Materials*, 228:30–36, 2016.

[123] Omid Veiseh, Jonathan W Gunn, and Miqin Zhang. Design and fabrication of magnetic nanoparticles for targeted drug delivery and imaging. *Advanced drug delivery reviews*, 62(3):284–304, 2010.

[124] Jonathan Viventi, Dae-Hyeong Kim, Leif Vigeland, Eric S Frechette, Justin A Blanco, Yun-Soung Kim, Andrew E Avrin, Vineet R Tiruvadi, Suk-Won Hwang, Ann C Vanleer, et al. Flexible, foldable, actively multiplexed, high-density electrode array for mapping brain activity in vivo. *Nature neuroscience*, 14 (12):1599–1605, 2011.

[125] Ivan Vlassiouk, Choong-Do Park, Sean A Vail, Devens Gust, and Sergei Smirnov. Control of nanopore wetting by a photochromic spiropyran: a light-controlled valve and electrical switch. *Nano letters*, 6(5): 1013–1017, 2006.

[126] Reecha Wadhwa, Carl F Lagenaur, and Xinyan Tracy Cui. Electrochemically controlled release of dexamethasone from conducting polymer polypyrrole coated electrode. *Journal of Controlled Release*, 110 (3):531–541, 2006.

[127] Dan Wang, Pengwei Jiao, Jianming Wang, Qiaolan Zhang, Lin Feng, and Zhenzhong Yang. Fast photo-switched wettability and color of surfaces coated with polymer brushes containing spiropyran. *Journal of Applied Polymer Science*, 125(2):870–875, 2012.

[128] Junwei Wang, Baodong Mao, James L Gole, and Clemens Burda. Visible-light-driven reversible and switchable hydrophobic to hydrophilic nitrogen-doped titania surfaces: correlation with photocatalysis. *Nanoscale*, 2(10):2257–2261, 2010.

[129] Huibin Wei, Bor-han Chueh, Huiling Wu, Eric W Hall, Cheuk-wing Li, Romana Schirhagl, Jin-Ming Lin, and Richard N Zare. Particle sorting using a porous membrane in a microfluidic device. *Lab on a chip*, 11(2):238–245, 2011.

[130] Otto W Witte, Hans-J Bidmon, Klaus Schiene, Christoph Redecker, and Georg Hagemann. Functional differentiation of multiple perilesional zones after focal cerebral ischemia. *Journal of Cerebral Blood Flow & Metabolism*, 20(8):1149–1165, 2000.

[131] J Xue, L Chen, HL Wang, ZB Zhang, XL Zhu, ET Kang, and KG Neoh. Stimuli-responsive multifunctional membranes of controllable morphology from poly (vinylidene fluoride)-graft-poly [2-(n, n-dimethylamino) ethyl methacrylate] prepared via atom transfer radical polymerization. *Langmuir*, 24 (24):14151–14158, 2008.

[132] Jing Yang, Wei-Dong He, Chen He, Jing Tao, Sheng-Qi Chen, Shao-Min Niu, and Shao-Lin Zhu. Hollow mesoporous silica nanoparticles modified with coumarin-containing copolymer for photo-modulated loading and releasing guest molecule. *Journal of Polymer Science Part A: Polymer Chemistry*, 51(18): 3791–3799, 2013.

[133] Mustafa S Yavuz, Yiyun Cheng, Jingyi Chen, Claire M Cobley, Qiang Zhang, Matthew Rycenga, Jingwei Xie, Chulhong Kim, Andrea G Schwartz, Lihong V Wang, et al. Gold nanocages covered by smart polymers for controlled release with near-infrared light. *Nature materials*, 8(12):935, 2009.

[134] Edmond WK Young, Michael WL Watson, Suthan Srigunapalan, Aaron R Wheeler, and Craig A Simmons. Technique for real-time measurements of endothelial permeability in a microfluidic membrane chip using laser-induced fluorescence detection. *Analytical chemistry*, 82(3):808–816, 2010.

[135] Ling Yu, Chang Ming Li, Yingshuai Liu, Jie Gao, Wei Wang, and Ye Gan. Flow-through functionalized pdms microfluidic channels with dextran derivative for elisas. *Lab on a Chip*, 9(9):1243–1247, 2009.

[136] Guangqun Zhai, SC Toh, WL Tan, ET Kang, KG Neoh, CC Huang, and DJ Liaw. Poly (vinylidene fluoride) with grafted zwitterionic polymer side chains for electrolyte-responsive microfiltration membranes. *Langmuir*, 19(17):7030–7037, 2003.

[137] Y. Zhang, W. M. Pardridge, and R. F. Keep. Neuroprotection in transient focal brain ischemia after delayed intravenous administration of brain-derived neurotrophic factor conjugated to a blood-brain barrier drug targeting system editorial comment. *Stroke*, 32(6):1378–1384, jun 2001. doi: 10.1161/01.str.32.6.1378. URL https://doi.org/10.1161/01.str.32.6.1378.

[138] Zhanxia Zhang, Dora Balogh, Fuan Wang, Ran Tel-Vered, Naomi Levy, Sohn Yang Sung, Rachel Nechushtai, and Itamar Willner. Light-induced and redox-triggered uptake and release of substrates to and from mesoporous sio2 nanoparticles. *Journal of Materials Chemistry B*, 1(25):3159–3166, 2013.

[139] Yingchun Zhu and Masahiro Fujiwara. Installing dynamic molecular photomechanics in mesopores: a multifunctional controlled-release nanosystem. *Angewandte Chemie International Edition*, 46(13):2241–2244, 2007.

[140] Bartosz Ziółkowski, Larisa Florea, Jannick Theobald, Fernando Benito-Lopez, and Dermot Diamond. Self-protonating spiropyran-co-nipam-co-acrylic acid hydrogel photoactuators. *Soft Matter*, 9(36):8754–8760, 2013.

[141] Joseph A Zuclich. Ultraviolet-induced photochemical damage in ocular tissues. *Health Physics*, 56(5):671–682, 1989.